INFORMATION TO USERS

This manuscript has been reproduced from the microfilm master. UMI films the text directly from the original or copy submitted. Thus, some thesis and dissertation copies are in typewriter face, while others may be from any type of computer printer.

The quality of this reproduction is dependent upon the quality of the copy submitted. Broken or indistinct print, colored or poor quality illustrations and photographs, print bleedthrough, substandard margins, and improper alignment can adversely affect reproduction.

In the unlikely event that the author did not send UMI a complete manuscript and there are missing pages, these will be noted. Also, if unauthorized copyright material had to be removed, a note will indicate the deletion.

Oversize materials (e.g., maps, drawings, charts) are reproduced by sectioning the original, beginning at the upper left-hand corner and continuing from left to right in equal sections with small overlaps.

Photographs included in the original manuscript have been reproduced xerographically in this copy. Higher quality 6" x 9" black and white photographic prints are available for any photographs or illustrations appearing in this copy for an additional charge. Contact UMI directly to order.

Bell & Howell Information and Learning
300 North Zeeb Road, Ann Arbor, MI 48106-1346 USA
800-521-0600

X-ray Scattering Study of the Spin-Peierls Phase Transition

by

MARK D. LUMSDEN

B.Sc. (St. Francis Xavier University) 1993

A Thesis
Submitted to the School of Graduate Studies
in Partial Fulfilment of the Requirements
for the Degree
Doctor of Philosophy

McMaster University

X-ray Scattering Study of the Spin-Peierls Phase Transition

DOCTOR OF PHILOSOPHY (1998)
(Physics)

McMaster University
Hamilton, Ontario

TITLE: X-ray Scattering Study of the Spin-Peierls Phase Transition

AUTHOR: Mark D. Lumsden

SUPERVISOR: Dr. B. D. Gaulin

NUMBER OF PAGES: xi, 167

Abstract

Scattering techniques are an essential tool in the experimental study of properties in the vicinity of a critical phase transition. Such techniques have been applied to the study of the spin-Peierls transition in pure and doped samples of $CuGeO_3$ and in the organic compound $MEM(TCNQ)_2$. The spin-Peierls phase transition occurs in one-dimensional S=1/2 Heisenberg spin chains with short-range, antiferromangetic interactions. Such a system is unstable against a dimerization of the chains with the subsequent appearance of a gap in the magnetic excitation spectrum. Such a gap acts to lower the magnetic energy in the system and, in the presence of coupling with the lattice, causes a phase transition to a dimerized, spin-Peierls, state.

High temperature stability measurements of the order parameter associated with this transition in the inorganic compound $CuGeO_3$ indicate a continuous phase transition at a temperature of 14.05 K with a corresponding critical exponent β of 0.345±0.03. This value is in agreement with conventional 3D universality and in closest agreement with 3D XY behaviour. We also observe a narrow asymptotic critical region which is largely responsible for the inconsistency in previously reported results. High resolution measurements of relative lattice constant changes, performed using a novel approach, indicate spontaneous strains which scale with the square of the order parameter expect near the transition temperature where differences are observed.

Similar order parameter measurements were performed on samples of $CuGeO_3$ doped with Zn, Si, and Cd. For the case of Zn and Si doping, we obtain and exponent β consistent with that for the pure material. Measurements on two Cd doped samples indicate results which clearly deviate from that observed in pure $CuGeO_3$ with an exponent β of about 0.5 consistent with mean field behaviour. We explain this change in behaviour as resulting from local strains induced by the presence of the much larger

Cd^{2+} dopant ion. Relative lattice constant measurements indicate spontaneous strains which scale with the square of the order parameter for the doped samples as was the case for pure $CuGeO_3$.

X-ray scattering measurements of both the order parameter and critical scattering in the vicinity of the transition temperature have been performed for the organic spin-Peierls compound $MEM(TCNQ)_2$. Order parameter measurements indicate a value of the exponent β of 0.35±0.06 consistent with 3D universality, as was observed in the inorganic spin-Peierls material $CuGeO_3$, and inconsistent with previous measurements which suggested mean-field behaviour. Critical scattering measurements suggest a lineshape not described by a traditional Ornstein-Zernike, Lorentzian, form but well described by a Lorentzian with a varying power or a Lorentzian+ Lorentzian^2. The latter form is reminiscent of recent x-ray scattering measurements of critical phenomena associated with structural phase transitions in perovskites or with magnetic x-ray scattering measurements on Ho, Tb, and some U-based compounds. Differences between this and previous measurements are discussed.

Acknowledgements

It is with sincere gratitude that I thank my supervisor, Bruce Gaulin, for his guidance, patience and support throughout my time at McMaster. Special thanks must also be extended to Marek Kiela for without his technical support, much of the work presented in this thesis could not have been completed. I would additionally like to thank Hanna Dabkowska for growing the pure and dilute $CuGeO_3$ crystals used in these experiements and for her useful suggestions and comments on the project.

I have benefited greatly from the friendship and assistance of many students and post-docs during my stay at McMaster, particularly Peter Mason, Jason Gardner, Marcy Lumsden, Chris Wiebe, Ming Mao, Oleg Petrenko, and Sonha Nguyen.

I am forever indebted to my parents for their years of support and encouragment. Finally I thank my wife, Mary, for her understanding, patience and love and our son Ian who provides me with a source of unending joy and pride.

Preface

The bulk of the original work in this thesis is included in Chapters 4, 5, and 6 which reproduces a series of three papers two of which have been peer-reviewed and published in Physical Review B and a third which has been submitted to this same journal. The first 2 papers are authored by myself, B.D. Gaulin, and H. Dabkowska with the third being co-authored by only B.D. Gaulin.

In each of the first two papers, H. Dabkowska grew the single crystals employed in the measurements. The experimental investigations and subsequent analysis were performed by myself under the guidance of B.D. Gaulin. I wrote each of the manuscripts with proofreading and editing assistance by B.D. Gaulin. Acknowledgements of helpful discussions are included in the individual papers themselves. I wrote all computer programs used in the course of the data analysis and all fits were performed using the nonlinear least-square fitting library, MINUIT, which is part of the CERNLIB libraries.

Contents

List of Figures

List of Tables

Chapter 1

Phase Transitions

The most pervasive example of a system in which a phase transition occurs is provided by the liquid which sustains all life on earth, water. We are all familiar with water freezing to form ice or boiling to form steam. Such processes are examples of phase transitions where a system is transformed from one state to another under the action of some external parameter. Other, less common, examples of phase transitions are crystalline structural transformations where the high temperature high-symmetry structure may transform to a lower-symmetry structure at low temperatures, and magnetic systems where the system may change from a high temperature phase with disordered magnetic moments to a low temperature phase with moments in a well-defined, ordered structure.

The state of any such system is described by a set of variables, known as thermodynamic variables, which fully describe the state of the system. For water, or any other fluid system, the set of such variables are the temperature, T, the pressure, P, and the density, ρ. The state of the system is defined by an equation of state which forms a surface in the space defined by the thermodynamic variables, P,ρ, and T in this case. The simplest way to consider this complicated surface is in the examination of its projection onto the various 2D planes, P-T, P-ρ, and ρ-T as shown in the left-

hand panels of Fig. 1.1 (Stanley 1971) (this is shown for a typical P,ρ,T system which differs slightly from that of water). These phase diagrams define a set of lines which separate the various phases from one another. Such lines are known as co-existence curves as they define lines along which the phases, in this case solid, liquid, and gas, are in thermodynamic equilibrium with one another.

Let us first consider the projection of the equation of state onto the P-T plane as shown in Fig. 1.1a. Here, we can see three well defined phases separated by coexistence curves and if the thermodynamic variables are manipulated in such a way as to cross these curves, the state of the system will transform discontinuously from one phase to another defining what is known as a discontinuous, or first-order, phase transition. Such a transition is accompanied by a latent heat of transformation which can be best understood by considering the transformation of water into steam. Heat is transferred to the water to drive the temperature up to the boiling point, but at this point, significantly more heat must be added, with no corresponding change in temperature, to drive the system fully into the gaseous state - such a heat transfer is a latent heat of transformation.

In contrast to the solid-liquid coexistence curve, the curve defining the boundary between the liquid and gas phases does not extend indefinitely, but rather can be seen to terminate at a point, defined by its thermodynamic variables P_c, ρ_c, and T_c, known as a critical point. One can imagine selecting a path in P-T space, as indicated by the dashed line in Fig 1.1a, such that the state of the system changes continuously from liquid to gas and the distinction between the two phases along this line is unclear. Such a continuous evolution of the state from one phase to another is known as a continuous or second-order phase transition. The behaviour of a system as it nears a critical point has been a topic of extensive study and such behaviour will constitute the bulk of this thesis for the case of one particular phase transition.

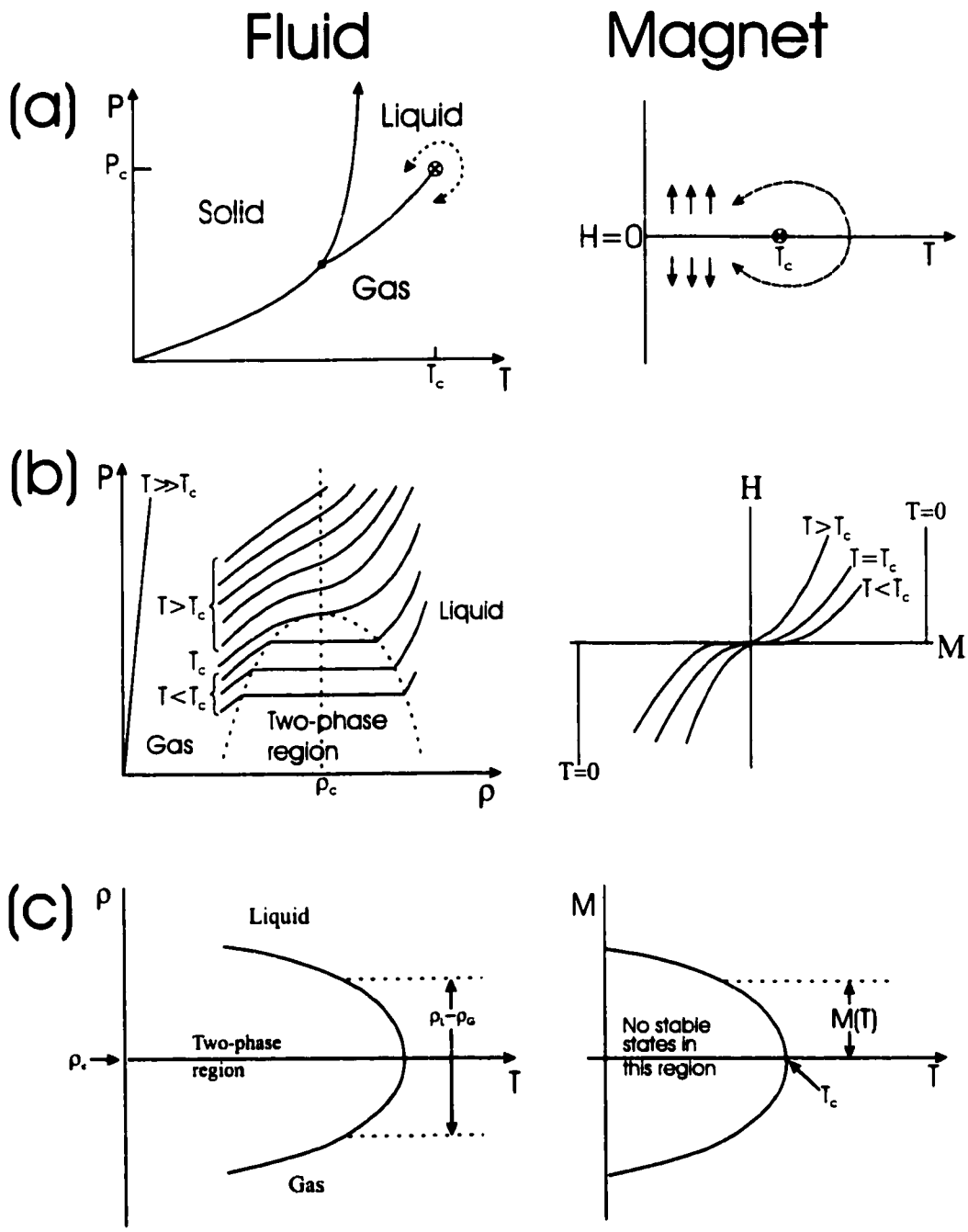

Figure 1.1: Projection of the equation of state onto the (a) P-T and H-T planes, (b) the P-ρ and H-M planes and (c) the ρ-T and M-T planes for a typical fluid system and magnetic system respectively. (Adapted from Stanley (1971))

To get a more detailed understanding of the behaviour near a critical point, let us consider the phase diagram in the P-ρ plane as shown in Fig. 1.1b. One can see that for temperatures well above T_c, the isotherm is a straight line, consistent with the ideal gas law, but as the temperature nears T_c, the isotherm exhibits substantial curvature. In fact, at T_c, the curvature at the critical density ρ_c becomes zero and such a flattening of the isotherm at T_c will correspond to a divergence in the isothermal compressibility, $\kappa_T = p^{-1}(\partial\rho/\partial P)_T$. The divergence of this and other experimentally measured quantities lies at the heart of so-called *critical phenomena* describing the behaviour of a system near a critical point.

One last, important concept can also be derived from the observation of the phase diagram in the P-ρ plane. One can see that the density of the liquid and gas states are very different for temperatures below T_c and this difference decreases progressively to zero as we approach T_c from below. The quantity $\rho_L - \rho_G$ which has a zero value above the transition temperature and is non-zero below, is called the *order parameter* for this particular phase transition. The existence of such an order parameter is a general property of all phase transitions and for a discontinuous transition, this quantity abruptly jumps to a finite value on passing through the transition temperature, while for a continuous transition, the order parameter increases progressively from zero. This represents a second physical quantity, the inverse of the order parameter, which diverges at the critical transition temperature.

1.1 Discontinuous/Continuous Phase Transitions

The distinction between discontinuous (first order) and continuous (second order or critical) phase transitions was first proposed by Ehrenfest who suggested that phase transitions be classified such that an *nth* order phase transition corresponds to

a discontinuity in the *nth* derivative of the free energy with respect to temperature. If we consider the free energy to be represented by G, the first derivative $(\partial G/\partial T) \sim dQ$, the heat transfer, and the second derivative $(\partial^2 G/\partial T^2) \sim C_v$, the specific heat. Such a representation works for a first-order phase transition as such a transition is accompanied by a latent heat of transformation, as mentioned previously, and consequently there is a discontinuity in the first derivative of the free energy, the heat transfer, dQ. However, this classification scheme typically fails for a second-order transition where the specific heat is often observed to exhibit a power law divergence upon approaching the transition temperature rather than a discontinuity. There are, however, cases where this classification scheme provides a good description of second-order transitions as well, with the best known examples being conventional superconductors and ferroelectrics (in fact, this scheme works for any continuous transition which can be classified as mean field).

Discontinuous phase transitions are characterized by a discontinuous change in the order parameter on passing through the transition, coexistence between the two phases in question, a latent heat of transformation and, often, by the presence of hysteresis. A continuous phase transition has an order parameter which evolves continuously on passing through the transition, no coexistence of phases, no hysteresis, and the presence of fluctuating microregions of one phase in the other whose size diverges at the transition temperature. Fluctuations may also occur in discontinuous phase transitions, but the length scale associated with such fluctuations does not diverge at T_c.

1.2 Magnetic Systems

To further discuss the behaviour near a critical point, it is constructive to change the focus from a typical fluid system to a magnetic system. Such a system involves a set of interacting magnetic moments which lie of the points of a crystalline lattice. Such a scenario occurs frequently in nature as the magnetic moments arise from unpaired electrons residing on the atoms in a crystalline solid. The magnetic moment of a free atom comes about from the spin angular momentum which the atom receives from the unpaired electrons and their orbital angular momentum about the nucleus. These moments interact with one another predominately through the electrostatic interaction which gains its dependence on magnetic moment direction through the Pauli exclusion principle. Such an interaction, known as an *exchange* interaction, can be shown to be predominately short-ranged and this represents one of the largest advantages provided by magnetic systems - the interactions can be treated as near neighbour interactions on a fixed crystalline lattice. One can easily imagine the advantage this provides in theoretical treatments when compared to more complex systems with long-range interactions such as fluid systems.

The state of such a magnetic system, for the case of ferromagnetic interactions where the spins preferentially align parallel to one another, can be described in terms of the thermodynamic variables H, the applied magnetic field, M, the magnetization, and T, the temperature, which can be thought to correspond directly to the variables P,ρ, and T. The corresponding projection of the equation of state onto the H-T, H-M and M-T planes are shown in the right side of Fig. 1.1 (Stanley 1971). As in the fluid system, there exists a critical point defined by H_c and T_c and we can construct a path, again represented by the dashed line in Fig. 1.1a, along which the state of the system can change in a continuous manner. As was the case for the isothermal compressibility, the flattening of the isotherms in the H-M plane correspond to a divergence of the

analogous response function, the magnetic susceptibility $\chi_T = (\partial M/\partial H)_T$. The relevant order parameter for such a system is the magnetization, M.

One can see an additional property of critical phase transitions by considering the M-T phase diagram shown in Fig. 1.1c. As the temperature is lowered below the transition temperature, the system selects one of two equivalent states, corresponding to +M or -M. Such a process is known as a *symmetry breaking* and is common to all critical phase transitions. There are three common symmetry breaking scenarios:

1. The magnetic moment has only a component in one crystalline direction. Such a symmetry breaking is known as discrete or Ising.
2. The spins are confined to a single plane - XY symmetry.
3. The spins are free to rotate throughout 3D space - Heisenberg symmetry.

The symmetry breaking that occurs in physical systems is often a result of anisotropies present due to the crystalline environment in which the magnetic moments reside.

1.3 Droplet Picture

The magnetic systems introduced in the last section are useful in furthering our understanding of the behaviour near a critical point. Let us consider a ferromagnetic system, where the spins prefer to be aligned in the same direction, at some temperature well below T_c. Here, the majority of the spins are aligned along some direction which we choose, arbitrarily, to be the $-z$ direction. Thermal fluctuations may drive a region of the system into a state where the spins are in the opposite direction with a corresponding increase in the free energy of the system. Such a process, as depicted in Fig. 1.2a (Kadanoff 1976), will be unlikely if the energy required in the formations of such a "droplet" is significantly greater than the thermal energy

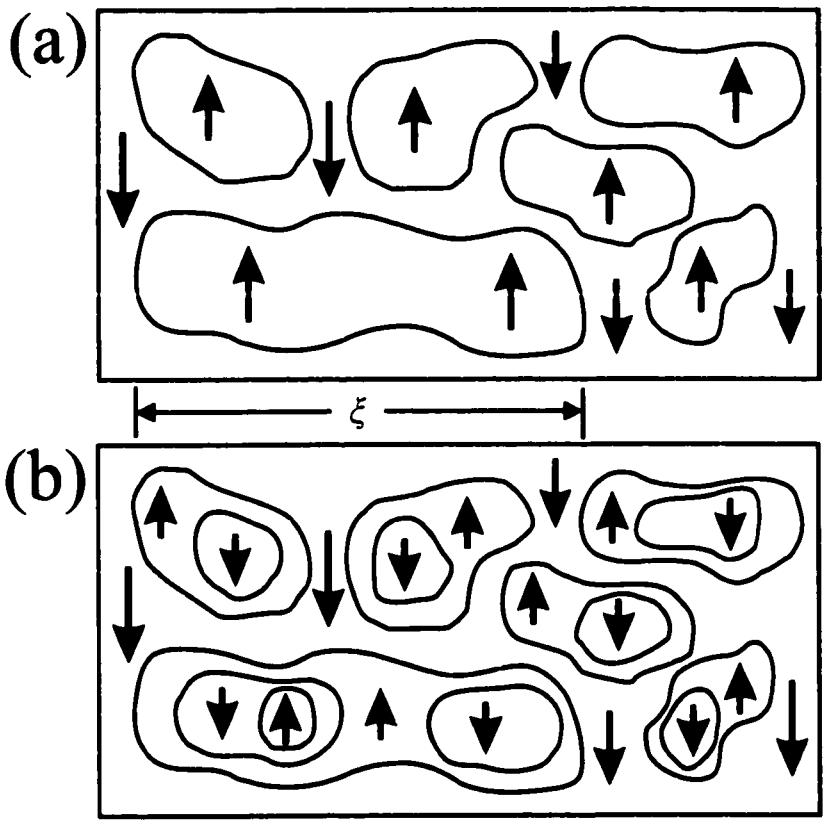

Figure 1.2: (a) Schematic of the formation of droplets of $+z$ spins in a system which was ordered with most spins down at low temperatures. Such a formation becomes energetically favourable as the temperature nears T_c. (b) Shows that the droplets formed in (a) were themselves critical regions and thus, droplets also form in their interior. For both panels, the individual arrows don't represent individual spins but rather regions containing a large number of spins with the specified orientation. (Adapted from Kadanoff (1976))

present in the system, kT. As the temperature increases, the thermal energy increases correspondingly and a larger number of these droplets are formed. However, as more droplets form, the magnetization, which is the number of $+z$ spins minus the number of $-z$ spins, approaches zero. Consequently, the energy of formation for a droplet decreases as $T \to T_c$ resulting in droplets whose size increase rapidly on approaching the transition. If we define the correlation length ξ to be the size of the largest such droplet, as shown in Fig. 1.2, then this quantity will diverge as $T \to T_c$.

However, each droplet is itself a critical region and thus smaller droplets will form within the larger droplets, as shown in Fig. 1.2b. In fact, at the transition temperature, the system will actually contain droplets of all sizes from the microscopic up to droplets which are comparable to the size of the system itself.

1.4 Critical Exponents and Universality

As we have seen previously, a number of physical quantities are found to diverge at a critical point. These include the susceptibility χ_T, the inverse order parameter, 1/M, and the correlation length ξ. These quantities, and several others, are experimentally found to exhibit power law behaviour in the immediate vicinity of the transition temperature.

$$f(T) \sim t^{-x} \tag{1.1}$$

where f(T) represents some physical quantity, the reduced temperature $t = (T - T_c)/T_c$, and the exponent x is defined to be a *critical exponent.*

In fact, the true behaviour of the measured quantity on approaching T_c will be a corrected power law of the form:

$$f(T) = f_0 t^{-x}[1 + Bt^y + ...] \tag{1.2}$$

and thus we arrive at the final definition of a critical exponent, x (Stanley 1971):

$$x \equiv \lim_{t \to 0} \frac{logf}{logt} \tag{1.3}$$

The precise form of the correction term, or so called correction-to-scaling term, shown in Eq. 1.2 will be discussed in more detail in Chapters 4 and 5.

One of the earliest, and simplest, predictions of critical exponents was provided by Weiss molecular field theory (Plischke & Bergersen 1989) which is an example

of a mean field theory. We can understand such a theory by considering the Ising ferromagnet which has spins constrained to lie in one specific direction and favours parallel alignment of these spins. The Hamiltonian describing such a system, for the particular case of spin-1/2, has the following form:

$$H = -J \sum_{<ij>} S_i S_j - h \sum_i S_i \tag{1.4}$$

where the spin at site i, S_i, can have the values $\pm\hbar/2$, the coupling constant J represents the strength of the interactions between neighbouring spins and the sum is over near-neighbour pairs $< ij >$. The second term in equation 1.4 represents an applied magnetic field and h is some measure of this field in units of energy. The order parameter for such a system, as mentioned before, is the magnetization, M, which is defined as the average value of any spin, i.e. M$\equiv <S_i>$.

Let us now consider the effect of such a Hamiltonian on some central spin, S_0 (see Plischke & Bergersen (1989)):

$$\begin{aligned} H(S_0) &= -S_0(J \sum_j S_j + h) \\ &= -S_0(qJM + h) - JS_0 \sum_j (S_j - M) \end{aligned} \tag{1.5}$$

where the sum is over near neighbours j and the number of near neighbours is q. The second expression results from recognizing that $qM = \sum_j M$. In this expression, the first term in Eq. 1.5 represents the central spin under the action of a *mean field* defined by the neighbouring spins and the applied field, while the second term represents fluctuations in the order parameter. For simplicity, we will neglect the second term and this simplification, the neglect of fluctuations, is the defining characteristic of mean field theory.

This model can then be used to calculate thermodynamic quantities such as

the magnetization, $M =< S_0 >$, which can be shown to be,

$$M = tanh\left[\frac{qJM + h}{k_B T}\right], \tag{1.6}$$

where M≡1 at T=0. For the specific case of zero field, this equation can be shown to describe a critical phase transition (Plischke & Bergersen 1989), consistent with the phase diagram shown in Fig. 1.1a, with a transition temperature $T_c = qJ/k_B$. If we expand Eq. 1.6 in the immediate vicinity of the transition temperature, the magnetization can be shown to have the following form (Plischke & Bergersen 1989):

$$\begin{aligned} M &= \pm 3^{\frac{1}{2}} \left(\frac{T}{T_c}\right)\left(1 - \frac{T}{T_c}\right)^{\frac{1}{2}} \\ &\sim t^{\frac{1}{2}} \end{aligned} \tag{1.7}$$

where the reduced temperature $t = 1 - T/T_c$. If we then define the critical exponent β such that

$$M \sim t^{\beta} \tag{1.8}$$

then mean field theory clearly predicts β to have a value of 1/2.

A similar calculation can be performed for the susceptibility, $\chi \equiv (\partial M/\partial h)_T$ and the specific heat C_h. This shows similar power law behaviour for the susceptibility with $\chi \sim t^{-1}$ and if we therefore define the critical exponent, γ, such that $\chi \sim t^{-\gamma}$, we see that $\gamma = 1$ in mean field theory. The specific heat shows different values as one nears T_c from above and below (Plischke & Bergersen 1989) and thus exhibits a discontinuity within the mean field approximation. Another quantity which can be calculated is the correlation length, ξ, but such a calculation cannot be performed directly from the Weiss theory, but must be extracted from another mean-field model, Landau-Ginzberg theory (see, for instance, Landau & Lifshitz (1969) or Plischke & Bergersen (1989)). Such a model predicts a power law behaviour for the correlation

length, $\xi \sim t^{-1/2}$ and with the critical exponent ν defined such that $\xi \sim t^{-\nu}$, we arrive at the prediction that $\nu = 1/2$.

Thus we have a theory which predicts very specific values for the exponents β, γ, and ν, of 1/2, 1, and 1/2 respectively and a discontinuous specific heat. The van der Waals equation (van der Waals 1873) is the analogue of Weiss theory for a fluid system and predicts identical values for the critical exponents. However, early measurements of critical exponents (see Guggenheim (1945) for early results on fluid systems) found values closer to $\beta \sim 0.3$, $\nu \sim 0.6$ and $\gamma \sim 1.2$ and shows a similar power law behaviour for the specific heat with an associated critical exponent α whose value is close to zero. This suggests that while mean field theory adequately describes the qualitative behaviour near a critical point, it fails drastically to reproduce quantitative results. Such a failure is a consequence of the major simplification in mean field theory, the neglect of fluctuations, which are essential to the behaviour near a critical point, as was discussed earlier with the droplet model.

However, the values of critical exponents are, in fact, not different for every given system under investigation, but, rather, are found to fall into a series of groups or so-called *universality classes*. The principle of universality, originally proposed by Kadanoff (Kadanoff 1966), states that the behaviour of a system in the vicinity of a critical phase transition depends only on a few general properties of the system, namely:

1. The dimensionality of the system
2. The symmetry of the order parameter
3. Whether the interactions in the system are short or long ranged.

Consequently, seemingly unrelated systems can behave in a completely analogous manner near the critical point, regardless of often striking differences in the micro-

scopics of the respective systems.

The principle of universality can be understood from the droplet picture of critical fluctuations discussed previously. As mentioned before, the length scale associated with the fluctuations diverges at the transition temperature and, hence, eventually reaches a size where it dominates over any other length scale in the system. Thus, the system achieves a state where the detailed microscopics become irrelevant and the behaviour is defined solely by the critical fluctuations which depend only on the three criteria mentioned above. If there exists a length scale in the system which is extremely large, one may never be able to attain a temperature in sufficient proximity to the transition temperature to observe the behaviour dominated by the fluctuations. Such systems, where we can neglect the fluctuations are examples of mean field systems, as discussed previously, and include systems such as conventional superconductors, where the coherence length is extremely large as well as ferroelectric materials.

Universality allows one to see the power in the use of magnetic systems in studying critical phenomena. As the system behaves in a universal manner, we can examine this behaviour by studying the simplest possible model found to display the characteristics of a particular class. The short range nature of the interactions present in magnetic systems and the ability to place the constituent moments on a regular lattice produces some of the simplest model systems which can be treated theoretically.

Prior to discussing the exponents expected for various universality classes, it is important to consider one-dimensional systems which take on added significance in light of the spin-Peierls phase transition which will be discussed in more detail in Chapter 3. For these 1D systems, there can be no phase transition at finite temperatures (see, for example, (Plischke & Bergersen 1989)). To see this, let us consider

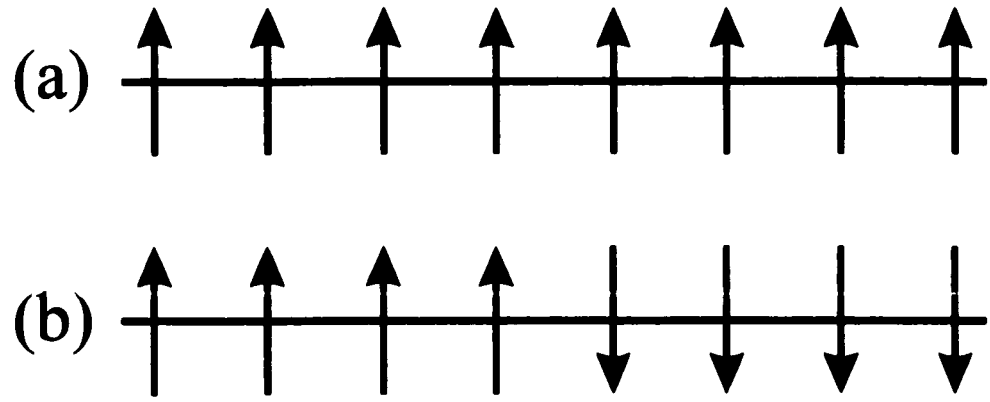

Figure 1.3: (a) The ground state of the Ising ferromagnet (b) The lowest energy excitation, a simple domain wall, which can be applied to such a state.

the 1D, spin-1/2, Ising ferromagnet described by the Hamiltonian, Eq. 1.4, with h=0. The ground state for such a system is the state with all spins pointing in one direction, chosen arbitrarily to be up, as shown in Fig. 1.3a. The lowest energy excitation in such a system is a simple domain wall as shown in Fig 1.3b. To examine the stability of such an excitation, we must consider the free energy, $G = E - TS$, where E is the internal energy and S is the entropy. The change in energy ΔE for the domain wall will be $\Delta E = 2J(\hbar/2)^2$ and the wall can be placed in N equivalent positions, where N is the number of sites on the chain, producing a change in entropy $\Delta S = k_B ln N$. Consequently the change in free energy, G, under the action of the domain wall is,

$$\Delta G = 2J\left(\frac{\hbar}{2}\right)^2 - k_B T ln N \tag{1.9}$$

As the size of the system $N \rightarrow \infty$, the change in free energy will always be less than zero for any finite temperature. Consequently, the state with a domain wall will always be stable at any finite temperature and therefore, there can be no phase transition to a long-range ordered state at a non-zero temperature in a 1D Ising system. This same argument can be extended, with added complication, to more complex 1D systems with the conclusion there can be no phase transition in a purely 1D system with short range interactions at finite temperatures.

Model	β	γ	ν	α	δ	η
Mean Field	0.5	1.0	0.5	-	3	0
1D Models	-	-	-	-	-	-
2D Models						
Ising	0.125	1.75	1	0	15	0.25
XY	-	-	-	-	15	0.25
Heisenberg	-	-	-	-	-	-
3D Models						
Ising	0.326	1.2378	0.6312	0.106	4.78	0.039
XY	0.345	1.316	0.669	-0.01	4.81	0.03
Heisenberg	0.367	1.388	0.707	-0.121	4.78	0.037

Table 1.1: Theoretical expectations for various critical exponents for conventional universality classes. (Collins 1989)

As discussed above, the universality class will be defined by the dimensionality of the system and the symmetry of the order parameter. The order parameter symmetry, as discussed before is typically either Ising, XY, or Heisenberg corresponding to 1,2, and 3 degrees of freedom respectively. The theoretical expectations for the critical exponents β, γ, ν, and α are shown in Table 1.1 (Collins 1989) for the various universality classes in addition to the exponents δ and η. The exponent δ describes the critical isotherm and is defined such that $m \sim h^{1/\delta}$ and the exponent η defines the correlation function such that $G(r) \sim r^{2-d-\eta}$ where d is the dimensionality of the system.

There are several important points which can be extracted upon observation

of this table. First, as mentioned above, 1D systems have no phase transitions at finite temperature and thus, no critical exponents are defined. Examination of 2D systems shows well defined exponents for the 2D Ising model as this model has been solved exactly by Onsager in 1944 representing the first major advancement beyond mean field theory. The 2D Heisenberg model has no phase transition (Mermin & Wagner 1966) and the 2D XY model is unconventional, exhibiting so-called Kosterlitz-Thouless behaviour (Kosterlitz & Thouless 1973, Kosterlitz 1974), and most exponents cannot be defined. The early experimental values ($\beta \sim 0.3$, $\gamma \sim 1.2$ and $\nu \sim 0.6$) can be seen to be consistent with 3D behaviour, an expected result, as the majority of physical systems are three dimensional. The glaring differences between mean field and 3D behaviour can easily be seen in this table.

By far the most powerful technique in the extraction of such critical exponents is scattering, both neutron and x-ray, and this technique, with emphasis on x-ray scattering, and its use in the study of critical phenomena will be discussed in detail in the next chapter.

Chapter 2

X-Ray Scattering

2.1 Generation of X-rays

X-rays were first discovered by Roentgen in 1895 (Roentgen 1895) and were so-named due to their, at that time, unknown nature. These mysterious rays were later shown to be short wavelength electromagnetic radiation. X-ray wavelengths vary from 10^{-13} m to 10^{-8} m placing them between , and not clearly separated from, the ultraviolet and gamma ray region of the electromagnetic spectrum.

Remarkably, despite over 100 years of innovation, the generation of x-rays for use in small laboratories and many medical applications has changed very little since the discovery by Roentgen (the one major exception to this is the recent development of large-scale synchrotron radiation facilities which produce very intense x-ray beams for research applications). The basic constituents of an x-ray generator are a source of high energy particles, typically electrons from a tungsten filament, a large potential difference across which these particles can be accelerated, and a target, or anode, which is typically composed of either copper or molybdenum.

The electrons strike the target first generating a continuous spectrum of radi-

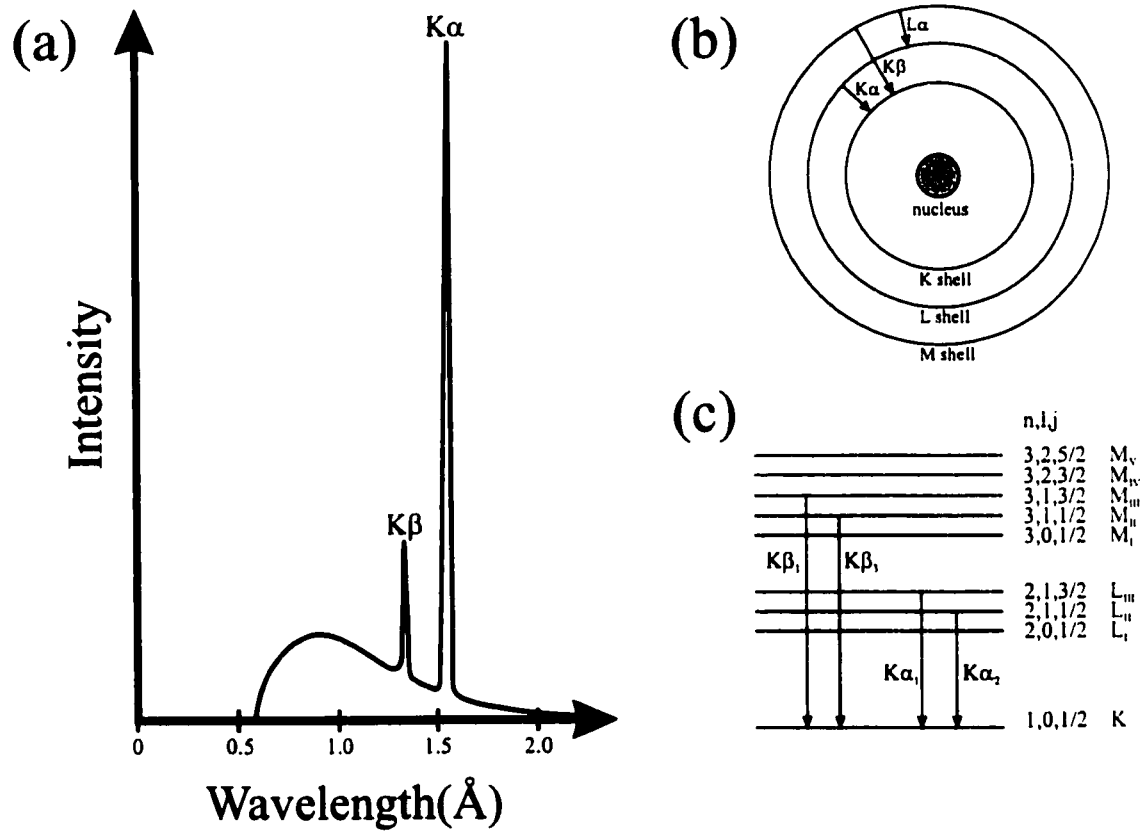

Figure 2.1: (a) Spectrum of emitted radiation from an x-ray generator with a copper target. (Cullity 1967) (b) Atomic shell model describing characteristic lines. (Cullity 1967) (c) Level diagram showing the relevant quantum numbers and the characteristic lines. (Landau & Lifshitz 1969)

ation resulting from the rapid deceleration of these charged particles upon impact, as can be seen in Fig 2.1a. From electromagnetic theory (Jackson 1975), an accelerated charged particle will emit radiation. However, not all electrons are decelerated in an identical manner with some losing all of their energy at once and others undergoing several collisions with the target atoms before coming to rest. Such variation in mechanisms of energy loss is responsible for the continuous nature of the spectrum of radiation. The most energy that can go into the production of x-rays is the energy eV passed to the electron by the accelerating voltage, V, where e is the electronic charge. Consequently, we can define a lower cutoff wavelength, $\lambda_{cuttoff}$, such that,

$$eV = h\nu_{max} = \frac{hc}{\lambda_{cutoff}}. \tag{2.1}$$

Consequently, the minimum wavelength of radiation which can be emitted is

$$\lambda_{cutoff} = \frac{hc}{eV} \tag{2.2}$$

and thus decreases as the accelerating voltage increases. Such a continuous spectrum of radiation is known as *Bremmsstrahlung* or braking radiation.

In addition to this continuous spectrum of radiation, once the voltage exceeds a specific value, which differs according to the target material used, intense, sharp peaks appear in the spectrum of radiation, as shown in Fig. 2.1a. The nature of these lines can be understood by considering the atoms in the target material. We will use a *shell model* (Cullity 1967) for the electronic structure of the atoms, as shown in Fig. 2.1b where the electrons form a series of shells around the nuclear core which are labelled as K,L,M,... with increasing distance from the nucleus (these letters K,L,M,... actually refer to principal quantum numbers n=1,2,3,...). When a bombarding electron of sufficient energy strikes a target atom, it may knock one of the electrons out of a low lying shell into a higher energy state. One of the higher energy electrons will then de-excite to fill in the gap left from this excited

electron and electronic transition is accompanied by the emission of a photon with an energy corresponding to the energy difference between levels. This explains the monoenergetic nature of the characteristic radiation, a property which is essential for the use of x-rays in diffraction studies as most measurements require a nearly monochromatic beam.

These characteristic lines are labelled according to the lower level involved in the transition process. For most x-ray studies, the radiation used is usually K radiation involving transitions to the K shell as shown in Fig 2.1b. If the gap left from the excitation of a K shell electron is filled by an L shell electron, the associated radiation is referred to as Kα, while if it filled by an M shell electron, the characteristic radiation is referred to as Kβ. The gap in the K shell is more likely to be filled by an L shell electron and hence Kα radiation is more intense than Kβ. Almost all x-ray studies involve the use of K-radiation and the corresponding wavelengths for a copper target, as used in the measurements which follow, are (Cullity 1967):

$K\alpha_1$: 1.54051 Å

$K\alpha_2$: 1.54433 Å

$K\beta_1$: 1.39217 Å

From this list, one can see that the Kα line is actually a doublet. To understand this, consider the level diagram shown in Fig. 2.1c (Landau & Lifshitz 1969). The L shell can be seen to be composed of three levels, which are indexed by the quantum numbers n,l,j as can be seen in the figure. The combined effects of relativity and spin-orbit coupling act to spilt levels of different total angular momentum quantum number, j. Those levels of the same n and j but different orbital angular momentum l are split by a quantum electrodynamic effect known as the Lamb shift. The only transitions which are allowed are those between levels such that $\Delta l = \pm 1$ and $\Delta j = 0, \pm 1$. Consequently, the Kα line representing transitions between the L and K shells will now

be two separate lines, representing transitions from the states L_{II} (n=2,l=1,j=1/2) and L_{III} (n=2,l=1, j=3/2) to the K state (n=1,l=0,j=1/2), which are labelled $K\alpha_2$ and $K\alpha_1$ respectively. The $K\alpha_1$ line is exactly twice as intense as the $K\alpha_2$ line.

The generation of x-rays is a very inefficient process with less than 1% of the bombarding electron energy being converted into radiation (Cullity 1967). The remainder of this energy takes the form of heat and it is advancements in the methods of heat removal which have constituted the majority of the technological developments over the years. The first advancement, as one may expect, involved the use of cooling water to remove heat from the target. The next major advancement, which allowed access to much higher energy electron beams, and, thus, higher flux x-ray beams, was the development of a rotating anode x-ray generator. Such a generator utilizes a target which rotates at high speeds ($\sim$ 3000 r.p.m.) such that the electron beam continuously strikes different portions of the target minimizing the amount of heat which is transferred into any single part of the target. This is coupled with water cooling to allow access to electron energies which would otherwise melt the anode and results in very intense x-ray beams.

2.2 X-Ray Diffraction

The diffraction of x-rays from crystalline material was first discovered by Laue (Friedrich, Knipping & Laue 1912, Laue 1912) and the use of this technique in structural determination was developed shortly thereafter by W.H. Bragg and W.L. Bragg (Bragg 1913, Bragg & Bragg 1913, Bragg 1914). The primary interaction between the x-rays and matter is through the electrostatic interaction between the electric field component of the electromagnetic wave and the constituent electrons. The magnetic field does not play a role in the principle mechanism of x-ray diffraction

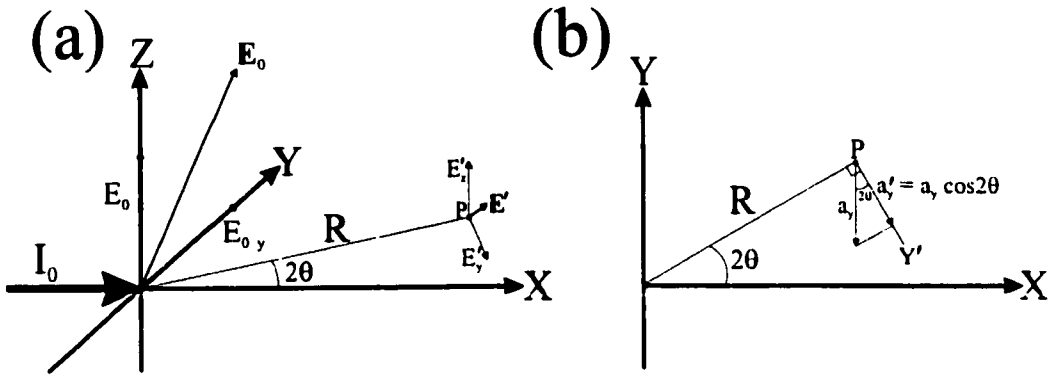

Figure 2.2: Scattering of an unpolarized incident beam by a single free electron at the origin. (b) shows the projection of (a) onto the X-Y plane. (Adapted from Warren (1990))

and hence will be ignored. In the following discussion, we will first consider the scattering of x-rays by a single free electron, combine these electrons to form an atom, and then combine atoms to form a single crystal. The form of the derivation closely follows that shown in Warren (1990).

2.2.1 Scattering by a Free Electron

We will first consider the interaction of a monochromatic beam of x-ray radiation with a single free electron. Although the process is quantum mechanical in nature, it is constructive to consider the process in classical terms as it arrives at the correct answer for elastically scattered x-rays with its primary failure being in the prediction of the inelastic, Compton scattered radiation. Classically, the process of x-ray scattering occurs due to an acceleration of the electrons under the action of the electric field present in the incident radiation. Such accelerated charges then re-radiate the incident radiation elastically (Jackson 1975).

First, let us consider a free electron located at the origin of Fig 2.2 and an incident beam propagating along the X-axis with intensity I_0. As such, the electric-field vector can take on all orientations in the Y-Z plane with equal probability, assum-

ing an unpolarized beam. We want to calculate the intensity of scattered radiation at point P chosen, for simplicity, to be in the X-Y plane. Initially, we will assume a specific direction for the electric field polarization and later average over all such orientations. The electric field in the incident beam will have components along Y and Z of:

$$\epsilon_{0Y} = E_{0Y}\ sin\ \omega t \qquad \epsilon_{0Z} = E_{0Z}\ sin\ \omega t \tag{2.3}$$

These components will exert a force on the electron producing accelerations,

$$a_Y = \frac{eE_{0Y}\ sin\ \omega t}{m} \qquad a_Z = \frac{eE_{0Z}\ sin\ \omega t}{m} \tag{2.4}$$

where e and m are the charge and mass of the electron, respectively.

From electromagnetic theory (Jackson 1975), the component of the acceleration normal to the vector, **R**, will determine the scattered electric field produced. Such normal directions are defined by the axes Y′ and Z and the components of the emitted electric field along these directions, as shown in Fig. 2.2, are,

$$\begin{aligned} \epsilon_{Y'} &= \frac{ea_{Y'}}{c^2R} = \frac{e^2E_{0Y}}{mc^2R}\ sin\ \omega t\ cos\ 2\theta \equiv E_{Y'}\ sin\ \omega t \\ \epsilon_Z &= \frac{ea_Z}{c^2R} = \frac{e^2E_{0Z}}{mc^2R}\ sin\ \omega t \equiv E_Z\ sin\ \omega t \end{aligned} \tag{2.5}$$

Considering the time-independent amplitudes of these electric fields,

$$E^2 = E_{Y'}^2 + E_Z^2 = \frac{e^4}{m^2c^4R^2}\left(E_{0Z}^2 + E_{0Y}^2 cos^2 2\theta\right) \tag{2.6}$$

If we then allow for an unpolarized beam, we can say $< E_{0Y} >=< E_{0Z} >= < E_0^2 > /2$ as the Y and Z directions are equivalent. Consequently,

$$< E^2 >=< E_0^2 > \frac{e^4}{m^2c^4R^2}\left(\frac{1 + cos^2 2\theta}{2}\right) \tag{2.7}$$

The measured quantity, the intensity, is the average energy per unit area per unit time and, in CGS units, is given by $I = c < E^2 > /8\pi$ and consequently,

$$I = I_0 \frac{e^4}{m^2c^4R^2}\left(\frac{1 + cos^2 2\theta}{2}\right). \tag{2.8}$$

This equation is the famous Thompson scattering equation for the scattering of electromagnetic radiation by a free electron. From this equation, one can understand why the predominant scattering in a solid is by the electrons and not the nucleus, which is also a charged entity. The intensity, Eq. 2.8 is inversely proportional to the square of the mass of the object which for a nucleus is considerably larger than that of an electron.

2.2.2 Scattering by an Atom

We now confine a set of such electrons to a small volume, typical of an atom. The question that jumps to mind is whether the scattering from a set of Z electrons confined to a small volume is simply Z times the scattering from a single electron. This may appear to be oversimplified, but it works exactly for the particular case of scattering in the forward direction ($2\theta = 0$) as the scattering from all the electrons are in phase and the amplitudes can be added directly. The finite size of the electron cloud introduces phase differences in the scattered waves from different electrons, provided the scattering angles are nonzero. This phase difference results in interference between the waves scattered from different electrons, resulting in a weaker intensity at finite scattering angles than that present in the forward direction. This interference is taken into account by a quantity known as the *atomic scattering factor*, f, which is the ratio of the amplitude of the electric field scattered by the atom to that of a single free electron. As such, it takes on a value of Z in the forward direction and falls away with increasing scattering angle.

This results in an intensity for the scattering of x-rays by an atom of,

$$I = I_0 \frac{e^4}{m^2 c^4 R^2} \left(\frac{1 + cos^2 2\theta}{2} \right) f^2. \tag{2.9}$$

The precise form for the atomic scattering factor, f, for a series of electrons in an atom is rather complex, but for the particular case of a spherically symmetric charge

distribution, it can be shown to have the following form,

$$f = \sum_n \int_0^\infty 4\pi r^2 \rho_n(r) \frac{sin\ Qr}{Qr} dr. \tag{2.10}$$

where the sum is over the n electrons composing the atom, $\rho_n(r)$ is the charge density, and the quantity Q is defined to be $4\pi sin\ \theta/\lambda$.

2.2.3 Scattering by a Small Single Crystal

Much in the same way as we combined electrons to form an atom, we will now combine atoms into a crystalline solid. We will consider the unit cell describing the crystal has primitive lattice vectors $\mathbf{a_1}$,$\mathbf{a_2}$, and $\mathbf{a_3}$. Thus, the position of any atom in the solid can be written in terms of a vector $\mathbf{R_n^m}$=$m_1\mathbf{a_1}$+$m_2\mathbf{a_2}$+ $m_3\mathbf{a_3}$+$\mathbf{r_n}$. Where the index m=(m_1,m_2,m_3) labels the specific unit cell in the crystal and the index n, defined by the vector $\mathbf{r_n}$ labels the different atoms within a unit cell. We will now consider the contribution to the scattering at point P from an atom described by $\mathbf{R_n^m}$, as shown in Fig. 2.3. The electric field generated by this atom will be given by:

$$\epsilon_P = \frac{E_0 e^2}{mc^2 R} f_n cos\left[\omega t - \frac{2\pi}{\lambda}(x_1 + x_2)\right] \tag{2.11}$$

This equation is simply the equation for a traveling wave with a path length $x_1 + x_2$ and an associated amplitude consistent with the expectation for scattering from an atom. The sum of all amplitudes from the atoms in the crystal will involve a sum over all such path lengths.

If we make the assumption of a plane scattered wave, which is reasonable provided the crystal is small in comparison to the distance R, then the distance $x_1 + x_2$ can be replaced by $x_1 + x_2'$. From Fig. 2.3, $2\pi(x_1 + x_2)/\lambda$ in Eq. 2.11 can then be replaced by $2\pi R/\lambda - (\mathbf{k'} - \mathbf{k}) \cdot \mathbf{R_n^m}$. For simplicity, we shall change notations to a complex exponential form which is valid provided one considers E^2=$\epsilon_P \epsilon_P^*$, where ϵ_P^*

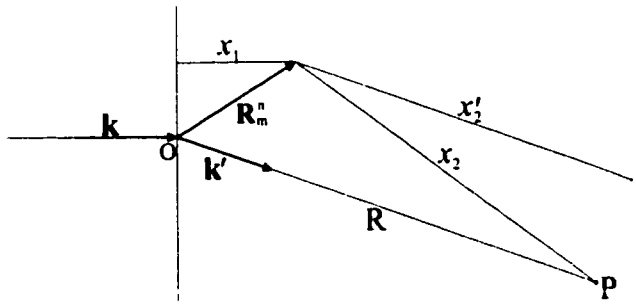

- **s** is unit vector along **k**
- **s'** is unit vector along **k'**
- $x_2' = \mathbf{R}\text{-}\mathbf{s}'\cdot\mathbf{R}_m^n$
- $x_1 = \mathbf{s}\cdot\mathbf{R}_m^n$
- $\frac{2\pi}{\lambda}(x_1+x_2') = \frac{2\pi}{\lambda}\mathbf{R}\text{-}(\mathbf{k}'\text{-}\mathbf{k})\cdot\mathbf{R}_m^n$

Figure 2.3: Diffraction by a small crystal. (Adapted from Warren (1990))

is the complex conjugate. This form gives,

$$\epsilon_P = \frac{E_0 e^2}{mc^2 R} f_n e^{i\left[\omega t - \frac{2\pi}{\lambda}R + (\mathbf{k}'-\mathbf{k})\cdot(m_1\mathbf{a}_1 + m_2\mathbf{a}_2 + m_3\mathbf{a}_3 + \mathbf{r}_n)\right]} \tag{2.12}$$

where we have substituted the above form for $\mathbf{R}_n^m$.

We now perform the sum over all atoms in the single crystal with the simplifying assumption that the edges of the crystal have lengths $N_1\mathbf{a}_1$, $N_2\mathbf{a}_2$, and $N_3\mathbf{a}_3$. We can then rewrite Eq. 2.12 in the following form:

$$\begin{aligned}\epsilon_P = &\frac{E_0 e^2}{mc^2 R} f_n e^{i\left[\omega t - \frac{2\pi}{\lambda}R\right]} \sum_n f_n e^{i(\mathbf{k}'-\mathbf{k})\cdot\mathbf{r}_n} \sum_{m_1=0}^{N_1-1} e^{i(\mathbf{k}'-\mathbf{k})\cdot m_1\mathbf{a}_1} \\ &\times \sum_{m_2=0}^{N_2-1} e^{i(\mathbf{k}'-\mathbf{k})\cdot m_2\mathbf{a}_2} \sum_{m_3=0}^{N_3-1} e^{i(\mathbf{k}'-\mathbf{k})\cdot m_3\mathbf{a}_3}\end{aligned} \tag{2.13}$$

One can see that the summation over the atoms within a unit cell is now separate from the remainder of the terms and, hence, we can define the *structure factor*, F to be,

$$F = \sum_n f_n e^{i(\mathbf{k}'-\mathbf{k})\cdot\mathbf{r}_n}. \tag{2.14}$$

This quantity describes the interference between waves scattered from various atoms within a unit cell and plays an essential role in structure determination as it is the only term in which the atomic positions appear.

Equation 2.13 above can then be simplified by noticing that the sums in m_1,m_2, and m_3 are geometric series whose solution can be written down exactly (Warren 1990). If we then calculate $E^2=\epsilon_P\epsilon_P^*$, the intensity can be written down following a similar method as with scattering for a single free electron. Performing this algebraic manipulation and assuming an unpolarized beam, we get the intensity of scattered x-rays from a small single crystal:

$$I_P = I_0 \frac{e^4}{m^2c^4R^2}\left(\frac{1+cos^2 2\theta}{2}\right) F^2 \frac{sin^2\frac{1}{2}(\mathbf{k'}-\mathbf{k})\cdot N_1\mathbf{a_1}}{sin^2\frac{1}{2}(\mathbf{k'}-\mathbf{k})\cdot \mathbf{a_1}} \times \frac{sin^2\frac{1}{2}(\mathbf{k'}-\mathbf{k})\cdot N_2\mathbf{a_2}}{sin^2\frac{1}{2}(\mathbf{k'}-\mathbf{k})\cdot \mathbf{a_2}} \frac{sin^2\frac{1}{2}(\mathbf{k'}-\mathbf{k})\cdot N_3\mathbf{a_3}}{sin^2\frac{1}{2}(\mathbf{k'}-\mathbf{k})\cdot \mathbf{a_3}} \tag{2.15}$$

Examination of Eq. 2.15 shows that it is composed of three terms of the form, sin^2Ny/sin^2y, where y=$\frac{1}{2}$(**k'**-**k**)·N_i**a**$_i$. As the value of N_i gets large, this function becomes strongly peaked at values of y which are integer multiples of π. In fact, for a real crystal where N_i will be extremely large, these functions will be zero everywhere except the points y=nπ, and hence the following three equations must be satisfied for the intensity to be finite:

$$\begin{aligned}(\mathbf{k'}-\mathbf{k})\cdot\mathbf{a_1} &= 2\pi h'\\ (\mathbf{k'}-\mathbf{k})\cdot\mathbf{a_2} &= 2\pi k'\\ (\mathbf{k'}-\mathbf{k})\cdot\mathbf{a_3} &= 2\pi l'\end{aligned} \tag{2.16}$$

where h',k',l' are integers. This set of three equations is known as the Laue conditions for x-ray diffraction. These can be rewritten in a more conventional form by first expanding the vector (**k'**-**k**) in the basis set defined by the primitive reciprocal lattice vectors,**b**$_1$, **b**$_2$, and **b**$_3$,

$$\mathbf{k'}-\mathbf{k} = h\mathbf{b_1} + k\mathbf{b_2} + l\mathbf{b_3}. \tag{2.17}$$

Substitution of Eq. 2.17 into the Laue equations, Eq. 2.16, and recognition of the defining characteristic of the primitive reciprocal lattice vectors, namely **a**$_i$· **b**$_j$=$2\pi\delta_{ij}$,

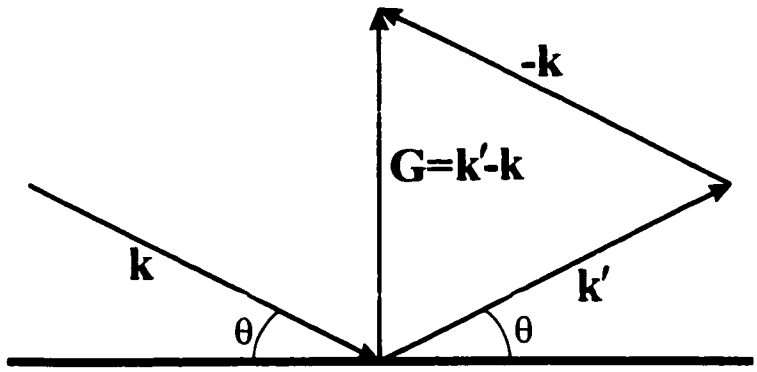

$$|\mathbf{k}|=|\mathbf{k}'|=\frac{2\pi}{\lambda}$$
$$|\mathbf{G}|=\frac{2\pi n}{d}$$
$$2k\sin\theta=\frac{2\pi n}{d}$$
$$2\left(\frac{2\pi}{\lambda}\right)\sin\theta=\frac{2\pi n}{d}$$
$$n\lambda=2d\sin\theta$$

Figure 2.4: Geometrical interpretation of the Laue equations. (Adapted from Ashcroft & Mermin (1976))

allows one to recognize that h=h', k=k', and l=l' and therefore, the indices h,k, and l in Eq. 2.17 must be integers. From this observation, Eq. 2.17 can be rewritten as,

$$\mathbf{k}' - \mathbf{k} = \mathbf{G} \tag{2.18}$$

where **G** defines the positions of reciprocal lattice points for our single crystal. This is the more familiar form for the Laue equations.

The geometrical implications of Eq. 2.18 are shown in Fig. 2.4. Considering elastic scattering where k'=k=$2\pi/\lambda$, and recognizing that the length of the reciprocal lattice vector, G, is equal to $\frac{2\pi n}{d}$ where d represents the real space separation between successive planes perpendicular to **G**, and n is an integer, we derive the expression,

$$n\lambda = 2d\ sin\theta \tag{2.19}$$

which is the famous *Bragg Law* for x-ray diffraction, the single most important equation in the use of scattering techniques.

It is worth noting that insertion of the Laue equation, Eq. 2.18, into the equation for the structure factor, Eq. 2.14, arrives at the more conventional form for the structure factor,

$$F = \sum_n f_n e^{i\mathbf{G}\cdot\mathbf{r}_n}. \tag{2.20}$$

Thus, from consideration of scattering from first a single free electron, then an atom composed of such electrons, and finally a single crystal composed of such atoms, we have arrived at the Bragg Law for x-ray diffraction. In the course of this derivation, we have introduced several important concepts in scattering such as the atomic form factor and the structure factor.

2.3 Critical Scattering

As mentioned previously, scattering techniques provide the single most valuable tool in the study of critical phenomena. To see this, let us consider the fluid system, described in Chapter 1, constrained to a volume V (Stanley 1971). Let us consider the position dependent density of particles,

$$n(\mathbf{r}) \equiv \sum_{i=1}^{N} \delta(\mathbf{r} - \mathbf{r}_i) \tag{2.21}$$

where $\mathbf{r}_i$ is the position of the i^{th} particle. We will define the average value of $n(\mathbf{r})$ to be n. This quantity, as discussed in Chapter 1 represents an effective order parameter for our fluid system (actually the order parameter is a density difference). For all arguments which follow, one can simply neglect the actual meaning of $n(\mathbf{r})$ and consider it to be the relevant order parameter for the system in question.

We will now introduce a quantity, $G(\mathbf{r}, \mathbf{r}')$ defined as,

$$G(\mathbf{r}, \mathbf{r}') \equiv \langle [n(\mathbf{r}) - \langle n(\mathbf{r}) \rangle][n(\mathbf{r}') - \langle n(\mathbf{r}') \rangle] \rangle, \tag{2.22}$$

where we define $\langle X \rangle$ to be the statistical average of the quantity X. From this expression, one can see that $G(\mathbf{r})$ is a measure of the correlation between fluctuations in the order parameter. We shall call it the density-density correlation function and it can be rewritten as,

$$G(\mathbf{r} - \mathbf{r}') = \langle n(\mathbf{r}) n(\mathbf{r}') \rangle - n^2. \tag{2.23}$$

where $n = \langle n(\mathbf{r}) \rangle$.

We will now consider the relevant response function for our fluid system, the isothermal compressibility, κ_T, which was shown in Chapter 1 to diverge at the transition temperature. One can show that κ_T is related to the fluctuations in the density and also to the density-density correlation function as,

$$\begin{aligned} \kappa_T &\propto \langle N - \langle N \rangle^2 \rangle \\ &\propto \frac{1}{n} \int d\mathbf{r}\, G(\mathbf{r}) \end{aligned} \tag{2.24}$$

We can see from Eq. 2.24 that a divergence in the response function corresponds to a divergence in the fluctuations in the order parameter and also the length scale associated with such fluctuations, represented by the range of the correlation function, $G(\mathbf{r} - \mathbf{r}')$. The above equation is a specific example of the fluctuation-dissipation theorem which relates measured response functions to the fluctuations in the relevant order parameter for the system. A similar result can be obtained for the isothermal susceptibility in terms of fluctuations in the magnetization.

We will now consider the scattering of electromagnetic radiation from such a system near the critical point. We will make the assumption that the scattering is quasielastic and that the energy of the incident radiation is much larger than typical excitation energies in the system. Such an approximation is known as the *static approximation* and is a very reasonable assumption for x-ray scattering where the energy of the incident radiation is on the order of keV, whereas typical excitations are on the order of meV (the assumption is much less easily made with neutron scattering where thermal neutrons have typical energies of about 10 meV). Within this assumption, we add the scattering from each particle in the system with the appropriate phase factor, and the intensity of scattered radiation can be shown to be

(Stanley 1971),

$$I(\mathbf{q}) \sim \frac{1}{N} \int d\mathbf{r} \int d\mathbf{r}' \; e^{-i\mathbf{q}\cdot(\mathbf{r}-\mathbf{r}')} \langle n(\mathbf{r}) n(\mathbf{r}') \rangle \tag{2.25}$$

$$\sim \frac{1}{N} \int d\mathbf{r} \int d\mathbf{r}' \; e^{-i\mathbf{q}\cdot(\mathbf{r}-\mathbf{r}')} \left[G(\mathbf{r}-\mathbf{r}') + n^2 \right], \tag{2.26}$$

where Eq. 2.26 comes from Eq. 2.25 and the definition of $G(\mathbf{r}-\mathbf{r}')$, Eq. 2.23. Eq. 2.26 can be rewritten as,

$$I(\mathbf{q}) \sim \frac{V}{N} \int d\mathbf{r} \; e^{-i\mathbf{q}\cdot\mathbf{r}} G(\mathbf{r}) + \frac{V^2}{N} n^2 \delta(\mathbf{q}). \tag{2.27}$$

This equation has two components, the first representing the fluctuations in the order parameter, as included through the density-density correlation function, and the second representing scattering which only exists at $\mathbf{q}$=0. This second component is a delta-function in $\mathbf{q}$, representing infinite range spatial correlations between particles, and is consequently an ordinary Bragg reflection. The amplitude of this component is a measure of the square of the order parameter, n^2. The first component has an associated length scale which will be the size of the fluctuating regions, or the correlation length, ξ. This quantity will be finite at all temperatures except the transition temperature T_c, and, hence, the scattering is not an infinite range Bragg reflection. This above expression applies to our fluid system, but can also be taken to apply to a structural phase transition, as is the case for the spin-Peierls transition, provided one bears in mind that $\mathbf{q}$ above will now be measured relative to some ordering wavevector, as opposed to $\mathbf{q}$=0. One typically writes Eq. 2.27 in terms of the Fourier transform of the density-density correlation function, which we will call the *scattering function*, $S(\mathbf{q})$,

$$S(\mathbf{q}) = \int d\mathbf{r} \; e^{-i\mathbf{q}\cdot\mathbf{r}} G(\mathbf{r}). \tag{2.28}$$

The first attempt to quantitatively model the correlation function, $G(\mathbf{r})$, was

performed by Ornstein and Zernike in 1914 (Ornstein & Zernicke 1914). The Ornstein-Zernike form results in a correlation function described by,

$$G(r) \sim \frac{e^{-\frac{r}{\xi}}}{r} \tag{2.29}$$

where ξ is the correlation length describing the size of the fluctuations. By taking the Fourier transform of $G(r)$, we obtain the scattering function,

$$S(q) \sim \frac{\kappa_T}{1 + q^2\xi^2} \tag{2.30}$$

where the amplitude of this Lorentzian form, κ_T, is the relevant response function, the isothermal compressibility in this case. This result is more commonly written in the form obtained for magnetic systems,

$$S(q) \sim \frac{\chi_T}{1 + q^2\xi^2} \tag{2.31}$$

where the response function for the magnetic system is the the isothermal, magnetic susceptibility.

Insertion of this form into the obtained expression for the intensity of scattered radiation results in,

$$I(\mathbf{q}) \sim \frac{V}{N}\left(\frac{\kappa_T}{1 + \xi^2 q^2}\right) + \frac{V^2}{N} n^2 \delta(\mathbf{q}). \tag{2.32}$$

This equation shows the power of using scattering techniques in the study of critical properties. As mentioned above, we get two component scattering, the first of which has an amplitude which gives a measure of the isothermal compressibility (or whatever the relevant response function is) and a width which measures the inverse correlation length. The second component of the scattering is a resolution limited Bragg component whose amplitude is a measure of the square of the order parameter. Thus, by measuring the q-dependent scattering as a function of temperature near the critical transition temperature, one can measure the temperature dependence of the

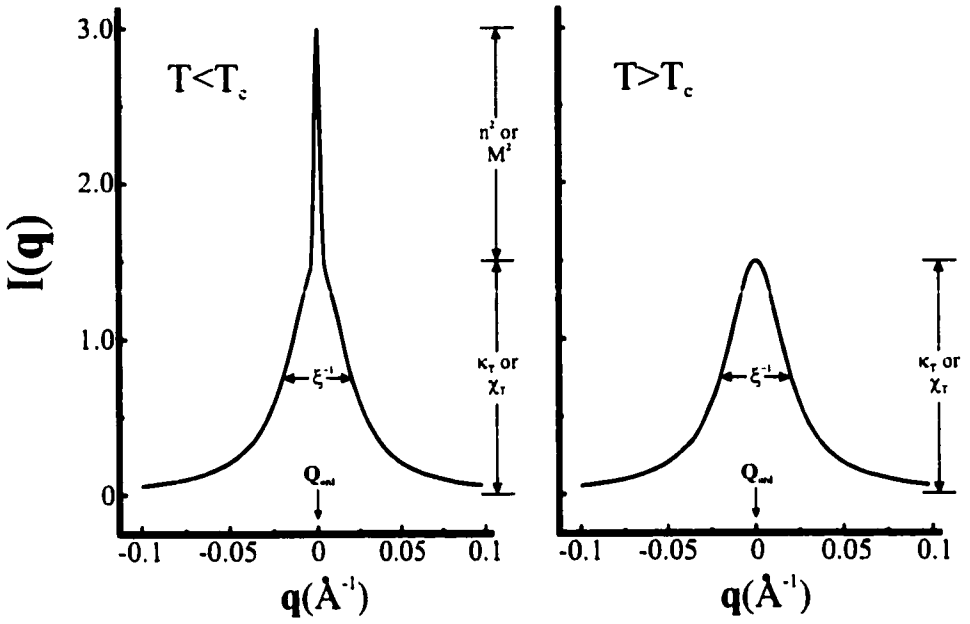

Figure 2.5: Expected intensity as a function of wavevector, **q** relative to some ordering wavevector for temperatures above and below T_c. The magnitude of the response function (κ_T or χ_T), the correlation length (ξ), and the order parameter squared (n^2 or M^2) are indicated on the plot.

response function, in this case κ_T, the correlation length, and the order parameter and thus can extract the associated critical exponents γ, ν, and β, respectively. This scattering is shown pictorially in Fig. 2.5 for temperatures both above and below the transition temperature, the difference being the nonzero order parameter above the transition temperature.

Subsequent theoretical developments have resulted in corrections to the Ornstein-Zernike correlation function of the following form (Fisher 1964, Fisher & Burford 1967),

$$G(r) \sim \xi^{(3-d)/(2-\eta)} r^{(1-d)/2} e^{-\frac{r}{\xi}} \tag{2.33}$$

where d is the dimensionality of the system. The above equation defines the critical exponent η whose value is shown in Table 1.1 for the various universality classes. We can see from this table that for 3D systems, $\eta \sim 0$ and consequently, to a very good

approximation, the correlation function shown in Eq. 2.33, can be represented by the original form of Ornstein and Zernike, Eq. 2.29.

2.4 Experimental

To allow for measurements of the critical behaviour of the divergent quantities mentioned above, we need to be able to carefully perform measurements in the 4-dimensional space defined by the 3 crystal axes and the energy transfer. The ideal instrument for such measurements is the *triple-axis-spectrometer*, originally developed by Brockhouse. Such an instrument, as applied to x-ray scattering studies, is shown schematically in Fig. 2.6. The three axes are from monochromator to sample, sample to analyzer, and from analyzer to detector. The analyzer crystal serves an important purpose in neutron scattering studies as it allows measurements to be made with different incident and scattered energies allowing for measurements of excitations in the sample under investigation. The same could be true of x-rays, but the high energy of typical x-ray beams, on the order of keV, means that typical excitations, which have energies on the order of meV, cannot be resolved using such an instrument. Consequently, for typical purposes in x-ray scattering measurements, the analyzer crystal serves only to improve background and for most of the reported measurements, it is actually removed, the instrument being used in a double-axis configuration instead. The double-axis configuration is ideal for x-ray measurements of critical phenomena as the detector integrates over all energy transfers rather efficiently and the static approximation is almost always valid. (in terms of cross-sections, $\mathbf{I(q)}$ discussed before is proportional to the differential cross-section $d\sigma/d\Omega$ which is the energy integral of the partial differential cross-section $d^2\sigma/d\Omega dE'$, and thus to get the correct results, the energy integration must be completely performed.)

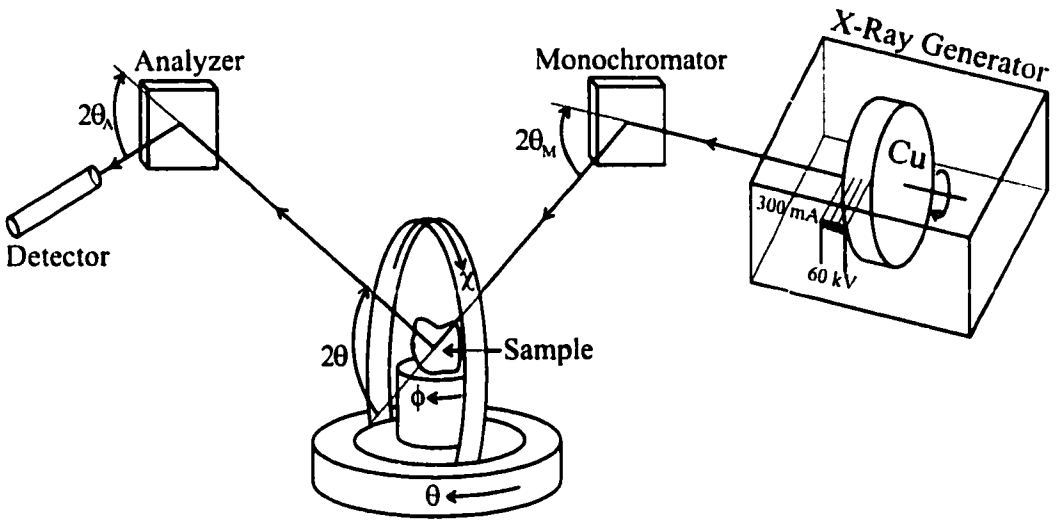

Figure 2.6: Schematic of the x-ray diffractometer used in these measurements.

Figure 2.6 shows a schematic of the instrument used in the measurements reported. X-rays are generated from an 18 kW rotating anode x-ray generator with a Cu-target resulting in a spectrum similar to that shown in Fig. 2.1. To improve the monochromaticity of the beam, the x-rays are Bragg scattered from a single crystal which for our instrument is either perfect single crystal Ge (1,1,1) or pyrolitic graphite, PG, (0,0,2). This reflection allows only Cu Kα radiation to pass through to the sample. In fact, for the Ge monochromator crystal, one can achieve separation of Kα_1 and Kα_2 allowing only Kα_1 radiation to be used. The radiation then strikes the sample whose orientation is defined by a series of three angles, θ, ϕ, and χ. Such an arrangement of angles is known as a Eulerian cradle and the particular cradle employed in these measurements allows a cryogenic unit, a closed-cycle He refrigerator, to be mounted. This allows careful control of the sample temperature from about 8 K to a maximum temperature of about 300 K. The x-rays are scattered from the sample and are measured in a single direction, defined by the scattering angle, 2θ. The x-rays are detected by a single NaI scintillation counter.

Between the monochromator and the sample, and between the sample and the detector, there are two sets of two tantalum coated slits. These slits define the collimation of the beam which plays an important role in the instrumental resolution. The resolution is also affected by the quality of the monochromator (and analyzer if it is employed) and the mosaic spread of the sample being examined. The extraction of the correlation length and the response function, as described in the preceding section, is complicated by the resolution of the instrument. In fact, the quantity which one measures is not $S(\mathbf{q})$ but rather a convolution of this quantity with the instrumental resolution function, $R(\mathbf{q})$.

$$I(\mathbf{q}) = \int R(\mathbf{q}')S(\mathbf{q} - \mathbf{q}')d\mathbf{q}' \tag{2.34}$$

As the quantity we want to extract is $S(\mathbf{q} - \mathbf{q}')$, one typically assumes a form for this function, often the Lorentzian form of Ornstein and Zernike, and convolutes this assumed scattering with the instrumental resolution which can be measured by measuring a resolution limited, Bragg reflection. This convolution process will be described in more detail in Chapter 6 and in Appendix A.

Chapter 3

Spin Peierls Transition

3.1 Introduction

As we have introduced critical phenomena and the use of scattering in their study, we will now go on to discuss the particular critical phase transition under investigation in these measurements, the spin Peierls (SP) transition (Bray, Interrante, Jacobs & Bonner 1983). The SP transition occurs in antiferromagnetically coupled quantum (low S) spin chains with short-range (nearest neighbour) interactions and continuous symmetry (either Heisenberg or XY). Typically the transition is described for S=1/2 Heisenberg spin chains, as these are the only examples found experimentally, and the remainder of the discussion will focus on this model.

To discuss the salient features of the SP transition, let us consider the excitation spectrum ($\epsilon(q) = E(q) - E_{GS}$, where E_{GS} is the ground state energy) shown in Fig. 3.1a for the particular case of uniform chains with the same antiferromagnetic (AF) coupling constant between all spins. The important feature of this spectrum is the lack of a gap between the singlet ground state and the triplet excited states causing the excitations at q=0,$\pm\pi/a$ to be infinitesimally close to the ground state

energy. Consequently, at T=0, zero point quantum fluctuations will cause some population of the excited states. However, if we now consider a dimerized spin chain, where neighbouring atoms are displaced in opposite directions from their equilibrium location, we obtain a doubled unit cell and alternating coupling constants, J_1 and J_2, as the exchange interaction depends on the physical separation between the spins. The excitation spectrum for such a dimerized chain is shown in Fig. 3.1b and can be seen to exhibit a gap separating a singlet ground state from a triplet of excited states. The presence of such a gap will prevent occupation of the excited states at T=0 as quantum fluctuations can not overcome the energy gap. This results in a system with a lower magnetic energy than in the uniform case and represents an inherent instability in the S=1/2 Heisenberg AF spin chain. For such a transition to occur in a physical system, the lowering of magnetic energy due to the gapped excitation spectrum must outweigh the increase in lattice energy which is required to dimerize the chains.

The above explanation describes the stability of the dimerized state at T=0, however, to allow measurements on physical systems, we require a finite transition temperature. As mentioned in Chapter 1, there can be no phase transition in a purely one-dimensional system and so there must be some higher dimensionality within the Hamiltonian, describing the energetics, to produce a finite transition temperature. Physical realizations of one-dimensional systems occur when geometrical considerations and exchange paths lead to interactions which are highly anisotropic, with much stronger interactions along one crystalline direction. Consequently, physical one-dimensional systems are only quasi-one-dimensional possessing weak interactions between chains. This interchain coupling will drive the quasi-1D system to a 3D long-range ordered AF (Néel) state at a transition temperature which is roughly the ratio of the interchain to intrachain coupling constants. Such a Néel state would

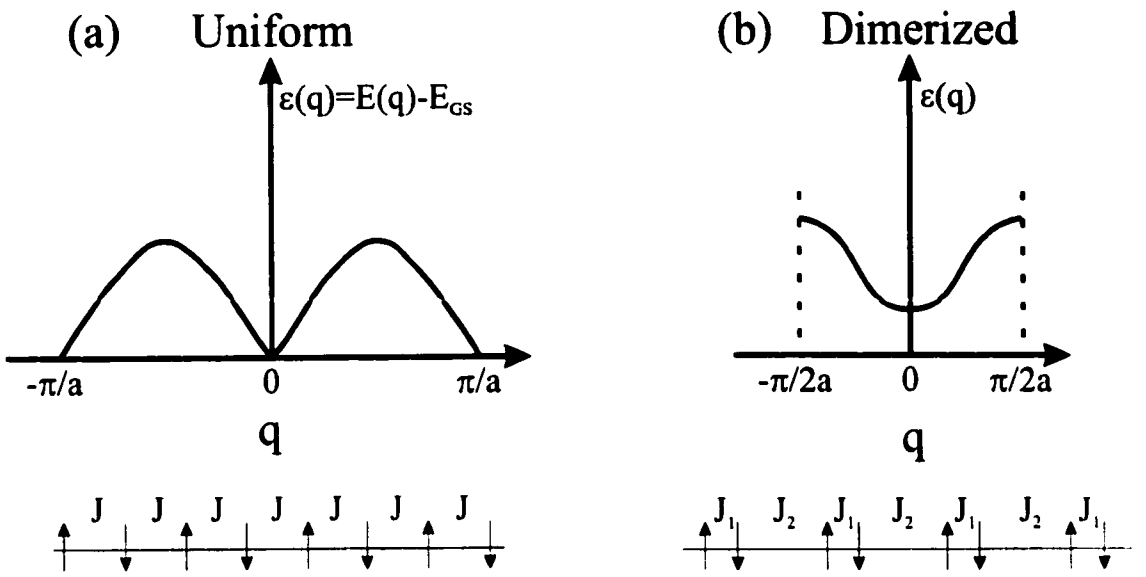

Figure 3.1: Excitation spectrum of (a) a uniform S=1/2 Heisenberg spin chain and (b) the same chain dimerized with alternating coupling constants. Below the spectra are cartoons of the interactions in the two systems. It is important to note that the ground state in both systems is a singlet state and not a Néel ordered state as appears to be indicated in these schematics. (Bray et al. 1983)

preclude the existence of a SP state, and so there must be some other 3D interaction which drives the SP transition. This interaction is called spin-phonon coupling (Bray et al. 1983) and occurs when the magnetism couples to the 3D phonons of the lattice, the phonons being the wavevector Fourier transform of the lattice vibrations. Such an interaction is present in all systems, as exchange interactions are dependent on atomic positions and, thus, dependent on 3D displacements of these atoms from their equilibrium positions. However, in most systems, these interactions are negligible in comparison with interchain coupling which is why there are very few SP systems occurring in nature.

It has been suggested (Bulaevskii, Buzdin & Khomskii 1978) that without some special property of the lattice, interchain coupling would always dominate, driving the system to a Néel state before the SP transition could occur. All

known SP systems have been shown to display an inherent lattice instability against a dimerization (Moncton, Birgeneau, Interrante & Wudl 1977, Tanaka, Satoh & Nagasaka 1990, Fujita, Ubukata, Arai, Tonegawa, Mino, Motokawa, Knight, Forsyth, Bennington, Akimitsu & Fujita 1996). Such an instability often manifests itself as a soft phonon mode, whose energy becomes small, thus lowering the associated lattice energy for the corresponding motion of the atoms. If the atomic motion associated with this soft phonon mode corresponds to the atoms in the chains beating against one another along the chain direction, then the lattice energy for a dimerization reduces substantially. As it is the competition between a lowering of magnetic energy and an increase in lattice energy which drives the SP transition, such a lattice instability makes the SP state more energetically favourable.

For physical systems, the SP transition occurs as the temperature is lowered below some transition temperature, T_{sp}. As the transition is a structural change induced by the energetics in the magnetic system, it is often referred to as *magnetoelastic* in nature. Experimentally,the dimerization is found to begin at the transition temperature and increase continuously as the temperature is lowered. Thus, the SP transition is a critical phase transition with an order parameter which is the degree of dimerization. (It is worth noting that there is a new SP compound, $\alpha' - NaV_2O_5$, which shows evidence of exhibiting a first-order SP transition (Köppen, Pankert, Hauptmann, Lang, Weiden, Geibel & Steglich 1998, Lumsden & Gaulin 1998)). The degree of dimerization can be measured as an inter- to intra-dimer density difference and is thus rather analogous to the fluid system described previously. It is the critical properties of the SP transition in several physical systems which constitutes the bulk of the work to be presented in this thesis.

As a point of note, the spin-Peierls transition was named due to an analogous transition occurring in one-dimensional conductors, the Peierls phase transition

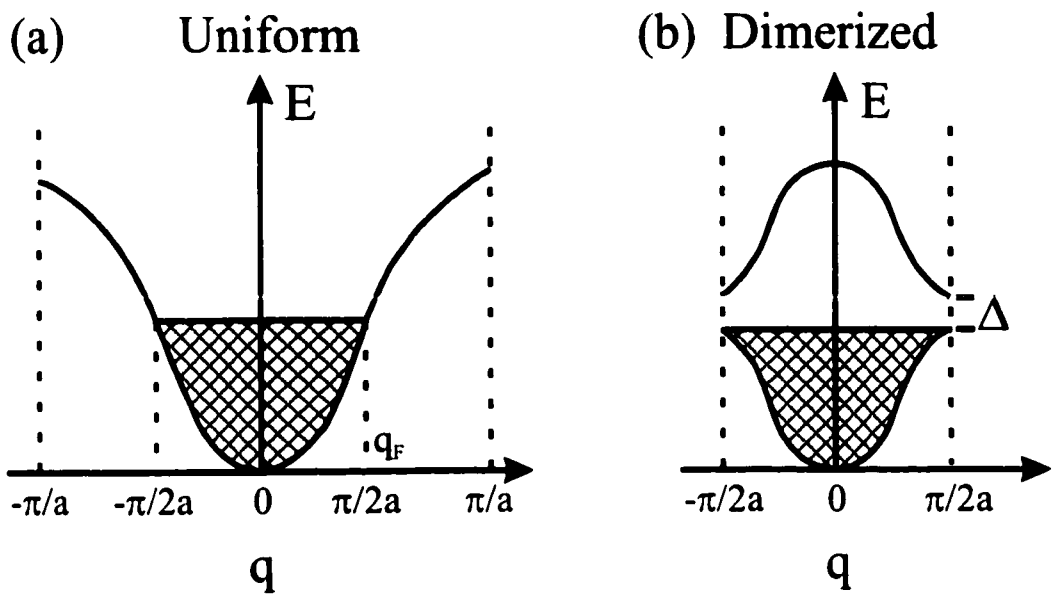

Figure 3.2: Electronic Peierls transition. (Bray et al. 1983)

(Peierls 1955). Peierls showed that a quasi-one-dimensional metal with a half filled conduction band, as shown in Fig. 3.2a, would be unstable against a dimerization of the chains. Such a dimerization doubles the chain periodicity changing the Brillouin zone boundary from $\pm\pi/a$ to $\pm\pi/2a$ and introducing a gap, Δ, in the band structure at the new zone boundary, as shown in Fig. 3.2b. This gap causes a lowering of the energy of the states at the Fermi level by $\Delta/2$. Consequently, there is a lowering of electronic energy and an inherent instability in the system. Such a transition converts a metal with a half-filled conduction band into an insulator with a filled conduction band. The correlations between this and the spin-Peierls transition are rather obvious and are responsible for the naming of the latter.

3.2 Experimental Characteristics

There are a number of physically measurable quantities which distinguish a phase transition as a SP transition. The first is a rapid and isotropic drop in the magnetic susceptibility ($\chi = M/H$) as the temperature is lowered through the SP transition, as shown in Fig 3.3a (Bray et al. 1983). Such a drop is due to the nonmagnetic (S=0) nature of the singlet ground state which becomes more strongly isolated from the excited states as the temperature drops below T_{sp}. The isotropic nature of the drop is due to the isotropic nature of the Heisenberg Hamiltonian and thus the curve shown in Fig. 3.3a could be representative of either measurements on a single crystal or a powder. This can be readily distinguished from the case of a set of quasi-1D spin chains which undergoes 3D Néel ordering. Here, χ drops to zero for, at most, one crystalline direction resulting in an anisotropy below the transition temperature. This is shown in Fig. 3.3b for both single crystals, with applied field both parallel and perpendicular to the ordering direction, and powder averages, represented by the dashed line. Fig. 3.3c shows the magnetic susceptibility for an alternating chain with a fixed, temperature independent, alternation ($\alpha = J_2/J_1 = 0.8$). It also exhibits an isotropic drop in the susceptibility, but this drop is much more gradual than for the SP transition as the alternation is always present and does not begin abruptly below some particular temperature.

The next physical characteristic of a SP system is the presence of a singlet-triplet gap in the magnetic excitation spectrum, as was shown in Fig 3.1b. Provided the density of magnetic moment is sufficient, such a gap can be measured directly with inelastic neutron scattering. The singlet-triplet nature of the gap can be determined by performing the inelastic neutron scattering measurements in the presence of a sufficiently large applied magnetic field. This field acts to split the triplet excited states through the Zeeman effect causing the single excitation to be separated into

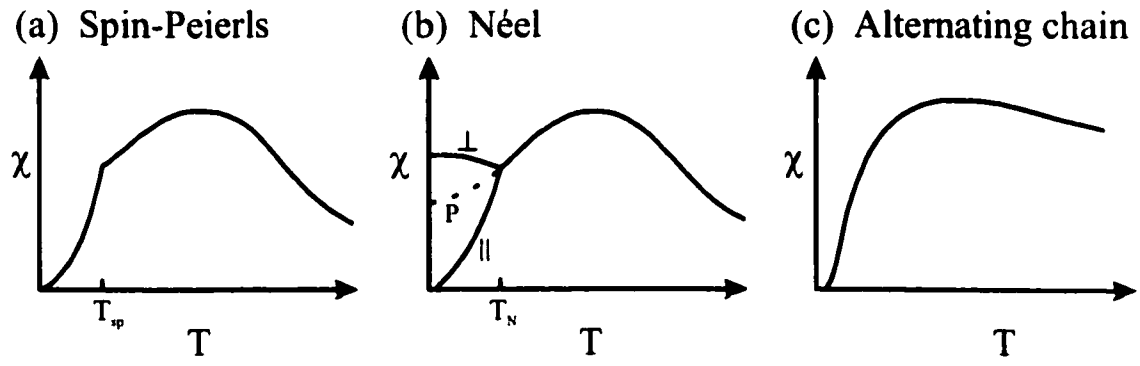

Figure 3.3: Magnetic susceptibility for (a) a spin-Peierls transition, (b) a long-range ordered antiferromagnetic (Néel) state, and (c) an alternating spin chain. (Bray et al. 1983)

three distinct excitations.

The third defining characteristic of a SP system is the presence of so-called *superlattice* Bragg reflections. These are peaks which appear below the transition temperature due to the new periodicity introduced by the dimerization. It is the magnitude of these peaks as a function of temperature which measures the square of the order parameter and the diffuse scattering around these positions which measures the critical fluctuations associated with the transition.

The final defining characteristic of a SP transition is the behaviour of the system in an applied magnetic field (Bray et al. 1983). Applying a magnetic field will have the effect of reducing the spin degrees of freedom by introducing anisotropies into the system analogous to the natural anisotropies that occur due to the action of crystal fields (such fields resulting from the local crystalline environment are responsible for lowering the spin degrees of freedom in a magnetic systems resulting in either XY or Ising symmetry). Lowering the spin degrees of freedom will reduce quantum fluctuations and it is this reduction which creates different effects in the Néel and SP states. Reducing fluctuations in a Néel state will actually increase the coherence between spins causing the transition temperature to initially increase until the Zeeman

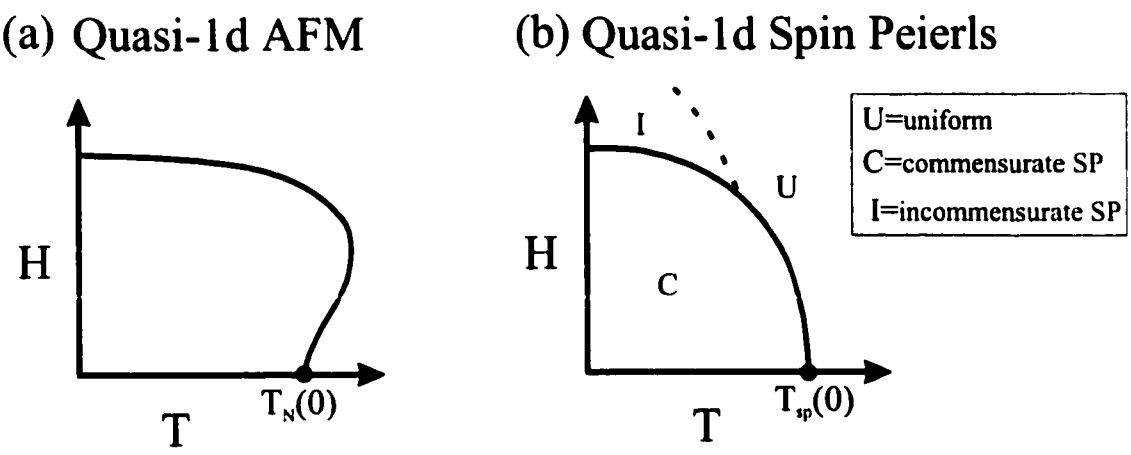

Figure 3.4: Behaviour in an applied magnetic field for (a) a long-range ordered antiferromagnetic system, and (b) a spin-Peierls system. (Bray et al. 1983)

interaction begins to destroy the ordered state lowering the transition temperature, as shown in Fig. 3.4a. For the SP system, the reduction in fluctuations actually reduces the energy available for the SP state, as it is the fluctuations which drives the system into such a state. Consequently, this couples with the Zeeman energy to destroy the SP state resulting in a continuous drop in T_{sp} with increasing field, as shown in Fig. 3.4b. Above some value of the field, the system enters into another state which has been characterized as a SP state with an ordering wavevector incommensurate with the underlying lattice (Bray et al. 1983).

3.3 Experimental Systems

3.3.1 MEM(TCNQ)$_2$

Theoretical work on the SP transition traces back to the early 1960's (McConnell & Lynden-Bell 1962), but the first true experimental realization did not occur until 1975 (Bray, Hart, Interrante, Jacobs, Kasper, Watkins, Wee & Bonner 1975) as the majority of quasi-one-dimensional systems undergo a transition to a 3D Néel ordered

state before the SP transition can take place. The first SP systems were composed of a combination of the organic donor tetrathiafulvalene (TTF) with a metal-organic acceptor, metal-bisdithiolene (mBDT) where the metal was either Cu or Au (Bray et al. 1975). Shortly thereafter, a second compound was found to exhibit the SP transition, methylethylmorpholinium-ditetracyanoquinodimethanide, or MEM(TCNQ)$_2$ for short (Huizinga, Kommandeur, Sawatzky, Thole, Kopinga, de Jonge & Roos 1979).

The structure of MEM(TCNQ)$_2$ (van Bodegom & Bosch 1981) consists of a series of planar TCNQ molecules which stack together forming one-dimensional chains. The structure is shown schematically in Fig. 3.5 (van Bodegom, Larson & Mook 1981). Above a temperature of about 335 K, the TCNQ molecules form uniform chains containing on average a charge of half an electron (i.e. $(TCNQ)_2^-$) and the system is a good electrical conductor (van Bodegom 1981). The system undergoes a phase transition at 335 K with a dimerization of the chains converting the metal into an insulator (van Bodegom 1981). Such a transition has been characterized as an electronic Peierls transition. Between 335 K and 18 K the system contains a single unpaired electron (S=1/2 magnetic moment) within each dimer (van Bodegom et al. 1981). From a magnetism point of view, this constitutes a set of uniform quasi-one dimensional S=1/2 spin chains. The one-dimensional nature is a result of the planar nature of the TCNQ molecules. Effectively, one can think of these molecules as pancake-like such that they stack close together in one direction and are well separated in the other two.

At a temperature of about 18 K, the system undergoes a second phase transition with a second dimerization of the chains (Visser, Oostra, Vettier & Voiron 1983). This transition exhibits all the characteristics of a SP phase transition. In Fig. 3.6a, we see the magnetic susceptibility as a function of temperature (Huizinga et al. 1979). The susceptibility is well described by a Bonner and Fisher theoretical prediction for

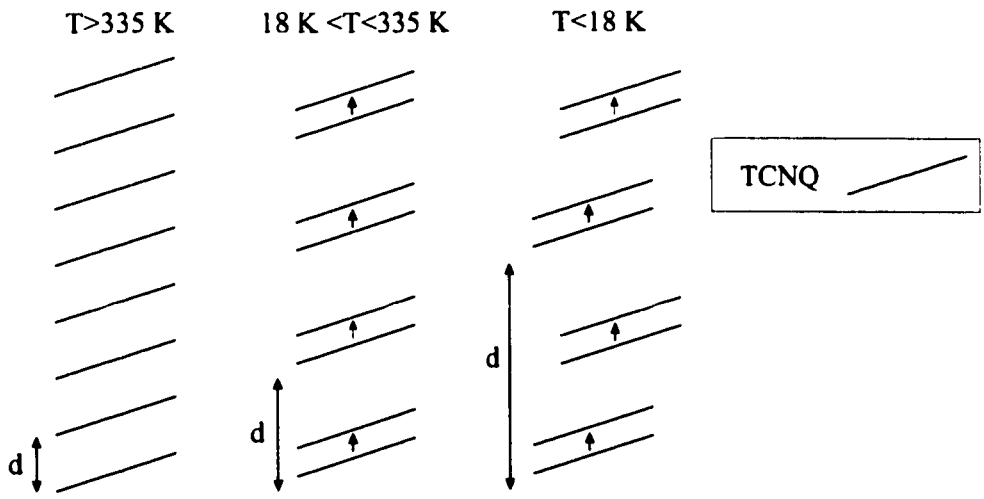

Figure 3.5: Schematic representation of the configuration of the planar TCNQ units of MEM(TCNQ)$_2$ for temperatures greater than 335 K, between 18K and 335 K, and below 18 K. (Adapted from (van Bodegom et al. 1981))

a one-dimensional S=1/2 Heisenberg spin chain (Bonner & Fisher 1964) from about 250 K down to about 18 K confirming the quasi-one-dimensional nature of the chains. Below 18 K, the susceptibility drops rapidly as one would expect for a SP phase transition. The dashed line represents fits to a mean field calculation for a SP model system which provides a good description of the data (Huizinga et al. 1979).

A gapped excitation spectrum could not be observed directly from inelastic neutron scattering due to a low density of magnetic moment (Aeppli, de Boer, Pouget & Shirane 1984). However, the presence of such a gap has been inferred from μSR measurements (Blundell, Pratt, Pattenden, Kurmoo, Chow, Takagi, Jestädt & Hayes 1997). The presence of superlattice peaks have been observed directly with x-ray and neutron scattering (van Bodegom et al. 1981, Visser et al. 1983) and indicate peaks described by Miller indices $(h, k, l/2)$ with l odd. These indices refer to the structure at room temperature and not the high-temperature structure above the electronic Peierls transition. A full characterization of the motion of the atoms upon entering the SP state has been performed through crystallographic determination

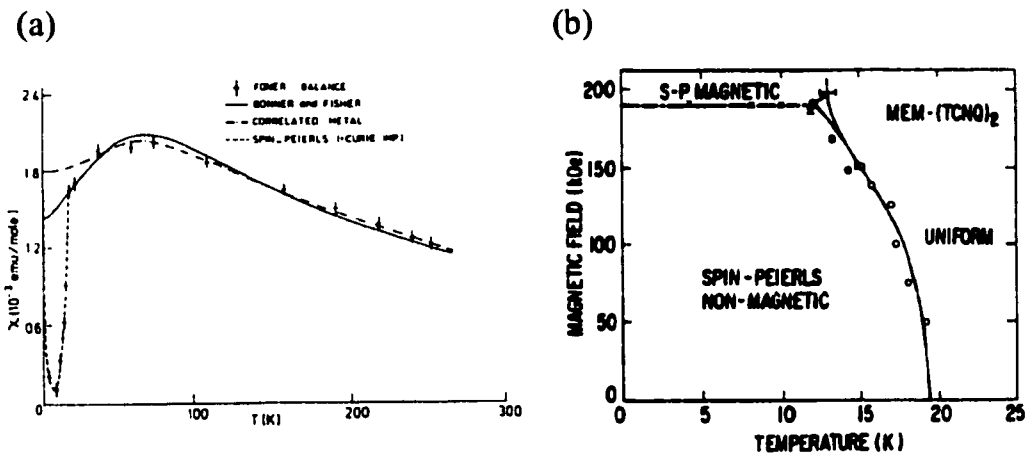

Figure 3.6: (a) Magnetic susceptibility as a function of temperature for a powder sample of MEM(TCNQ)$_2$ (Huizinga et al. 1979). (b) The H-T phase diagram as obtained from high-field magnetization (Bloch et al. 1981).

(Visser et al. 1983), but is rather complicated due to the large number of atoms within a unit cell and will not be described here for simplicity sake. Scattering studies also show the presence of substantial critical scattering on approaching the transition temperature (van Bodegom et al. 1981) but a quantitative lineshape analysis has not been performed and, consequently, no attempt has been made at extraction of critical exponents.

Finally, the H-T phase diagram has been mapped out by performing high-field magnetization measurements and is shown in Fig. 3.6b (Bloch et al. 1981). We see a similar phase diagram to that predicted theoretically (see Fig. 3.4b) with a SP transition temperature which drops continuously with increasing field and a high-field phase whose nature has not been fully characterized experimentally.

Consequently, we can see that MEM(TCNQ)$_2$ exhibits all the characteristic features of a SP transition with a transition temperature of about 18 K. Measurements of the critical properties associated with this phase transition will be discussed in Chapter 6.

3.3.2 $CuGeO_3$

Prior to 1993 all known SP systems were composed of complex organic molecules with a rather large number of atoms per unit cell and a low density of magnetic moment. Consequently, it was difficult to perform a complete experimental characterization of the SP transition using these systems. This changed dramatically when Hase, Terasaki & Uchinokura (1993) reported the characteristic isotropic susceptibility drop below a temperature of about 14 K in a structurally simple, inorganic compound, $CuGeO_3$.

The structural simplicity is shown in Fig. 3.7a where we show the crystal structure of $CuGeO_3$. The unit cell is orthorhombic belonging to the Pbmm space group and the structure essentially consists of chains of Cu-O octahedra which stack along the c-axis and are separated from one another along a by chains of Ge-O tetrahedra (Völlenkle, Wittman & Nowotny 1967). The Cu ions are in the +2 oxidation state which gives rise to a Hund's rule S=1/2 state with orbital angular momentum quenched by crystal field effects. Consequently, we have a spin 1/2 system and the quasi-one-dimensional nature of the magnetic system can be partially understood by examination of the crystal structure. The shortest Cu-Cu distance is along the c-axis and the exchange in this direction is enhanced by strong superexchange mediated by the O^{2-} ions which are shared between adjacent octahedra. The interactions along the a-axis are substantially weaker as the magnetic moments are isolated from one another by the Ge-O tetrahedra. The interactions along b will also be weaker than along c due to larger Cu-Cu and Cu-O-Cu distances giving rise to weaker direct exchange and super-exchange. As a result, we would expect rather strong interactions along c with weaker exchange along b and the weakest along the a crystalline direction and, consequently, we anticipate quasi-one-dimensional spin chains.

Following the initial susceptibility measurements of Hase, there were a num-

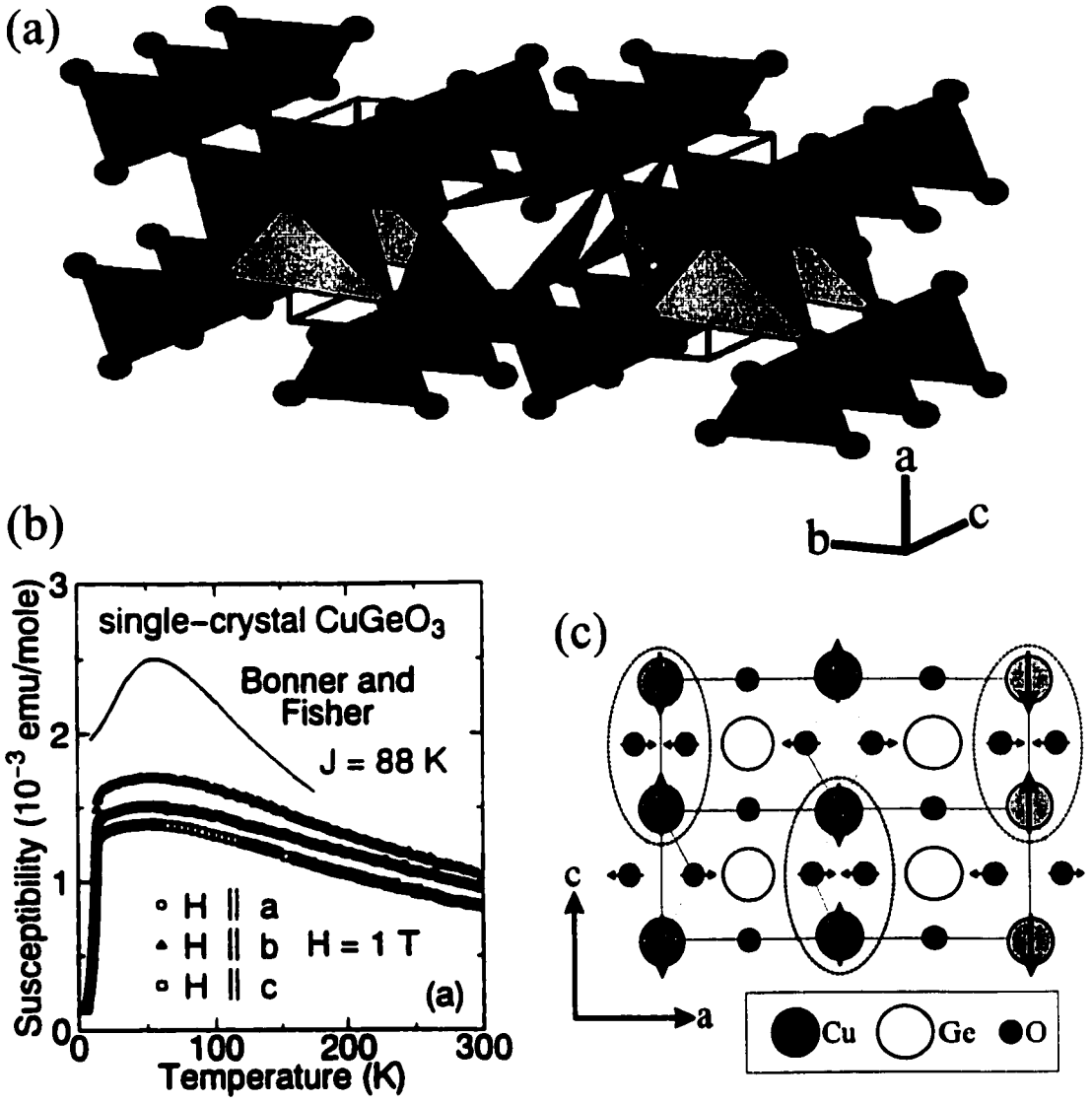

Figure 3.7: (a) Room temperature crystal structure of $CuGeO_3$. (b) Single crystal magnetic susceptibility (Hase, Terasaki & Uchinokura 1993). (c) Projection of crystal structure onto the a-c plane with arrows indicating the atomic motions on entering the SP state (Hirota et al. 1994).

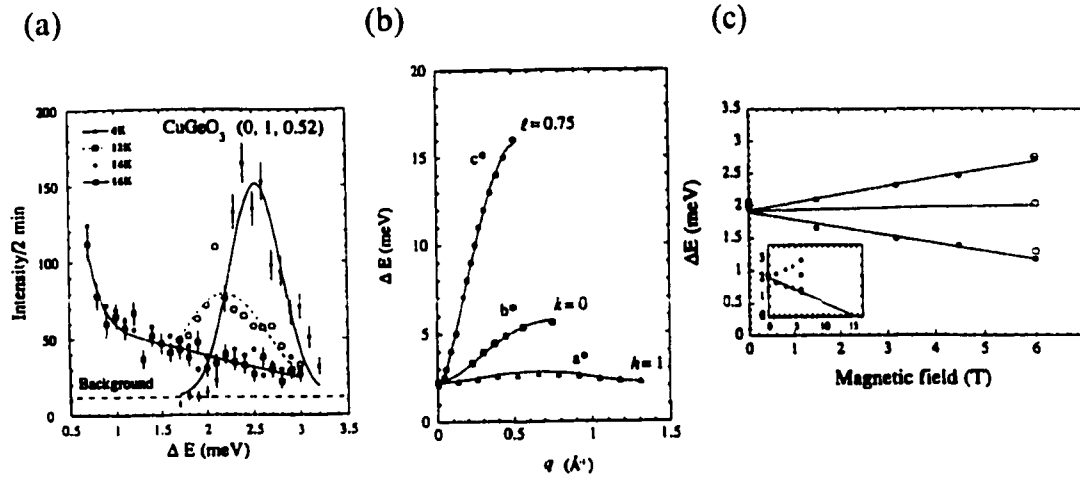

Figure 3.8: (a) Constant-Q scan showing presence of an excitation (Nishi et al. 1994). (b) Dispersion curve showing a gapped excitation spectrum and quasi-one-dimensional interactions (Nishi et al. 1994). (c) Triplet nature of the gap revealed with inelastic neutron scattering in the presence of an applied magnetic field (Fujita et al. 1995).

ber of experiments performed in an effort to characterize the SP state and confirm that the 14 K transition was indeed of the SP nature. Inelastic neutron scattering measurements showed the presence of a gapped excitation spectrum and allowed the excitations to be mapped out along the three crystalline directions (Nishi et al. 1994). This is shown in Fig. 3.8a where we first show a typical constant-Q scan showing the presence of a well-defined excitation which appears below 14 K and in Fig. 3.8b where the resulting dispersion curves are presented (Nishi et al. 1994). The solid lines represent fits to these dispersion curves giving values for the coupling constants of $J_c \sim$ 120 K, $J_b \sim 0.1J_c$ and $J_a \sim -0.01J_c$ (Nishi et al. 1994). This confirms the quasi-one-dimensional nature of the magnetic system and also indicates a coupling along b which is a substantial fraction of that along the chain direction. Consequently, the interchain coupling is large and the presence of a SP transition is unexpected. Its appearance suggests some inherent lattice instability and phonon and lattice constant measurements do bear this out (Fujita et al. 1996).

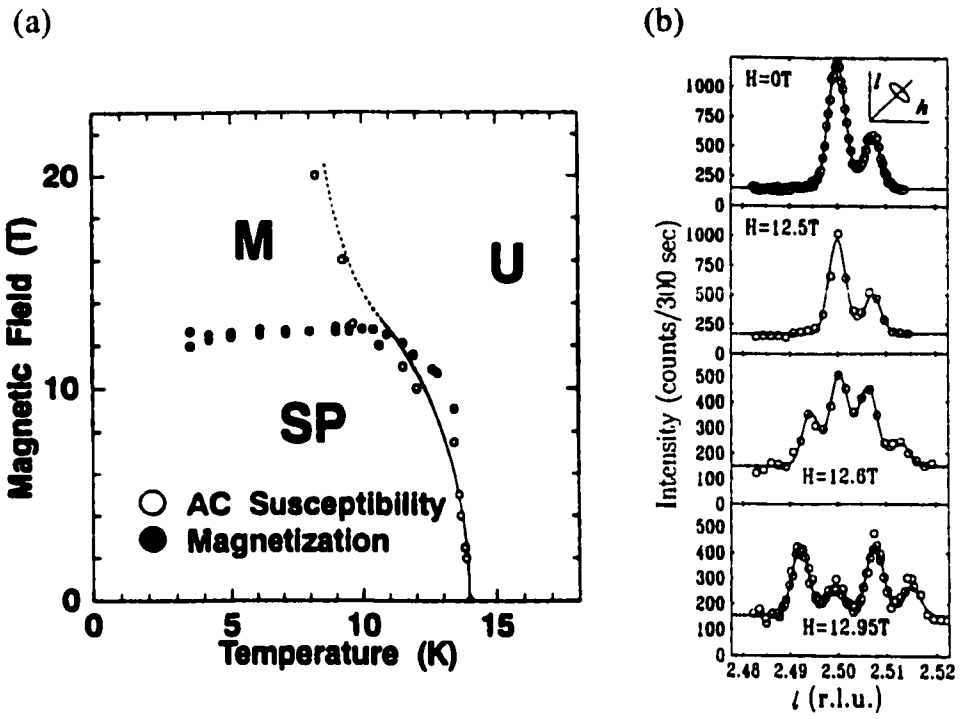

Figure 3.9: (a) H-T phase diagram for $CuGeO_3$ (Hamamoto et al. 1994). (b) X-ray scattering showing the incommensurate nature of the high field phase (Kiryukhin & Keimer 1995).

In addition to the observation of a gapped excitation spectrum, the nature of the excitations across this gap were examined by performing the inelastic neutron scattering measurements in the presence of an applied magnetic field (Fujita et al. 1995). The resulting excitation energy, as shown in Fig. 3.8c, splits into three distinct excitations with a splitting that increases linearly with applied field, indicating the singlet-triplet nature of the excitation.

Observation of superlattice reflections due to the new periodicity induced by the dimerization of the spin chains was slow in coming, but was finally found by Pouget, Regnault, Ain, Hennion, Renard, Veillet, Dhalenne & Revcolevschi (1994) using x-ray scattering techniques. These reflections were found to exhibit Miller indices $(h/2, k, l/2)$ where h and l are odd. Consequently, we see not only a doubling

of the unit cell along the chain direction, but an additional a-axis dimerization, the presence of which was unexpected and was responsible for the delay in observation of these reflections. The reason for this additional dimerization can be understood by considering the projection of the crystal structure onto the a-c plane as shown in Fig. 3.7c (Hirota et al. 1994). The Cu ion displacements are accompanied by O ion displacements which act to enhance the exchange within the dimers (represented by the dashed ellipse) while reducing that between dimers as a result of the superexchange interaction which they mediate. To facilitate the observation of a doubled unit cell along a, it was postulated that the Cu ion displacements are out of phase from one chain to the next, along a, resulting in a doubly dimerized unit cell as can be seen in Fig. 3.7c (Hirota et al. 1994).

Finally, the behaviour of the transition temperature under the action of an applied magnetic field was examined carefully, through high field magnetization and AC susceptibility measurements (Hase, Terasaki, Uchinokura, Tokunaga, Miura & Obara 1993, Hamamoto et al. 1994), with the resulting phase diagram shown in Fig. 3.9a. This is consistent with that theoretically predicted for the SP transition and the nature of the high field phase was examined carefully by performing x-ray scattering measurements in the presence of a sufficiently large magnetic field (Kiryukhin & Keimer 1995). On passing through the high-field phase boundary, the superlattice peaks are observed to split, as shown in Fig. 3.9b, suggesting a structure incommensurate with the lattice (Kiryukhin & Keimer 1995).

3.3.3 Doped $CuGeO_3$

Prior to 1993, all known SP systems were composed of large, complex organic molecules and these systems did not readily accept dopant ions. Consequently, there had been no work done studying the effects of impurities on the SP phase transition.

However, $CuGeO_3$ readily accepts dopants on either the Cu^{2+} site or the Ge^{4+} site, and a plethora of experimental and theoretical investigations were undertaken to study these doped samples.

One of the more interesting consequences of these studies is the nature of the phase diagram with doping concentration. With dopants on either the Cu^{2+} (Hase, Terasaki, Sasago, Uchinokura & Obara 1993, Oseroff, Cheong, Aktas, Hundley, Fisk & L.W. Rupp 1995, Sasago, Koide, Uchinokura, Martin, Hase & Hirota 1996) or Ge^{4+} (Oseroff et al. 1995, Renard, Dang, Veillet, Dhalenne, Revcolevschi & Regnault 1995, Regnault, Renard, Dhalenne & Revcolevschi 1995, Poirier, Beaudry, Castonguay, Plumer, Quirion, Razavi, Revcholevschi & Dhalenne 1995) site, the SP transition temperature decreases rather rapidly and there appears a second antiferromagnetically ordered phase which has been observed to coexist with the SP phase. This is a surprising result as the SP phase and an AF ordered phase are often considered to be mutually exclusive. The phase diagram as a function of doping concentration is shown in Fig. 3.10 for the replacement of (a) Zn^{2+} for Cu^{2+} (Sasago et al. 1996) and (b) Ge^{4+} for Si^{4+} (Renard et al. 1995). We can clearly see the SP transition temperature falling away with increasing concentration until some maximum concentration is reached above which this phase ceases to exist. The Néel phase transition occurs at a lower temperature than the SP transition and its transition temperature increases with increasing dopant concentration reaching a plateau at roughly the same concentration as the SP phase disappears.

The existence of this Néel phase is yet to be fully explained. One difficulty comes in describing very similar phase diagrams for doping both within the chains (replacing Cu^{2+}) and between chains (replacing Ge^{4+}). Some theoretical predictions do exist suggesting interesting effects such as a spatially varying magnetic moment in the AF phase with the moment attaining its largest value near the doping centre and

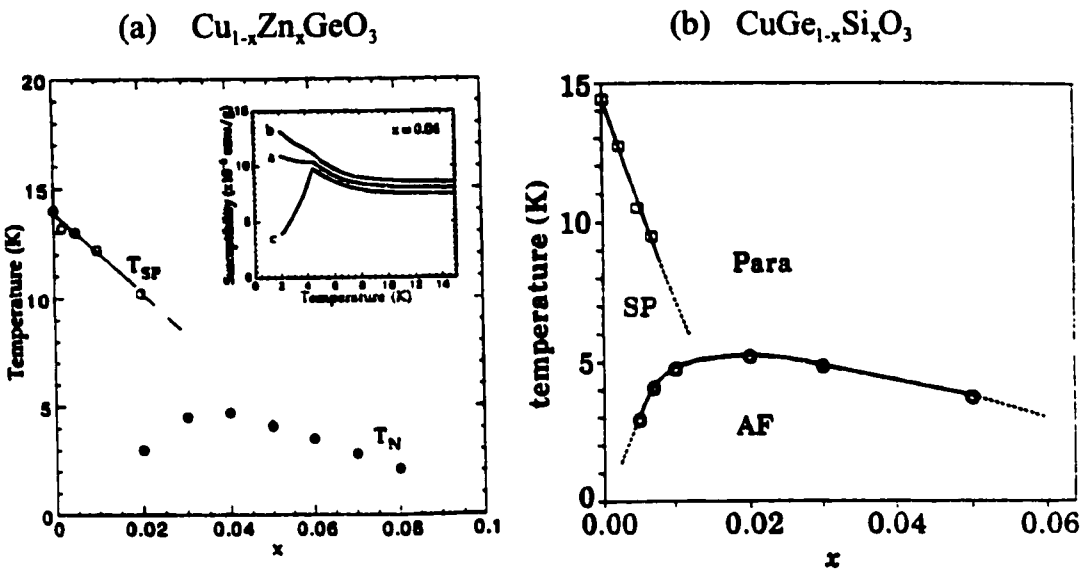

Figure 3.10: Phase diagram as a function of dopant concentration for (a) Zn^{2+} substituted for Cu^{2+} (Sasago et al. 1996)and (b) Si^{4+} substituted for Ge^{4+} (Renard et al. 1995).

falling away as one proceeds away from this position (Fukuyama, Tanimoto & Saito 1996). Experimentally, the AF phase has been observed for dopant concentrations as low as 0.1% which corresponds to replacing every 1000th atom (it is worth noting experimentally that determination of concentrations at this level is rather difficult and it somewhat suspect) (Manabe, Ishimoto, Koide, Sasago & Uchinokura 1998, Grenier, Renard, Veillet, Paulsen, Calemczuk, Dhalenne & Revcolevschi 1998). This seems to contradict theoretical treatments which suggest some lower cutoff concentration below which the Néel phase ceases to exist (Fukuyama et al. 1996).

The effects of impurities on critical phenomena has been a topic which has received much attention over the last 25 years. Harris made arguments that the effects of impurities would depend crucially on the critical exponent α, describing the specific heat (Harris 1974). Namely, he claimed that the critical exponents would change under the influence of impurities if α was greater than zero. These arguments were

later confirmed by more rigorous renormalization group studies (Harris & Lubensky 1974). From Table 1.1, we can see that for 3D systems, 3D Ising should be affected by impurities with both 3D XY and Heisenberg having values of α which are less than zero.

Chapter 4

Critical Properties of $CuGeO_3$

Despite the plethora of experimental studies of the SP transition in $CuGeO_3$, the critical phenomena associated with this transition had not been examined in detail. Consequently, we have studied these properties through the use of x-ray diffraction techniques and the resulting measurements are presented in the following chapter which incorporates the article "X-Ray diffraction study of critical phenomena at the spin-Peierls transition in $CuGeO_3$" reprinted from Physical Review B, Vol. 57, No. 22, pp.14097-14104, June 1, 1998.

X-Ray Diffraction Study of Critical Phenomena at the Spin Peierls Transition in $CuGeO_3$

M.D. Lumsden, B.D. Gaulin, and H. Dabkowska

Department of Physics and Astronomy, McMaster University, Hamilton, Ontario, L8S 4M1, Canada

Abstract

We have performed x-ray diffraction measurements of the critical phenomena associated with the spin Peierls phase transition in $CuGeO_3$. Measurements of the order parameter indicate a value of the critical exponent β of 0.345±0.03 consistent with conventional three dimensional (3D) behavior and in closest agreement with 3D XY universality, as expected on theoretical grounds. This work also indicates a rather narrow asymptotic critical region which explains much of the inconsistency reported in previous critical exponent estimates. Measurements of the relative changes in lattice constants have also been carried out to allow for detailed comparison between the spontaneous strains present below the transition temperature and the order parameter. The order parameter and lattice constant measurements were performed in identical thermal environments on the same sample to allow for direct comparison with no adjustment of transition temperature. This comparison suggests good agreement between the two except near the transition temperature where fluctuation effects are observed in the spontaneous strain which are less evident in the order parameter.

Reprinted from Physical Review B Vol.57 No.22 pp.14097-14104 (1998)

I. INTRODUCTION

Quantum fluctuations in low dimensional magnetic systems are known to result in unique and exciting phenomena. One particularly interesting effect is the spin-Peierls (SP) transition which occurs in quasi-one-dimensional S=1/2 Heisenberg spin chains with antiferromagnetic interactions. In the presence of strong magneto-elastic coupling, the chains are found to undergo a dimerization at low temperatures and a concomitant gap in the magnetic excitation spectrum separating a non-magnetic singlet ground state from a triplet of excited states. The presence of this gap yields an isotropic drop in the magnetic susceptibility below the transition temperature (T_{sp}).

Experimentally realized SP systems are rare as three dimensional (3D) magnetic interactions usually drive the system to a Néel ordered state before the magneto-elastic SP transition can occur. Previously, the only known systems to undergo such a transition were composed of large, complex organic molecules,[1] such as $MEM(TCNQ)_2$ and TTF(CuBDT), with a very low density of magnetic moment. However, interest in this phase transition has been renewed with the discovery of a structurally simple, inorganic SP system, $CuGeO_3$. It is now well established that $CuGeO_3$ undergoes a SP transition at $T_{sp} \sim 14$ K.[2–6] The isotropic magnetic susceptibility drop and characteristic decrease in T_{sp} in the presence of a magnetic field were first observed by Hase *et al.*[2] The gap in the excitation spectrum has been directly observed with neutron scattering[3] and the singlet to triplet nature of the gap has been confirmed under application of a magnetic field.[4] Finally, the dimerization has been observed using x-ray,[5] neutron,[5] and electron diffraction.[6]

$CuGeO_3$ has an orthorhombic unit cell with space group Pbmm and room temperature lattice constants of a = 4.81 Å, b = 8.47 Å, and c = 2.94 Å.[7] (Recent

measurements suggest a different but related crystal structure for $CuGeO_3$ with space group $P2_12_12$ and lattice constants $a = 9.60$ Å, $b = 8.47$ Å, and $c = 11.78$ Å.[8] However for the remainder of this paper we will refer to the conventional crystal structure.) The structure consists of chains of CuO_4 octahedra stacked along the c-axis which are separated from each other by chains of GeO_3 tetrahedra. The one dimensional (1D) spin chains are formed by Cu^{2+} ions stacked along the c-axis and the one-dimensionality arises from a strong superexchange interaction mediated through the O atoms. There exist, however, non-negligible interchain couplings with $J_b \sim 0.1 J_c$ and $J_a \sim -0.01 J_c$.[3] It has been proposed that the c-axis dimerization is out of phase between neighboring chains[9] and this, together with slight displacements of the O atoms results in a doubling of the unit cell along the a-axis in addition to the expected dimerization of the spin chain. Consequently, the unit cell is doubled along both a and c and superlattice reflections of the form $(h/2,k,l/2)$ with h and l odd have been observed.

The measurements to date of the critical phenomena associated with the SP transition in $CuGeO_3$ have produced a rather murky picture with exponents spanning several universality classes. Early neutron measurements produced results consistent with tricritical behavior ($\beta \sim 0.25$)[10,11] whereas more recent neutron diffraction studies on a crystal with a reduced T_{sp} (~ 13.26 K) have determined a value of β consistent with 3D universality (0.33 ± 0.03).[12] Thermal expansion measurements have yielded estimates of β ranging from 0.30 to 0.35[13,14] while ultrasonic attenuation has produced a β estimate of 0.25.[15] Specific heat measurements have resulted in an equally unclear picture with an early measurement producing a rather large value of $\alpha \sim 0.4$[16] while later measurements estimate values of α consistent with conventional 3D universality, $-0.15 \leq \alpha \leq 0.12$.[17] While no clear picture as to the true universality of

the SP transition in $CuGeO_3$ has existed, one thing that is clear is that the results for $CuGeO_3$ are not the same as those for the previously studied organic SP systems where critical phenomena consistent with mean-field behavior have been observed.[18,19] The immature status of this experimental field led us to carefully examine the temperature dependence of the superlattice peak intensity using x-ray diffraction with high temperature stability. A preliminary report of these results has been published previously.[20]

Previous neutron[21] and x-ray diffraction[10] measurements indicated a spontaneous strain in the b-axis lattice constant which develops below T_{sp} and scales with the square of the order parameter. The x-ray diffraction results also seemed to indicate a slight upturn in the a-axis lattice constant but the resolution was insufficient to ascertain whether this spontaneous strain also scales with the order parameter.[10] Later neutron work[22] and high-resolution capacitance dilatometry measurements[13] indicated spontaneous strains along all three crystal axes. In order to understand the relationship between the order parameter and the spontaneous strains, we have performed high temperature stability, high resolution x-ray diffraction measurements of the temperature dependence of all three lattice constants. Our apparatus provides a unique opportunity to perform the spontaneous strain and order parameter measurements on the same sample in identical sample environments with identical thermometry. Both measurements can be performed with very high temperature stability and the results can be compared directly with no compensation for temperature calibration. This should allow for detailed comparisons to be made and systematic deviations between the two quantities can be observed.

II. EXPERIMENTAL DETAILS

The single crystal used in these measurements was grown from a CuO flux by slow cooling from 1220°C. The dimensions of the crystal were approximately $2\times1\times0.5$ mm^3 and the sample was of good quality with a mosaic spread of about 0.04° half width at half maximum (HWHM). For both the order parameter and thermal expansion work, the sample was mounted in a Be can in the presence of a He exchange gas. This can was connected to the cold finger of a closed-cycle He refrigerator and a temperature stability of about 0.005 K was obtained over the temperature range of interest. The incident radiation was Cu Kα radiation from an 18 kW rotating anode x-ray generator. For the order parameter measurements, a vertically focusing PG (0,0,2) monochromator crystal was used in order to maximize the number of photons incident on the sample. For the lattice constant measurements, a flat, perfect single crystal of Ge (1,1,1) was used as the monochromator and the incident radiation consisted of Cu Kα_1 only with Cu Kα_2 being removed by distance collimation before the sample.

III. ORDER PARAMETER

A. Experimental Results

The temperature dependence of the (1/2,5,1/2) superlattice Bragg peak was examined in order to measure the order parameter associated with the SP transition in $CuGeO_3$. This reflection was chosen due to its relative strength when compared to other possible reflections.[9] It is important to note that our measurements, as well as previously reported structure factor calculations,[9] indicate that this superlattice

peak is reduced in intensity by a factor of $\sim 10^{-4}$ when compared to principal Bragg peaks such as (0,4,0) and, consequently, extinction effects should be negligible.

Prior to performing our measurements, the effect of spontaneous strains present below T_{sp} on the peak position and lineshape of the superlattice peak were examined carefully. Both longitudinal and transverse scans through (1/2,5,1/2) were performed at temperatures near the transition and also well below the transition and the resulting longitudinal scans at 7 K and 13 K are shown in Fig. 1. The solid lines represent best fits to a single Gaussian with resulting peak positions of 57.804(5) at 7 K and 57.807(5) at 13 K and corresponding widths of 0.44(1) at 6 K and 0.44(1) at 13 K. We certainly expected any changes in position or lineshape which occur below the transition temperature to be negligible given the relatively low Q resolution configuration employed in these measurements. However, to emphasize this point, the inset shows the same data background subtracted and normalized to unity. Once again, there is no noticeable change in position or lineshape. Consequently, the peak intensity will be proportional to the square of the order parameter and the observed temperature dependence of the peak intensity for the (1/2,5,1/2) reflection is shown in Fig. 2.

B. Analysis and Discussion

In order to determine the critical behavior of the order parameter, the measured data was fit to a power law in the reduced temperature $t=1 - T/T_{sp}$:

$$Intensity = I_o t^{2\beta} + Background \tag{1}$$

This power law is expected to be valid in the so-called asymptotic critical region, near T_{sp}, where the length scale associated with fluctuations in the order parameter

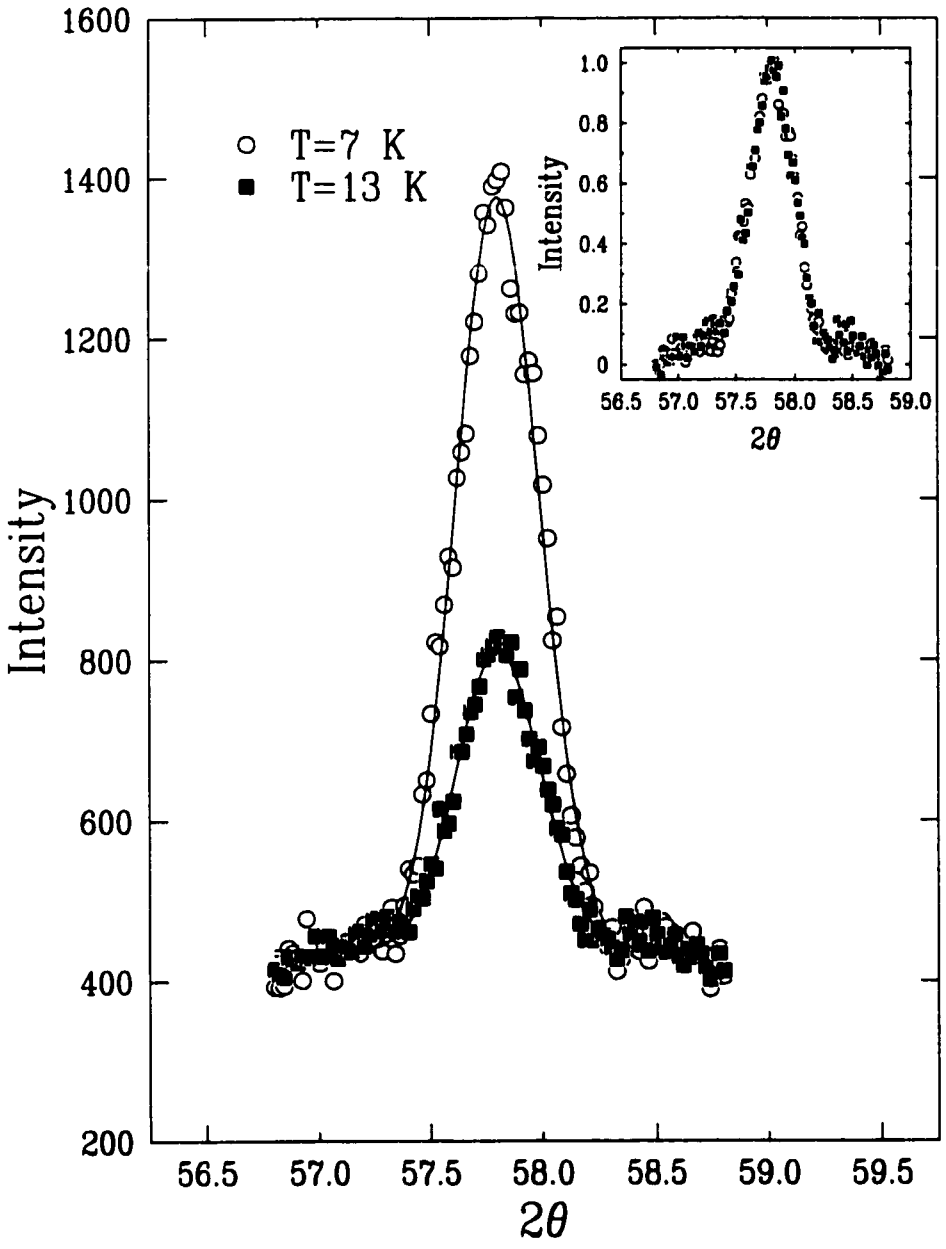

Figure 1: Longitudinal scans through the (1/2,5,1/2) superlattice reflection at temperatures of 7 K and 13 K. The solid lines represent best fits to a single Gaussian resulting in peak positions of 57.805(5) at 7 K and 57.807(5) at 13 K with corresponding widths of 0.44(1) and 0.44(1). The inset shows the two curves background subtracted and normalized to unity.

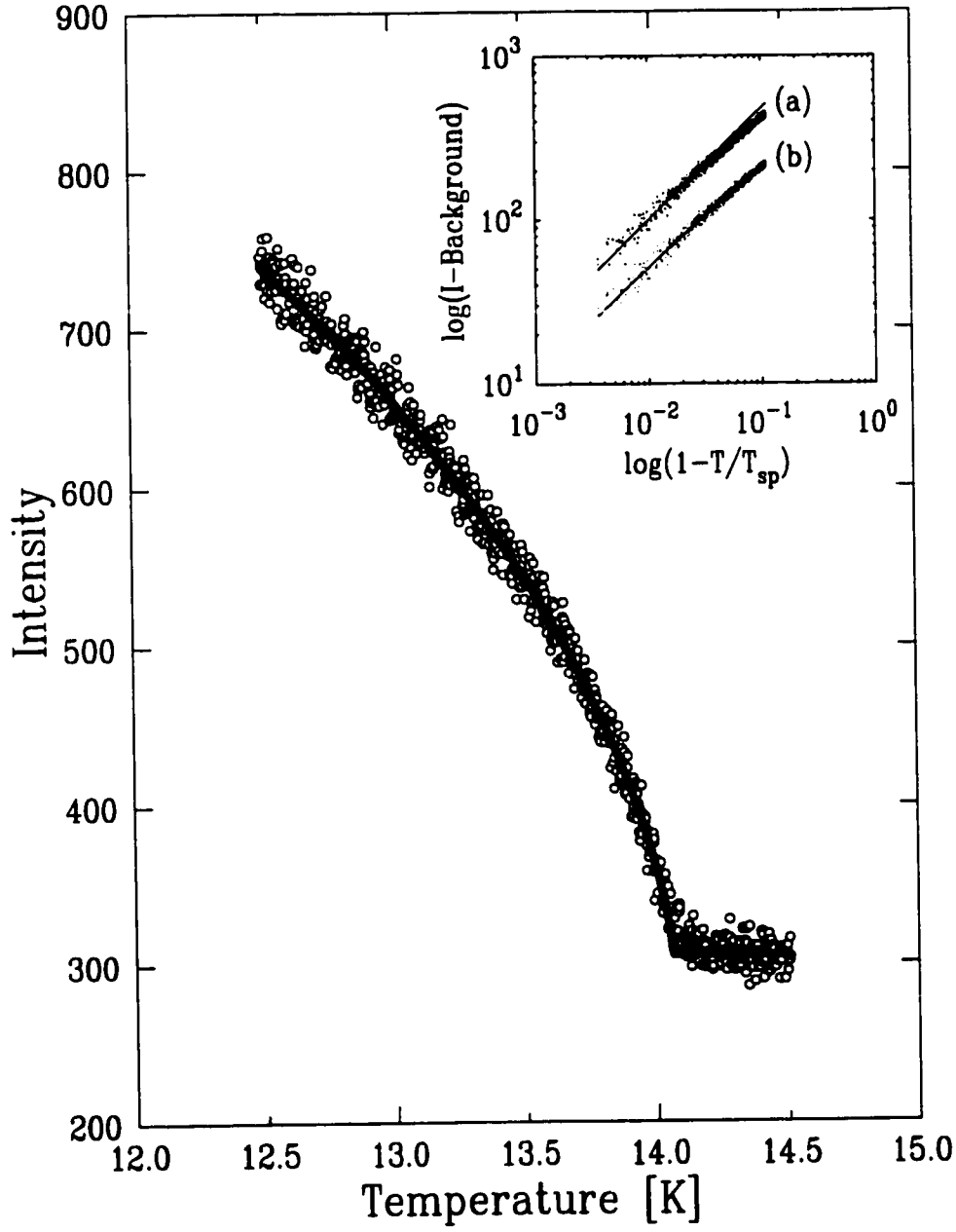

Figure 2: X-ray scattering peak intensity of the (1/2,5,1/2) superlattice reflection as a function of temperature. The solid line represents the best fit to a power law with the first correction-to-scaling term added [Eq. (2)]. The inset shows the same data, background subtracted, on a logarithmic scale [(a) and (b) have been displaced vertically]. The solid line in (b) represents the same fit as in the main panel while that in (a) represents a fit of the data at small reduced temperature, t, to a simple power law.

dominates over all other relevant length scales in the system. As one moves below the asymptotic region in temperature, the expected power law behavior must be modified by successive correction-to-scaling confluent singularity terms,[23] the first of which is shown in Eq. (2).

$$Intensity = I_o t^{2\beta}(1 + At^{\Delta}) + Background \tag{2}$$

where the exponent Δ has an approximate value of 0.5. In fitting the data to Eq. (2), the exponent Δ was first treated as a variable parameter, but was never found to deviate from 0.5 in any significant manner. As a result, Δ was fixed at 0.5 for the remainder of the analysis.

An important point of note is that the sign of the correction amplitude, A, should be negative resulting in a correction term ($1+At^{\Delta}$) which is less than unity for temperatures below T_{sp}. This point is discussed in detail in the appendix.

The fit represented by the solid line in Fig. 2 represents the best fit using the modified power law [Eq. (2)] and yields an exponent β of 0.345±0.03 at a transition temperature of 14.05±0.01 K. The inset of Fig. 2 represents the same peak intensity data, background subtracted, plotted on logarithmic scales with fits to the simple power law (a) as well as the power law with the first correction-to-scaling term included (b). The corrected power law describes the data very well over the entire temperature range whereas the ordinary power law fit is seen to deviate from and exceed the data for reduced temperatures in excess of about 0.03. To correct for this deviation, one clearly needs a correction term which will be less than unity for temperatures below T_{sp} and thus the correction amplitude, A, in Eq. (2) must be less than zero as expected.

The deviation of the data from the simple power law at low temperatures

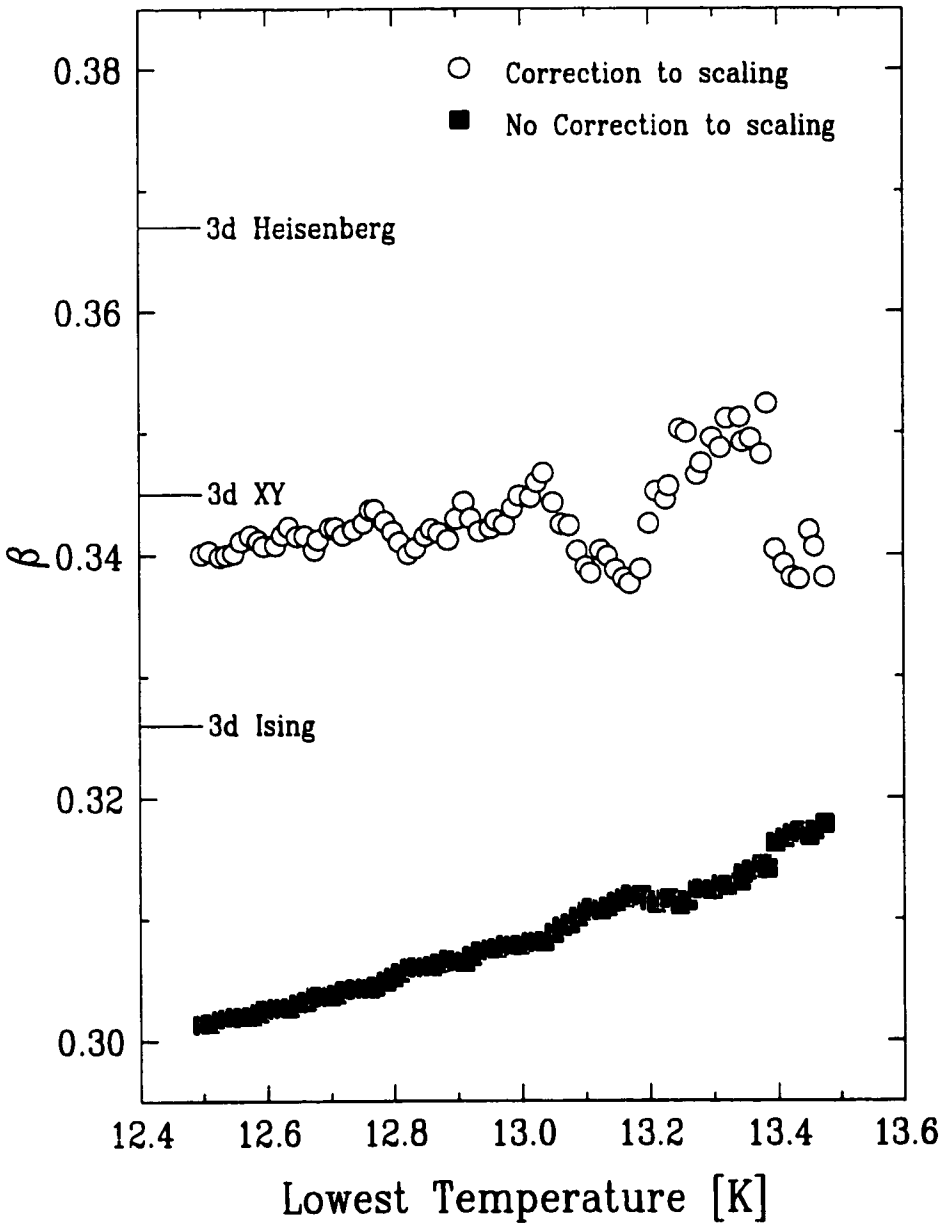

Figure 3: The dependence of the critical exponent β on the range of data included in the fits for fits to a simple power law [Eq. (1)] and to a power law with the first correction-to-scaling term added [Eq. (2)]. All fits are performed with the same highest temperature. For reference, the predicted values of β for 3D Ising, XY, and Heisenberg universality are also included.

motivated us to examine in more detail the dependence of the fits on the range of data included. Thus, fits were carried out as a function of the lowest temperature included as this temperature is varied from about 12.5 K up to about 13.5 K. The results could not be extended much beyond 13.5 K as the uncertainty in the fits became excessive. The obtained results for β as a function of lowest temperature are shown in Fig. 3 for fits to both the ordinary power law [Eq. (1)] as well as the power law with the first correction-to-scaling term included [Eq. (2)]. Expectations for the 3D Ising, 3D XY, and 3D Heisenberg universality classes are included in the figure as a point of reference.[24] The value of β obtained from the ordinary power law varies continuously over the entire temperature range of interest and we feel that this strong variation is largely responsible for the wide range of values of critical exponents reported in previous measurements. The fits to the corrected power law [Eq. (2)] show little dependence on the range of data included. The fact that the value of β obtained from the ordinary power law varies over the entire temperature range is taken as direct evidence that the asymptotic region is rather narrow. The robust nature of the corrected power law fits indicates that only the first order correction term in necessary to adequately describe the data at least over the temperature range which was investigated. Fits were also performed using a power law with the first two correction-to-scaling terms included and, as expected, no significant differences were observed.

The extraction of the exponent β is generally made much more difficult due to presence of critical scattering from fluctuations in the order parameter in the immediate vicinity of the transition temperature. These fluctuations provide additional scattering at the ordering wave vector which attains its maximum at the transition temperature where the size of the correlated regions diverge. This causes substantial

curvature in the order parameter near the transition temperature and makes the data in its immediate vicinity unusable. However, in contrast to more traditional SP systems, there has been a great deal of difficulty in observing these critical fluctuations in $CuGeO_3$,[5,9–11] although recent measurements have made progress in this respect.[12,25] Detailed scans were performed through the (1/2,5,1/2) position at temperatures near T_{sp} and no evidence of critical scattering was observed. The absence of critical scattering in our measurements makes it impossible to determine exponents associated with the Q-dependent susceptibility, $\chi(Q)$, and the correlation length, ξ. It does, however, allow for a much more accurate determination of the exponent β associated with the order parameter than is usually possible.

The dependence of the value of β on the chosen transition temperature, T_{sp}, was investigated in some detail as this largely determines the accuracy of most critical exponent estimates. This dependence is shown in Fig. 4 where β as well as the goodness-of-fit parameter χ^2 are plotted versus the chosen value of transition temperature, T_{sp}. As can be seen the value of β obtained from these fits is a smooth function of T_{sp}, indicating that, as expected, it is the uncertainty in T_{sp} and not the statistical quality of the diffraction data that is responsible for the uncertainty in β.

For reference, the expected values of β for tricritical, 3D Ising, 3D XY, and 3D Heisenberg universality are indicated. The plot of χ^2 versus T_{sp} has a very pronounced minimum at a T_{sp} of about 14.05 K with a corresponding β value of about 0.345. The value of β obtained from these measurements is consistent with conventional 3D behavior and strongly supports recent theoretical work[26] based on a Landau-type description of the free energy where the displacements of both Cu and O are taken into consideration, which predicts 3D XY universality for which β has been estimated theoretically to be 0.3455 ± 0.002.[27]

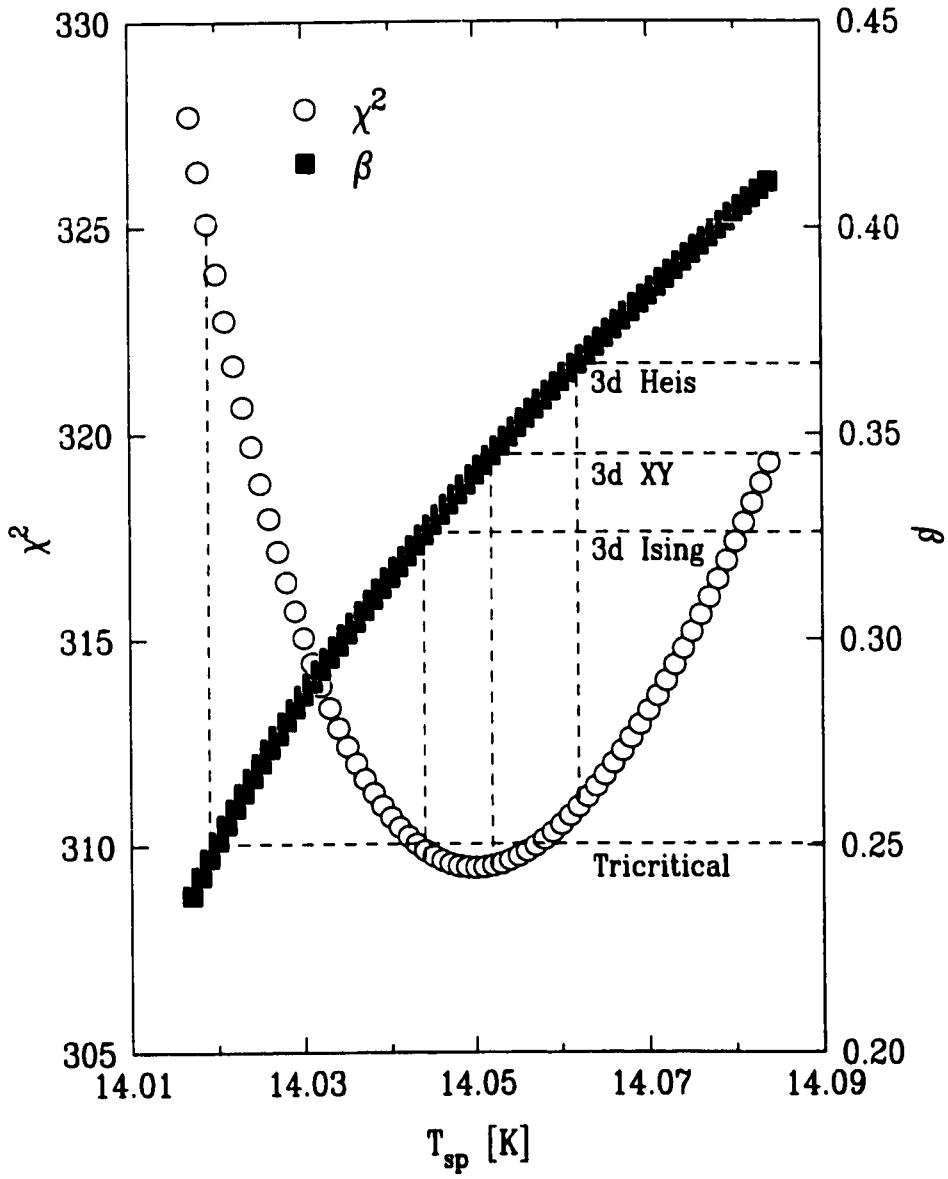

Figure 4: The dependence of the goodness-of-fit parameter, $\chi^2=\Sigma_i[I_{calc}(T_i) - I_{obs}(T_i)/\sigma(I_{obs}(T_i))]^2$ and the critical exponent β on the chosen value of the transition temperature T_{sp}. The results were obtained from fits to the power law with first correction-to-scaling term included [Eq. (2)]. The predicted values of β for 3D Ising, XY, and Heisenberg universality, as well as for tricritical mean-field behavior are included.

IV. LATTICE CONSTANTS

Our first set of measurements of the lattice parameters in $CuGeO_3$ using a conventional approach led us to conclude that such measurements would lack the resolution necessary for detailed comparison to the order parameter. The limiting factor was the mosaic quality of the single crystal and the subsequent lowering of Bragg peak intensity. The crystal used in these measurements has a mosaic spread of about 0.04° HWHM. (As a point of reference, the crystal used in the diffraction measurements of Harris *et al.* had a reported mosaic of 0.009° HWHM.[10]) The conventional approach consists of performing detailed longitudinal scans of the relevant Bragg peaks and then extracting peak positions from lineshape analysis.

A. Experimental Description

The alternative approach which we implemented is shown schematically in Fig. 5. As the temperature is changed, the peak in a longitudinal scan shifts position from point A to point B, and thus the intensity at point C undergoes a rather large change ending at point D. In this way small changes in peak position correspond to rather large intensity changes for those positions on the longitudinal scan whose slope is large. Large changes in position, such as those shown in Fig. 5, could easily be measured using conventional techniques, but this alternative approach has significant advantages for measuring very small changes in lattice constant such as those which occur in $CuGeO_3$ (the shift in peak position shown in Fig. 5 has been exaggerated to allow for easier description of the technique). The technique allows high statistic measurements to be made as the time allotted per temperature now is the time involved in measuring a single point as opposed to that required for

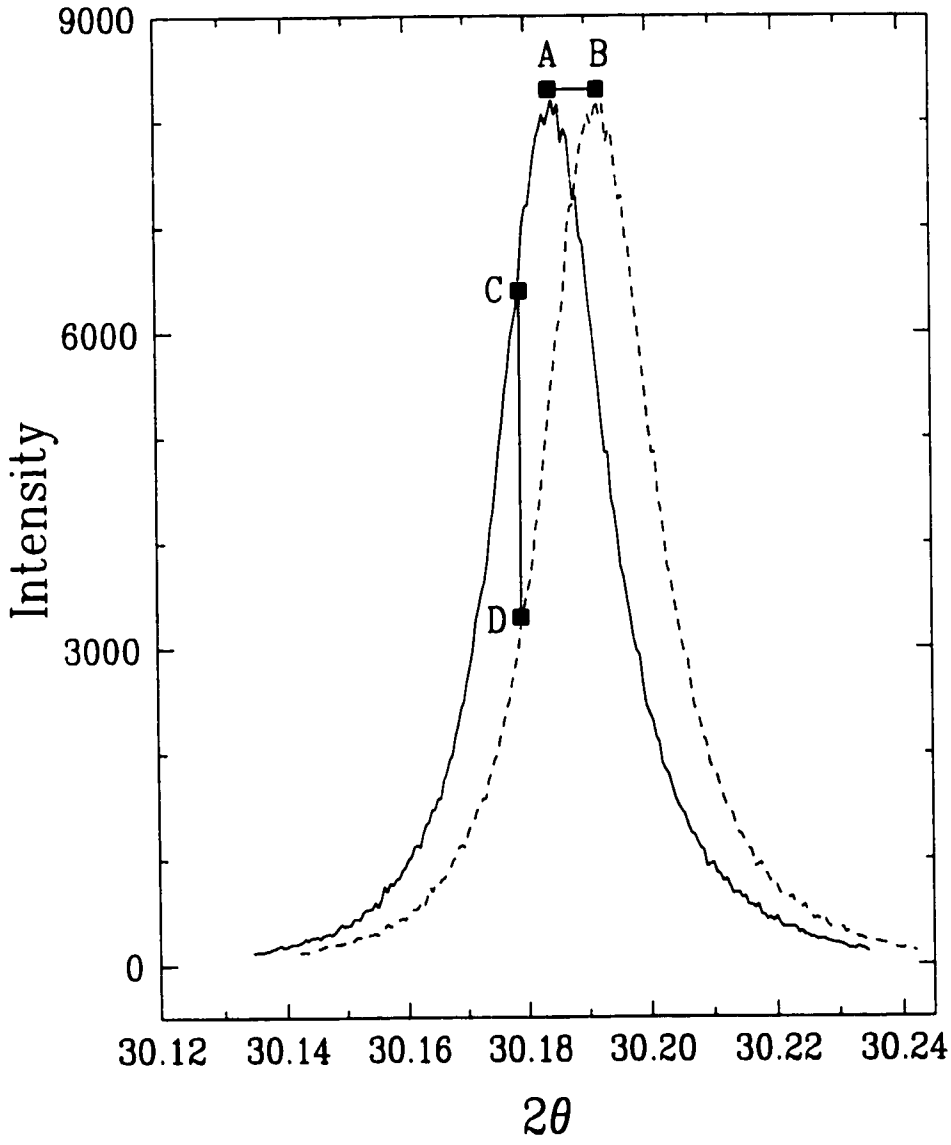

Figure 5: A sample longitudinal scan through the (0,0,1) Bragg reflection. With a shift in peak position from A to B, the intensity at point C changes by a large amount, to that at point D. The changes in peak position represented by this figure are exaggerated and are shown to demonstrate the novel approach employed in the lattice constant measurements.

a detailed lineshape. We estimate that this approach provided about an order of magnitude increase in sensitivity, resulting in measured $\Delta L/L \sim 10^{-6}$.

The actual determination of the temperature dependence of the lattice constants consisted of the following procedure. The longitudinal lineshape of a Bragg peak, such as that shown in Fig. 5 for the (0,0,1) reflection, was measured in detail. An appropriate position on the lineshape (such as point C in Fig. 5) was selected so as to maximize changes in intensity. The temperature dependence of the intensity at that point was then measured. Initially, on ramping the temperature, successive runs showed essentially the same relative changes, but from one run to the next, there were often small offsets in intensity. This was attributed to slight twists of the sample-mount-cryostat system and to correct for this, following each change in temperature, transverse scans were performed and the position was re-centered in the transverse direction. This alleviated the offset problem as evidenced by the reproducibility of runs taken with both temperature increasing and decreasing. The resulting data, shown in Figs. 6 and 7, were typically made up of 8-10 runs with half done on warming and half on cooling. Finally, changes in peak position were determined from changes in intensity using the detailed lineshape measurement.

Potential problems exist with this approach, such as systematic changes in the lineshape, due to, for example, slight re-alignment of the grains which make up the mosaic single crystal. Throughout our measurements, we periodically performed longitudinal scans, such as those shown in Fig. 5, as a check for these and related effects. In addition, as mentioned above, the results were reproducible over many independent warming and cooling runs.

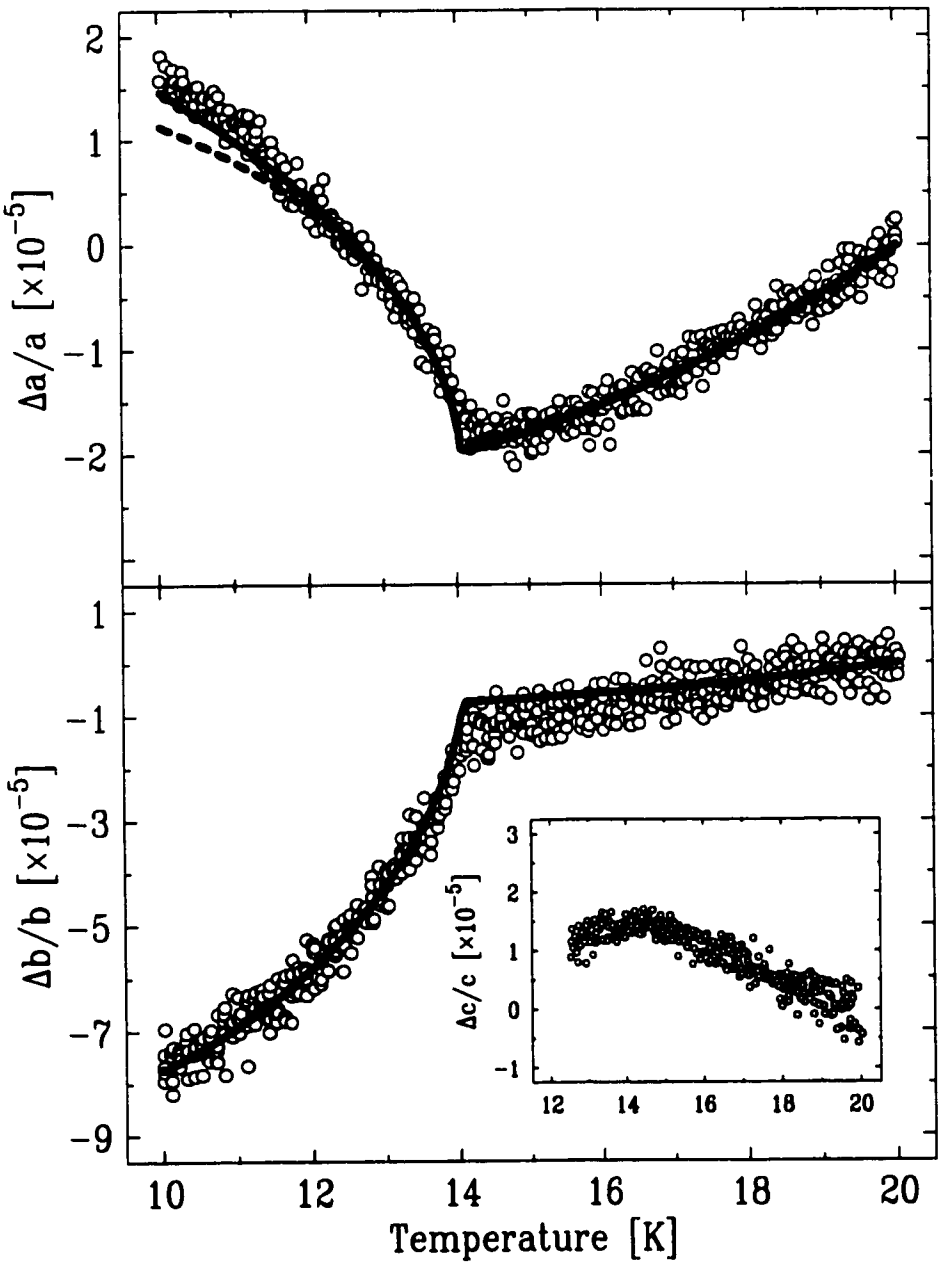

Figure 6: Relative changes in the a, b, and c lattice constants as a function of temperature normalized to produce a $\Delta l/l$ of zero at 20 K. The solid line represents the background obtained from measurements on a 5% Zn-doped sample in addition to the order parameter squared, as obtained from fits to the superlattice reflection data shown in Fig. 2. The dashed line in the upper panel represents the results obtained with a background fit using the data on the pure sample for temperatures between 16 K to 20 K, well above the transition temperature.

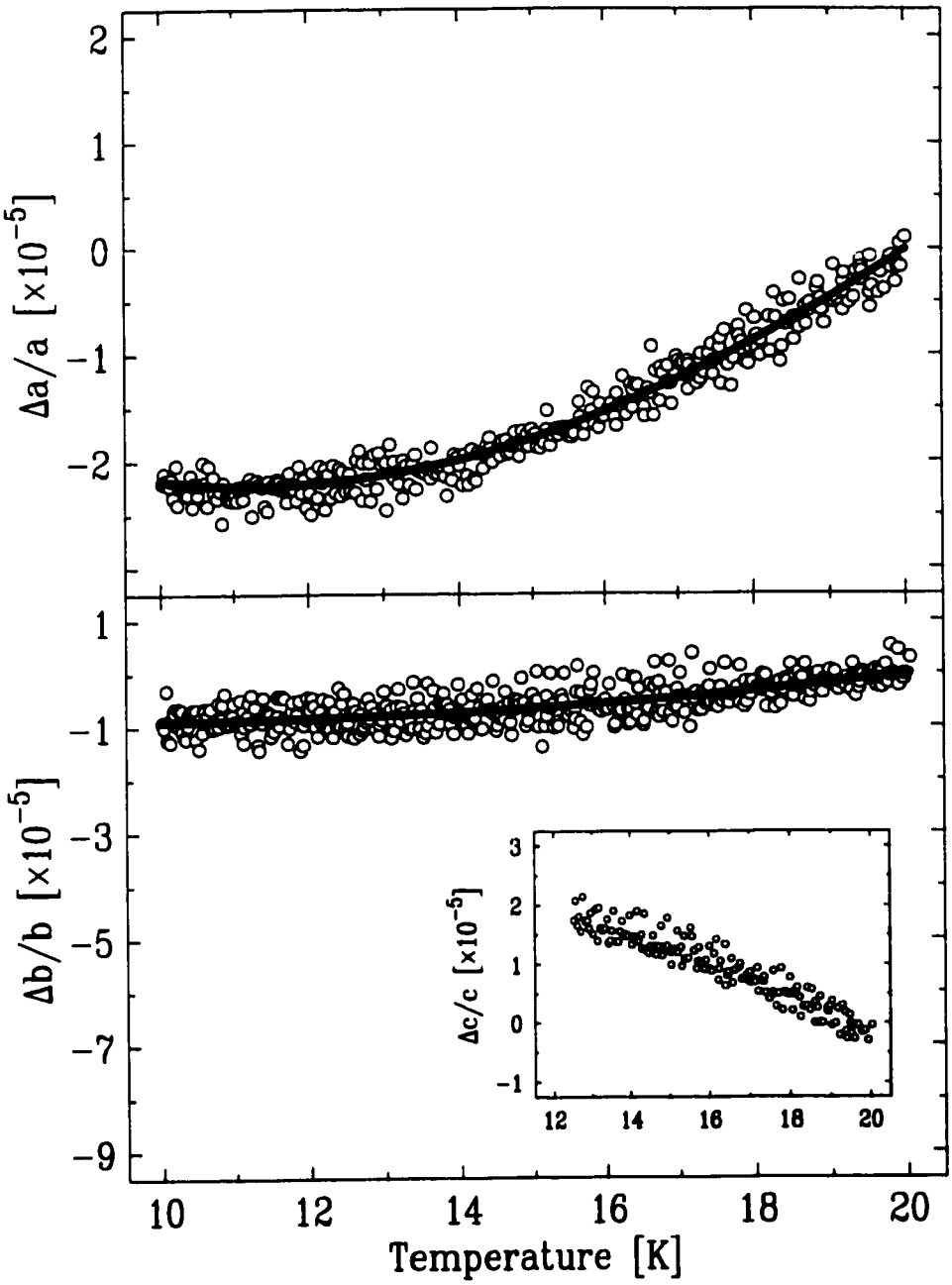

Figure 7: Relative changes for the a, b, and c lattice constants as a function of temperature for a single crystal of $Cu_{1-x}Zn_xGeO_3$ with x~0.05. Again the data was normalized to produce a $\Delta l/l$ of zero at 20 K. The solid lines represent the best polynomial description of the data. This was taken as an independent measure of the thermal expansion of pure $CuGeO_3$ in the absence of the SP transition.

B. Results and Discussion

The results obtained for the temperature dependence of the three lattice constants of $CuGeO_3$ are shown in Fig. 6. The results are presented as relative changes in lattice constant normalized to give a $\Delta l/l$ of zero at a temperature of 20 K. For all lattice constants, the highest Q reflection possible was measured to maximize resolution. The a lattice constant was measured using the (4,0,0) reflection while the b lattice constant was measured using (0,8,0). The c lattice constant was measured from changes in the (0,0,1) peak position as this was the highest attainable (0,0,L) reflection due to geometrical constraints. The low Q reflection used in measuring c, coupled with the smaller magnitude of the spontaneous strain along this direction,[13] is responsible for the inferior results obtained for this lattice constant compared with the other two.

As is evident from Fig. 6, there exist spontaneous strains below T_{sp} for all three lattice constants. As a further consistency check, the magnitude of the changes in length were compared to those obtained in previous capacitance dilatometry measurements.[13] We obtain relative length changes between 12.5 and 14 K of 0.002%, 0.004%, and 0.0004% for a, b, and c respectively and these are in very close agreement with dilatometry measurements where changes of 0.002%, 0.004%, and 0.0003% were obtained.[13] We are therefore very confident that the novel approach employed in measuring the spontaneous strains is free of systematic error.

It is important to note that this represents a substantial improvement over previous x-ray diffraction results where measurements of the a-axis lattice constant indicated only a small upturn below T_{sp} and it had been suggested that the changes in the c-axis lattice constant were too small to be observed using such techniques.[10]

Our results show clear changes in both a and c and the spontaneous strains along both a and b have been measured with sufficient accuracy to allow for quantitative analysis.

A difficulty in extracting the spontaneous strain from the relative changes in lattice constant comes from determining the background, representing the expected thermal expansion in the absence of the phase transition. This contribution must be subtracted from the overall signal to isolate both the spontaneous strain below T_{sp} and any possible fluctuation effects near T_{sp}. Typically, the data well above the transition temperature would be fit to a suitable polynomial and this fit would be taken to represent this background. In order to provide an independent measure of this background, lattice constant measurements were also performed on a $Cu_{1-x}Zn_xGeO_3$ single crystal with x~0.05. The first studies on the influence of Zn impurities on the SP transition in $CuGeO_3$ indicated that this level of doping was sufficient to suppress the SP transition completely with only an antiferromagnetic phase transition at much lower temperatures.[28] However, later measurements suggest that a sample with this concentration of Zn should exhibit a SP transition at a temperature of about 11 K[29] in addition to a lower temperature Néel phase. While the precise nature of the phase diagram for the $Cu_{1-x}Zn_xGeO_3$ system is somewhat controversial, it is clear that Zn doping at the 5% level should be disruptive to the SP state displayed by the pure material, and thus this doped system may well serve for an appropriate background determination. The temperature dependence of the three lattice constants in the 5% Zn-doped sample was measured using the approach described above and the resultant relative changes are shown in Fig. 7. No evidence of spontaneous strains can be seen for temperatures between 10 K and 20 K indicating the absence of a SP transition over this temperature range. This appears inconsistent with the presence of a SP

transition at 11 K, as suggested by Sasago *et al.*,[29] and is consistent with the absence of such a transition as suggested by the earlier measurements of Hase *et al.*[28] Of course, any comparison between our present results and those of both Sasago *et al.*[29] and Hase *et al.*[28] rely on accurate determinations of the Zn concentration present in the crystals employed in these studies.

The solid lines in Fig. 7 represent the best polynomial fit describing the strain data for the 5% Zn-doped sample. The b lattice constant was fit to a T^4 behavior as expected for the low temperature thermal expansion of an insulator where the thermal expansion coefficient exhibits a T^3 behavior.[10]

$$b = b_o(1 + AT^4) \tag{3}$$

The a lattice constant could not be described by such an expression as it is observed to increase slightly at lower temperatures. These data were fit to:

$$a = a_o[1 + A(T - T_0)^2] \tag{4}$$

The best fit line shown yields a value of T_0 of about 11.5 K indicating an increase in the a lattice constant for temperatures below this value. One may argue this upturn to be indicative of a SP transition at this temperature, as would be expected from the phase diagram of Sasago *et al.*[29] However, no evidence of such a transition is seen in the b lattice constant where the magnitude of the spontaneous strain is greatly enhanced and hence, we conclude that no SP transition occurs in this sample over the temperature range of interest.

These best fit polynomial lines were taken to represent the thermal expansion of the pure material in the absence of the SP transition. Thus, the solid lines shown in Fig. 6 represent this background with the order parameter squared added for temperatures below T_{sp}=14.05 K. The order parameter was obtained from the best

fit to the superlattice reflection data shown in Fig. 2 using the modified power law [Eq. (2)]. As the measurements were carried out on the same crystal using the same thermometry, no adjustment of the transition temperature was required and the only tunable parameter is the overall amplitude [I_o in Eq. (2)]. This was scaled to provide agreement at T$\sim$12.5 K as this is the lowest temperature included in the order parameter measurements. The solid line in Fig. 6 gives a good description of the data for both the a-axis and b-axis lattice constants and, consequently, we conclude that the spontaneous strain does indeed scale well with the order parameter squared.

The importance of the independent background measurement can be appreciated by consideration of the dashed line in the upper panel of Fig. 6. This dashed line assumes a background which is taken from a polynomial fit to the high temperature (16 - 20 K) data for the a lattice constant on the pure sample. One can see that this provides an inferior description of the data and it is evident that the independent background determination is necessary to properly describe the data. The better agreement with the background obtained from the Zn-doped sample indicates that the upturn in the a-axis lattice constant observed for this sample is, in fact, a good representation of the true background occurring in pure $CuGeO_3$. This line still lies somewhat lower than the data, suggesting that the true increase in background strain for the a-axis lattice constant below about 11.5 K in the pure material is slightly greater than that observed in the 5% Zn-doped sample.

We have examined systematic deviations of the spontaneous strains from the order parameter squared. The data shown in Fig. 6 are subtracted from the model calculation represented by the solid lines in the same figure. The resulting subtracted data were binned into groups of 5 and the results for both the a-axis and b-axis are

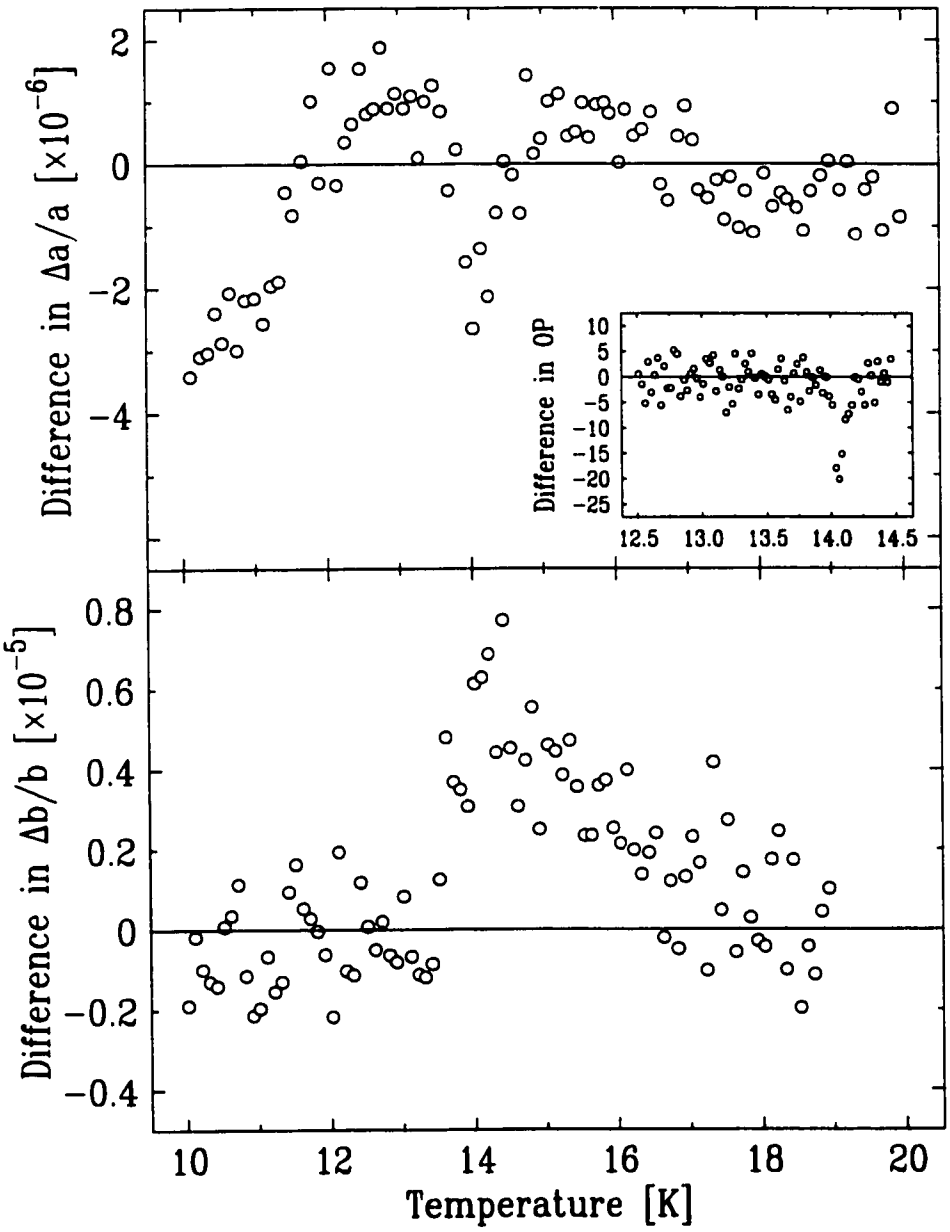

Figure 8: Difference between the data and the model of the spontaneous strain being proportional to the square of the order parameter (shown as the solid lines in Fig. 6). The inset shows the difference between the superlattice reflection data and the best fit to the power law with correction-to-scaling included, which is the solid line shown in Fig. 2. For both the thermal expansion and order parameter data, the resulting differences have been binned into groups of 5 to improve statistics.

shown in Fig. 8. As a point of reference, the difference between the superlattice reflection data and the order parameter fit, as shown in Fig. 2, is plotted in the inset. For the order parameter, significant deviations from the fit are only observed for temperatures within about 0.1 K of the transition temperature consistent with the absence of fluctuations. However, for both the a-axis and b-axis spontaneous strain measurements, significant deviations are observed within about 1 K of T_{sp} for the a-axis and within about 2 K for the b-axis. We interpret these differences as the presence of fluctuation effects in the spontaneous strain data which are less evident in the order parameter data. It is important to note that critical scattering from fluctuations in the order parameter has been observed in several previous measurements[5,12,25] and the absence of such scattering in our order parameter measurements is likely a consequence of poor signal-noise. However, this scattering is much more clearly observed in the spontaneous strain measurements. Deviations are also observed in the case of the a-axis lattice constant at low temperatures (< 12 K), however, this is a consequence of the slight difficulty in the background subtraction, as previously discussed. It is important to note that this slight difference in background does not alter the fluctuation effects observed in the vicinity of T_{sp} as this is largely determined by the shape of the order parameter and the value of the transition temperature.

V. SUMMARY

In summary, we have performed high temperature stability measurements of the order parameter associated with the SP transition in $CuGeO_3$ in the vicinity of T_{sp} and obtain a value of the exponent β of 0.345±0.03 at a transition temperature of 14.05±0.01 K. This value of β is consistent with conventional 3D universality and

strongly supports the theoretical argument[26] for 3D XY behavior, where the predicted value of β is 0.3455 $\pm$ 0.002.[27] Our results also demonstrate that the asymptotic critical region is rather narrow and this factor is most likely responsible for the inconsistency of critical exponent estimates obtained from previous measurements.

In addition, high resolution, high temperature stability x-ray diffraction measurements of relative lattice constant changes have been performed using a novel approach and this has allowed for a detailed comparison between the spontaneous strains present below T_{sp} and the order parameter. This comparison shows the spontaneous strains to be well accounted for by the order parameter squared with fluctuation effects present in the spontaneous strains, near T_{sp}, over a temperature range of at least 1 K. These fluctuation effects, easily observed in the spontaneous strain measurements, are much more difficult to observe in the order parameter with little evidence seen in our results. The nature of this additional contribution to the spontaneous strain is not clear, but the peak observed in the difference plots shown in Fig. 8 are reminiscent of those typically seen in measurements of heat capacity or the Q-dependent susceptibility due to the build up of critical fluctuations near typical continuous phase transitions.

ACKNOWLEDGMENTS

It is a pleasure to acknowledge helpful discussions with J. McGuire, T. Rööm, C.V. Stager, T. Timusk, and especially M. Plumer. This work was supported by NSERC of Canada and the OCMR of Ontario.

APPENDIX: THE FIRST CORRECTION-TO-SCALING AMPLITUDE

For a modified power law with the first correction-to-scaling term included, the amplitude of this term [represented as A in Eq. (2)] should be less than zero.

To appreciate this, let us consider the case of mean field theory where one commonly considers the solution to be:

$$m \sim t^{\frac{1}{2}} \tag{A1}$$

where m is the order parameter and $t = 1 - T/T_{sp}$. This result is only valid near the asymptotic critical region with the temperature near the transition temperature. In fact within mean field theory, the full solution of the order parameter as a function of temperature is known[30]:

$$m = tanh(\frac{T_{sp}}{T}m) \tag{A2}$$

where the order parameter is normalized to unity at T=0. The lowest order expansion of this transcendental equation for temperatures near T_{sp}, where m is small, results in:

$$m = 3^{\frac{1}{2}}(\frac{T}{T_{sp}})t^{\frac{1}{2}} \tag{A3}$$

So one does obtain the commonly used form shown in Eq. (A1), but even the lowest order expansion is modified by a term T/T_{sp}. One would expect the correction-to-scaling term in Eq. (2), when applied to mean field theory, to modify the order parameter in a manner consistent with the T/T_{sp} term shown in Eq. (A3). As this will act to reduce the order parameter for temperatures below T_{sp}, one would expect the same for the correction term ($1+At^{\Delta}$) in Eq. (2) and, hence, the first correction-to-scaling amplitude A should be less than zero.

References

[1] See J.W. Bray, L.V. Interrante, I.S. Jacobs, and J.C. Bonner, in *Extended Linear Chain Compounds*, edited by J.S. Miller (Plenum Press, New York, 1983), Vol. 3, p.353, and references therein.

[2] M. Hase, I. Terasaki, and K. Uchinokura, Phys. Rev. Lett. **70**, 3651 (1993).

[3] M. Nishi, O. Fujita, and J. Akimitsu, Phys. Rev. B **50**, 6508 (1994).

[4] O. Fujita, J. Akimitsu, M. Nishi, and K. Kakurai, Phys. Rev. Lett. **74**, 1677 (1995).

[5] J.P. Pouget, L.P. Regnault, M. Ain, B. Hennion, J.P. Renard, P. Veillet, G. Dhalenne, and A. Revocolevschi, Phys. Rev. Lett. **72**, 4037 (1994).

[6] O. Kamimura, M. Terauchi, M. Tanaka, O. Fujita, and J. Akimitsu, J. Phys. Soc. Jpn. **63**, 2467 (1994).

[7] H. Völlenkle, A. Wittman, and H. Nowotny, Monatsh. Chem. **98**, 1352 (1967).

[8] M. Hidaka, M. Hatae, I. Yamada, M. Nishi, and J. Akimitsu, J. Phys.:Condens. Matter **9**, 809 (1997).

[9] K. Hirota, D.E. Cox, J.E. Lorenzo, G. Shirane, J.M. Tranquada, M. Hase, K. Uchinokura, H. Kojima, Y. Shibuya, and I. Tanaka, Phys. Rev. Lett. **73**, 736 (1994).

[10] Q.J. Harris, Q. Feng, R.J. Birgeneau, K. Hirota, K. Kakurai, J.E. Lorenzo, G. Shirane, M. Hase, K. Uchinokura, H. Kojima, I. Tanaka, and Y. Shibuya, Phys. Rev. B **50**, 12606 (1994).

[11] M. Fujita, M. Arai, K. Ubukata, H. Ohta, M. Mino, M. Motokawa, K. Knight, R.

Ibberson, J.B. Forsyth, S.M. Bennington, O. Akimitsu, and J. Fujita, Physica B **213 & 214**, 288 (1995).

[12] Q.J. Harris, Q. Feng, R.J. Birgeneau, K. Hirota, G. Shirane, M. Hase, and K. Uchinokura, Phys. Rev. B **52**, 15420 (1995).

[13] H. Winkelmann, E. Gamper, B. Büchner, M. Braden, A. Revcolevschi, and G. Dhalenne, Phys. Rev. B **51**, 12884 (1995).

[14] T. Lorenz, U. Ammerahl, T. Auweiler, B. Büchner, A. Revcolevschi, and G. Dhalenne, Phys. Rev. B **55**, 5914 (1997).

[15] M. Saint Paul, P. Monceau, and A. Revolevschi, Solid State Commun. **93**, 7 (1995).

[16] S. Sahling, J.C. Lasjaunias, P. Monceau, and A. Revcolevschi, Solid State Commun. **92**, 423 (1994).

[17] X. Liu, J. Wosnitza, H. von Lohneysen, and R.K. Kremer, Z. Phys. B **98**,163 (1995); **75**, 771 (1995).

[18] D.E. Moncton, R.J. Birgeneau, L.V. Interrante, and F. Wudl, Phys. Rev. Lett. **39**, 507 (1977).

[19] B. van Bodegom, B.C. Larson, and H.A. Mook, Phys. Rev. B **24**, 1520 (1981).

[20] M.D. Lumsden, B.D. Gaulin, and H. Dabkowska, Phys. Rev. Lett. **76**, 4919 (1996).

[21] J.E. Lorenzo, K. Hirota, G. Shirane, J.M. Tranquada, M. Hase, K. Uchinokura, H. Kojima, I. Tanaka, and Y. Shibuya, Phys. Rev. B **50**,1278 (1994).

[22] M. Fujita, K. Ubukata, M. Arai, T. Tonegawa, M. Mino, M. Motokawa, K. Knight, B. Forsyth, S.M. Bennington, J. Akimitsu, and O. Fujita, Physica B **219 & 220**,

95 (1996).

[23] A. Aharony and G. Ahlers, Phys. Rev. Lett. **44**, 782 (1980).

[24] M.F. Collins, *Magnetic Critical Scattering* (Oxford University Press, New York, 1989).

[25] K. Hirota, G. Shirane, Q.J. Harris, Q. Feng, R.J. Birgeneau, M. Hase, and K. Uchinokura, Phys. Rev. B **52**, 15412 (1995).

[26] M.L. Plumer, Phys. Rev. B **53**, 594 (1996).

[27] J.C. le Guillou and J. Zinn-Justin, Phys. Rev. B **21**, 3976 (1980).

[28] M. Hase, I. Terasaki, Y. Sasago, and K. Uchinokura, H. Obara, Phys. Rev. Lett. **71**, 4059 (1993).

[29] Y. Sasago, N. Koide, K. Uchinokura, Michael C. Martin, M. Hase, K. Hirota, and G. Shirane, Phys. Rev. B **54**, R6835 (1996).

[30] See, for example, M. Plischke and B. Bergersen, *Equilibrium Statistical Physics* (Prentice Hall, New Jersey, 1989).

Chapter 5

Critical Properties in Doped $CuGeO_3$

With a firm understanding of the critical properties associated with the SP transition in pure $CuGeO_3$, we decided to investigate these properties for doped samples in search for any systematic differences in the presence of impurities. Consequently, we performed measurements similar to those reported in Chapter 4 on several different samples with several different dopants. In particular, we have performed measurements on samples with Zn^{2+} and Cd^{2+} substituted for Cu^{2+} and with Ge^{4+} replaced with Si^{4+}. These measurements are presented in the following article entitled, "Critical phenomena at the spin-Peierls transition in doped $CuGeO_3$" published in Physical Review B, Vol. 58, No. 18, pp.12252-12259, November 1, 1998.

Critical Phenomena at the Spin Peierls Transition in Doped $CuGeO_3$

M.D. Lumsden, B.D. Gaulin, and H. Dabkowska

Department of Physics and Astronomy, McMaster University,

Hamilton, Ontario, L8S 4M1, Canada

Abstract

We have examined the critical properties of several lightly doped samples of $CuGeO_3$ through x-ray diffraction measurements of the order parameter. We obtain an exponent β consistent with that obtained for pure $CuGeO_3$, where β=0.345±0.03, for 0.1% Zn-doped, 0.2% Si-doped, and 0.4% Si-doped samples. Measurements on two 0.1% Cd-doped samples produce results clearly inconsistent with those for the pure compound and well described by mean field behaviour. This change in critical phenomena from three-dimensional behaviour to mean field behaviour is interpreted as a consequence of local strain fields induced by the presence of larger dopant ions. Lattice constant measurements on the same doped samples indicate the presence of spontaneous strains which scale with the square of the order parameter, as was the case for pure $CuGeO_3$.

Reprinted from Physical Review B Vol.58 No.18 pp.12252-12259 (1998)

I. INTRODUCTION

The spin-Peierls (SP) phase transition has received renewed attention in recent years following the discovery of the first inorganic SP system, $CuGeO_3$.[1] The SP transition occurs in Heisenberg S=1/2 spin chains which are strongly coupled to the three-dimensional phonons of the lattice. These chains can lower their magnetic energy via a lattice dimerization with the concomitant appearance of an energy gap in the spectrum of magnetic excitations separating a singlet ground state from a triplet of excited states. The characteristic drop in magnetic susceptibility due to the nonmagnetic singlet ground state,[1] the lattice dimerization,[2,3] and the energy gap[4,5] have all been observed in $CuGeO_3$ and it is well established that that system does indeed undergo a SP transition at a transition temperature (T_{sp}) of about 14 K.

Prior to the discovery of $CuGeO_3$, the SP transition had only been observed in a few complex organic systems, TTF-Cu(Au)BDT and $MEM(TCNQ)_2$, containing a single unpaired electron localized on the molecular units with a subsequent low density of magnetic moment.[6] $CuGeO_3$ has the S=1/2 spins localized on the Cu^{2+} ions which form effective 1D spin chains along the c-axis. The unit cell of $CuGeO_3$ is orthorhombic with lattice constants a=4.81 Å, b=8.47 Å, and c=2.94 Å.[7] The crystal structure consists of chains of CuO_4 octahedra separated by chains of GeO_3 tetrahedra both of which stack along the c-axis.

The effects of impurities on the SP transition had not been examined in the past due the low solubility of dopants in previously known organic SP systems. $CuGeO_3$ has been shown to readily accept substituted ions on either the Cu^{2+} or the Ge^{4+} sites and this touched off a number of interesting experiments performed with various dopants (most commonly nonmagnetic (Zn^{2+})[8–11] or magnetic (Ni^{2+})[9,10] substituted

for Cu^{2+} as well as (Si^{4+})[9,12–14] for Ge^{4+}). The presence of these dopants leads to a sharp decrease in the SP transition temperature, and the coexistence, at temperatures below the SP transition temperature, of an additional long-range ordered Néel phase.[8–14] The exact forms of the phase diagrams as a function of concentration have been well examined but still remain somewhat controversial.[8,9,11–13]

One motivation in examining the critical properties of doped samples of $CuGeO_3$ is based on a heuristic argument due to Harris[15] regarding the effects of impurities on critical phenomena (this heuristic argument was later confirmed by renormalization group studies[16]). He argued that the critical behaviour would be unaltered by small randomness provided the exponent α, associated with the specific heat, was less than zero. For conventional 3D systems, this means the only affected system would be the Ising system with both XY and Heisenberg systems having α values less than zero.[17] For this reason, measurements of lightly doped $CuGeO_3$ systems may allow different 3D universality classes to be differentiated in the pure material. A potential caveat is that the difference between the pure and dilute Ising values for the exponent β is about 0.024 (pure Ising: 0.326[17], random Ising: 0.35[18]) and this difference is at the limit of our sensitivity (the value found for the pure material was 0.345 ± 0.03[19]). However, the effects of impurities on the critical properties associated with this novel ordered state are clearly of interest in their own right and, as will be discussed, the critical behaviour is unexpectedly rich changing dramatically in the presence of certain dopants. Measurements have been performed on samples with three different dopant ions, Zn^{2+} and Cd^{2+} replacing Cu^{2+}, and Si^{4+} substituted for Ge^{4+}. The ionic radii of Zn^{2+}, Cd^{2+}, and Cu^{2+} are 0.74, 0.97, and 0.72 Å respectively while those of Si^{4+} and Ge^{4+} are 0.42 and 0.52 Å respectively[20]. Thus, Si^{4+} represents a smaller dopant ion, Zn^{2+} a dopant ion of roughly the same size, and Cd^{2+} a substantially

larger dopant ion. This series of samples should allow for comparisons of the critical phenomena as a function of relative ionic size.

II. EXPERIMENTAL DETAILS

Single crystals of $CuGeO_3$, $Cu_{1-x}Zn_xGeO_3$ ($x \sim 0.001$), $CuGe_{1-x}Si_xO_3$ ($x \sim 0.002$ and $x \sim 0.004$) and $Cu_{1-x}Cd_xGeO_3$ ($x \sim 0.001$) were grown from CuO flux by slow cooling. The dopant concentrations were kept low in an attempt to ensure good sample homogeneity which is essential for proper estimates of critical exponents, a point which will be discussed in more detail later. To determine dopant concentrations, single crystals were placed in an HCl solution and gently heated until completely dissolved. Concentrations of Zn, Si, and Cd were determined by atomic emission spectroscopy. In this technique, a high-temperature inductively coupled plasma source is used to excite the atoms in the solution. These atoms then de-excite and the resulting emitted light is analyzed with a high resolution spectrometer. Concentrations were measured on several samples from the same crystal growth to ensure reproducible results. In addition, for the Zn-[8] and Si-doped[12] samples, the phase diagrams as a function of temperature have been studied in some detail. This allows the transition temperature to be a good measure of the dopant concentration. For the Zn-doped and two Si-doped samples, the measured transition temperature and the inferred concentration from previous phase diagram measurements are in agreement with the results obtained from the atomic emission measurements. For the Cd-doped samples, two different compositions were investigated, but both were found to have roughly the same transition temperature, indicating comparable concentrations of about 0.1% Cd despite the fact that the concentrations used in the starting materials were 1%

and 5%. This indicates a rather low solubility limit for Cd, as expected from the difference in ionic radius between Cu^{2+} and Cd^{2+} (0.72 Å for Cu^{2+} compared with 0.97 Å for Cd^{2+}).[20] However, the transition temperature is slightly reduced from that observed in the pure compound indicating a nonzero amount of Cd present in both crystals.

All samples were loaded in a Be can in the presence of a He exchange gas which was mounted on the cold finger of a closed-cycle He refrigerator. For all the measurements, the temperature was stable to approximately 0.005 K over the temperature range of interest. The incident radiation was Cu Kα radiation from an 18 kW rotating anode x-ray generator and this was further monochromatized using a vertically focusing PG (0,0,2) monochromator crystal. In all cases, the (1/2,5,1/2) superlattice reflection was examined for the order parameter analysis to provide directly comparable results between samples.

III. ORDER PARAMETER

A. Results

As mentioned above, sample homogeneity is essential in the determination of critical properties for these doped samples. Inhomogeneity can lead to a distribution of transition temperatures producing significant curvature in the order parameter near T_{sp} and making detailed analysis very difficult. Figure 1 shows the results for the peak intensity of the (1/2,5,1/2) reflection, proportional to the order parameter squared, for pure $CuGeO_3$, as well as for the Zn and Si-doped samples. The intensity is normalized to unity at a temperature about 1.5 K below the respective transition temperature. The transition temperature is clearly reduced for all doped samples and the measured

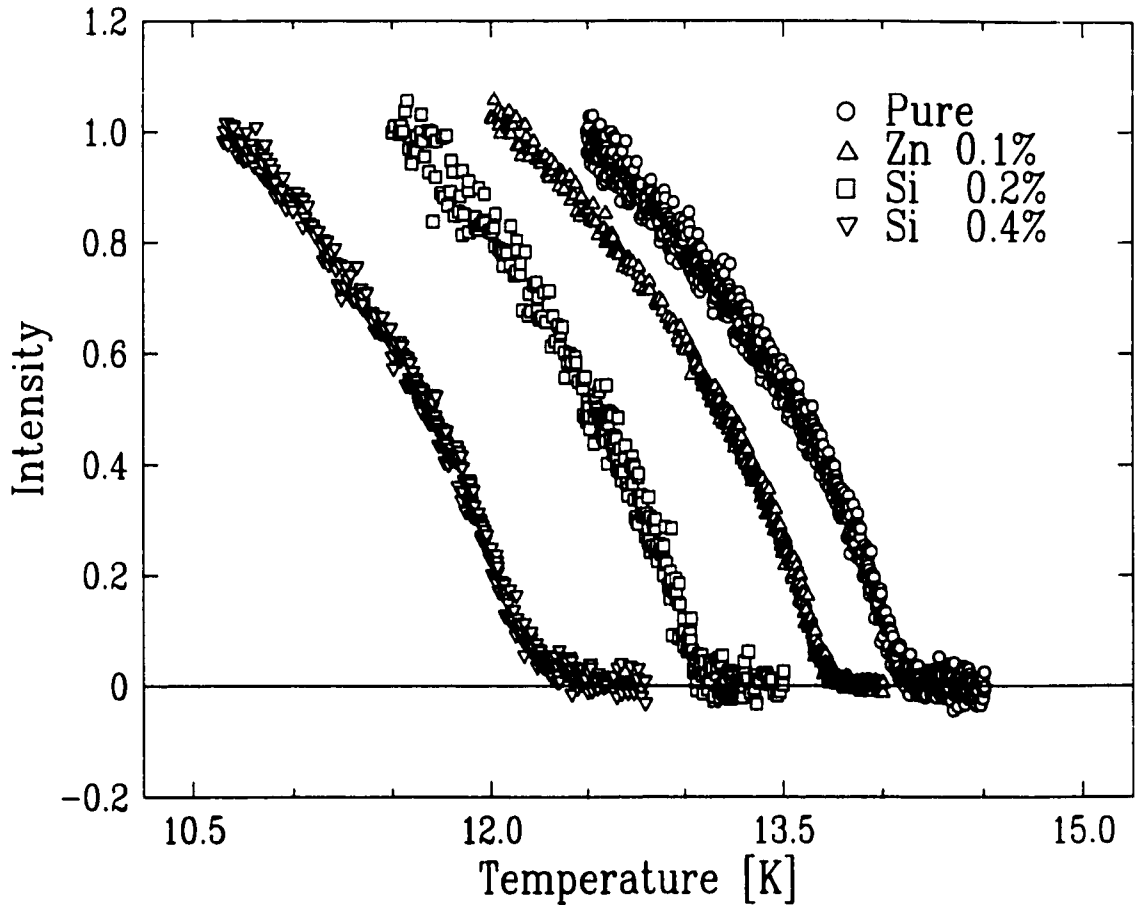

Figure 1: Peak intensity of the (1/2,5,1/2) reflection, normalized to unity at roughly 1.5 K below T_{sp}, for pure $CuGeO_3$, 0.1% Zn-doped, 0.2% Si-doped, and 0.4% Si-doped samples. The transitions in the doped samples are nearly as sharp as that observed in the pure sample indicating no substantial gradients in doping concentration. The order parameter of the highest concentration Si-doped sample exhibits slightly more curvature near T_{sp} demonstrating the difficulty in obtaining homogeneous samples as the amount of dopant increases.

T_{sp} and concentrations are consistent with the phase diagrams observed in earlier measurements of both Zn-doped[8] and Si-doped[12] samples. One can clearly see, for the Zn and lowest concentration Si-doped samples, that no significant curvature is observed near the transition temperature indicating homogeneous samples. The last data set included, for the 0.4% Si-doped sample, shows significant curvature near the transition temperature indicating the difficulties that can arise in maintaining homogeneity in samples with higher concentration of dopant. As is clear from the data, extraction of the proper critical behaviour from fits to the 0.4% Si-doped data will be more difficult as the data very near T_{sp} is unusable.

Prior to performing extensive quantitative analysis of the order parameter, it is useful to compare the raw data obtained for the doped materials to that for the pure compound. Previous analysis on pure $CuGeO_3$ yielded a value of the exponent β of 0.345±0.03 consistent with 3D XY behaviour.[19] Figures 2 and 3 show the peak intensity data for the doped samples, background subtracted, plotted as a function of $T - T_{sp}$, and normalized to unity at a $T - T_{sp}$ of -1.5 K, overlayed on the data for the pure compound. Figure 2 shows the results for the Zn and two Si-doped samples and in all three cases, excellent agreement with the pure data is observed indicating critical behaviour very similar to that obtained for the pure compound. There is a difference for the 0.4% Si-doped sample near the transition temperature, as shown in the inset of Fig. 2 where the data in the immediate vicinity of the transition temperature is magnified. This difference can be attributed to an inhomogeneous distribution of dopants as was suggested from Fig. 1. For this sample, the quantitative analysis will be performed up to a maximum temperature chosen so as to avoid this rounding near T_{sp}.

The only compound which showed clear deviation from the data obtained for

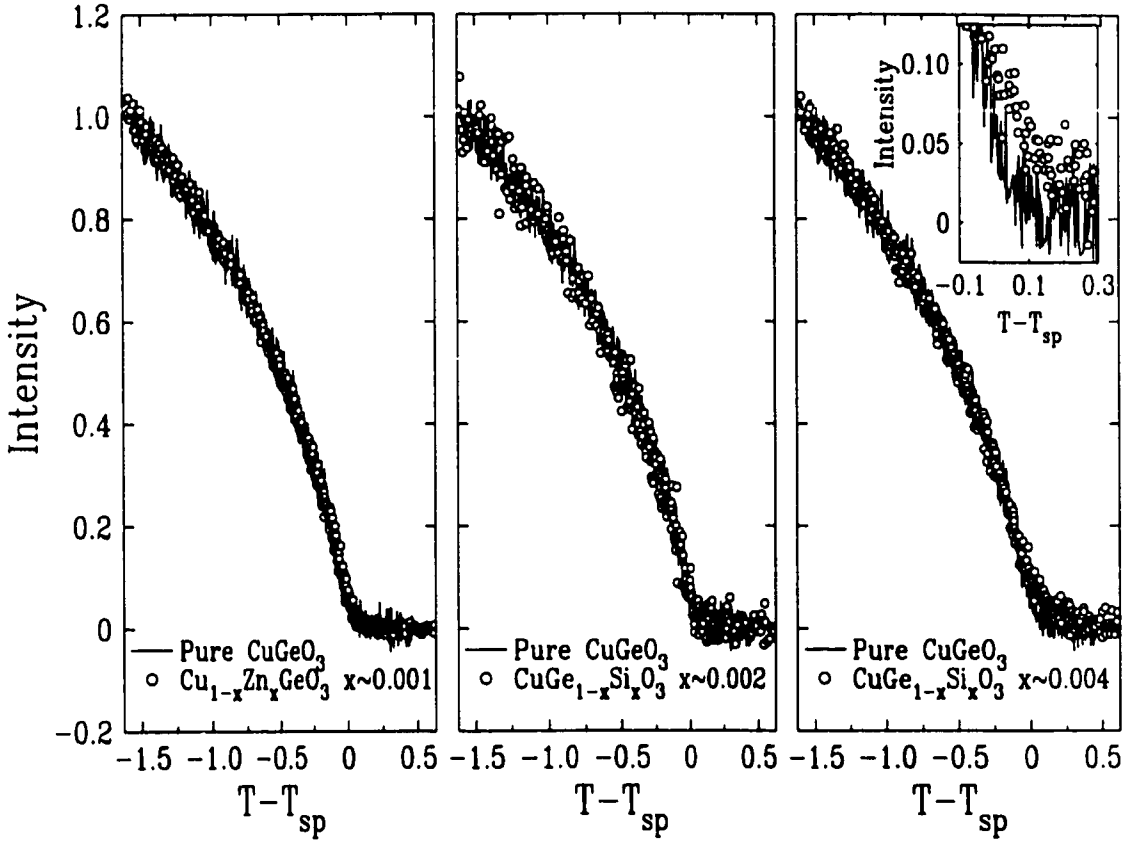

Figure 2: Peak intensity data plotted as a function of $T-T_{sp}$ and normalized to unity at $T-T_{sp}$=-1.5K. The left panel shows the results for 0.1% Zn-doped sample overlayed on the results from the pure sample. The centre and right panel show the same results for the 0.2% and 0.4% Si-doped samples, respectively. In all three cases, the data from the doped samples are in excellent agreement with that from pure $CuGeO_3$ suggesting no differences in the critical properties. The 0.4% Si-doped sample shows deviations from the pure data near the transition temperature, as shown in the inset which magnifies the region near T_{sp}, which can be attributed to an inhomogeneous distribution of dopant throughout the crystal.

the pure material is that for the Cd-doped samples as shown in Fig. 3. This data shows results from two samples taken from two independent sample growths. The data for sample 1 (left panel) shows clear deviation from the pure data over the entire investigated temperature range and the intensity seems to be exhibiting linear behaviour over this range. Measurements were also performed on a second Cd-doped sample with a different starting concentration of Cd and the results for this second sample are shown in the right panel of Fig. 3. Although less dramatic than the first Cd sample, there are again clear deviations from the pure data and, once again, the behaviour seems rather linear for temperatures within about 0.6 K of the transition temperature. Thus, for both Cd samples, the asymptotic behaviour of the order parameter appears to be linear suggesting a value of the exponent β consistent with mean field behaviour (2β=1).[21] To further emphasize this point, the solid line shown in both panels represents the lowest order expansion of the full mean field solution, namely,[21]

$$m = 3^{\frac{1}{2}} t^{\beta} \left(\frac{T}{T_{sp}} \right) \tag{1}$$

where the reduced temperature $t = 1 - T/T_{sp}$. As the intensity at the superlattice peak is proportional to the square of the order parameter, the resulting intensity is

$$I = I_o t^{2\beta} \left(\frac{T}{T_{sp}} \right)^2 + background. \tag{2}$$

This form describes the data very well in the vicinity of the transition temperature confirming the suggested mean field behaviour as can be clearly seen in Fig. 3. An important point of note, as was the case with the other doped samples, is that no obvious rounding in the order parameter is observed near the transition temperature suggesting, once again, homogeneous samples.

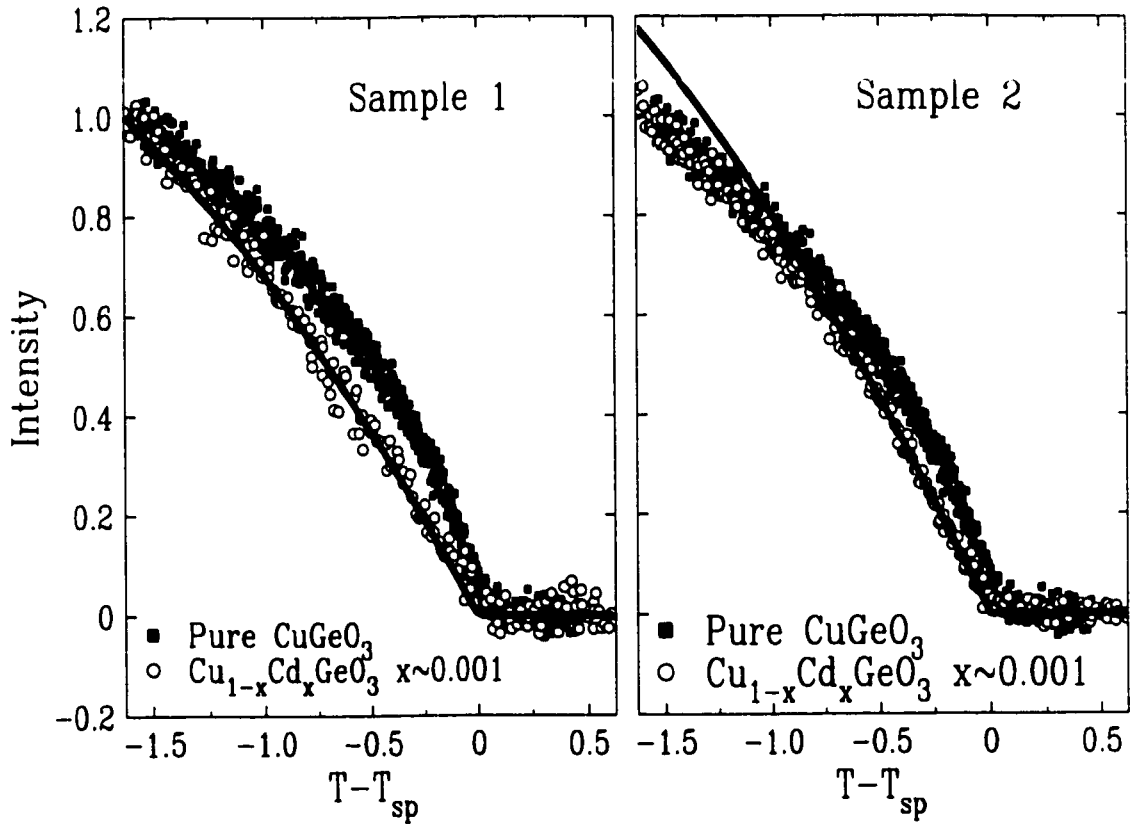

Figure 3: Peak intensity data plotted as a function of $T - T_{sp}$ normalized to unity at 1.5 K below the transition temperature for two samples of $Cu_{1-x}Cd_xGeO_3$ with x~0.001. The two crystals were taken from two independent sample growths with two different starting concentrations of Cd (1% for sample 1 and 5% for sample 2). The data are superposed on that obtained for pure $CuGeO_3$ and in both cases clear deviations are observed. The solid line represents the lowest order expansion of the full mean field solution [Eq. (2)] and we can see good agreement in both cases in the vicinity of the transition temperature indicating mean field behaviour.

B. Analysis

In order to quantitatively describe the critical behaviour of the order parameter, the data was fit to a power law in the reduced temperature, t=1-T/T_{sp},

$$Intensity = I_o t^{2\beta} + background. \tag{3}$$

This power law behaviour is expected to be valid in the asymptotic critical region, near T_{sp}, where the length scale associated with fluctuations in the order parameter dominates over all other relevant length scales. As the temperature is lowered below the asymptotic region, the power law behaviour must be modified by successive correction to scaling confluent singularity terms[22], the first of which is included in the modified power law of Eq. (4).

$$Intensity = I_o t^{2\beta}(1 + At^{\Delta}) + Background \tag{4}$$

where the exponent Δ is known to have an approximate value of 0.5 for three dimensional systems.[22]

For mean field behaviour, the first correction to the simple power law, Eq. (3), is known exactly and is represented by the $(T/T_{sp})^2$ term as shown in Eq. (2). Thus for the Cd-doped samples, where we expect mean field behaviour, the modified form of the power law will be that represented by Eq. (2).

From previous work on pure $CuGeO_3$, the extracted value of the exponent β using the simple power law [Eq. (3)], was strongly dependent on the range of data included in the fits.[19] The fits to the modified power law [Eq. (4)] were rather robust, but the value of β extracted from fits to the ordinary power law [Eq. (3)], increased systematically over the entire range of temperatures examined. This is shown in the upper panel of Fig. 4 where the results from the previous analysis on the pure compound

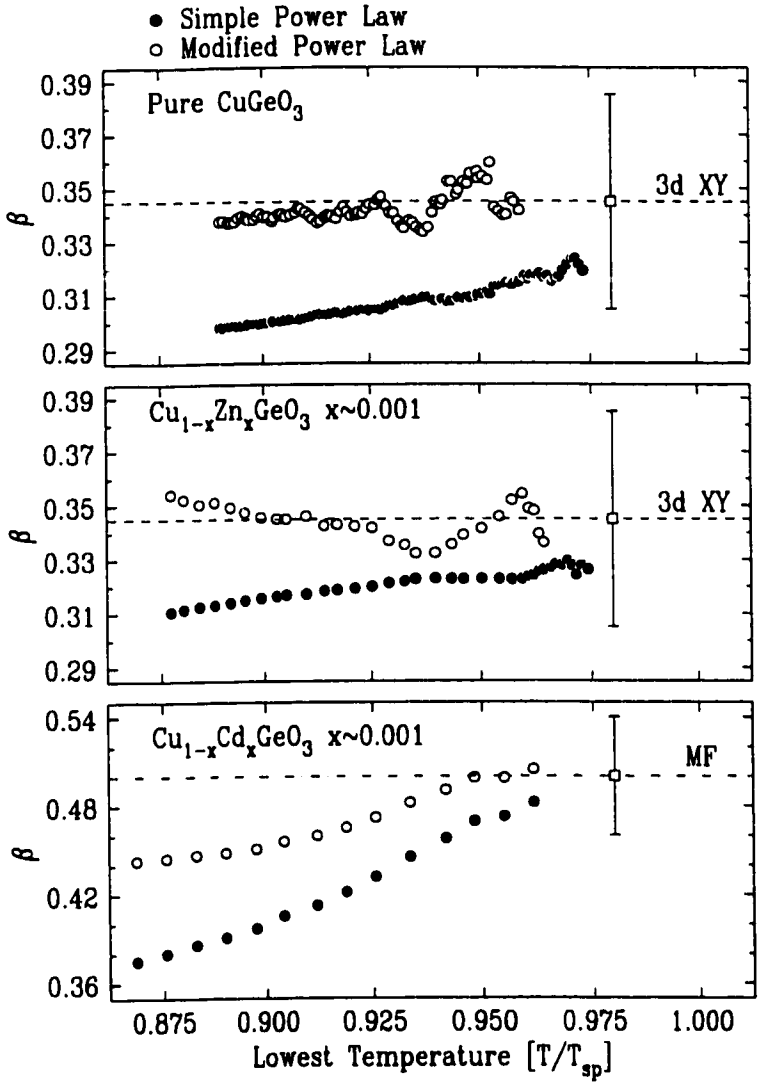

Figure 4: Value of the exponent β as a function of the lowest temperature included in the fits (plotted as T/T_{sp}) for pure $CuGeO_3$, the 0.1% Zn-doped sample and the 0.1% Cd-doped sample. The results consist of values of β extracted from best fit curves to an ordinary power law [Eq. (3)] as well as a modified power law with the first correction term included (this is represented by Eq. (4) for the pure and Zn-doped samples and Eq. (2) for the Cd-doped sample). As suggested by the data presented in Fig. 2, the results of the pure $CuGeO_3$ and the Zn-doped compounds are consistent with one another and also consistent with 3D XY universality. The error bars shown on the plot are largely a consequence of the uncertainty in T_{sp}. The third panel shows the results for the Cd-doped sample and, as suggested by the data shown in Fig. 2, this clearly deviates from the results obtained for pure $CuGeO_3$. It gives a value of β consistent with mean field behaviour and clearly inconsistent with 3D XY behaviour.

are presented. This plot represents the best fit value of β as determined from both the ordinary and modified power laws plotted as a function of the lowest temperature (relative to T_{sp}) included in the fits as this lowest temperature is increased toward the transition temperature. Theoretical expectation for 3D XY universality is represented by the dashed line. The two lower panels of Fig. 4 represent the same results obtained from the analysis on the Zn-doped sample and one Cd-doped sample (sample 2 in Fig. 3). The modified power law for the Cd-doped data, represents the exact lowest order expansion of the mean field result [Eq. (2)]. The results for the Zn-doped sample again show robust behaviour for the modified power law and a clear upward trend for the ordinary power law as the lowest temperature employed in the fits is increased. In addition, the values for the exponent are very close to that obtained for the pure material confirming the qualitative arguments made by examination of the raw data (Fig. 2).

However, also as indicated by the raw data, there is a very definite difference observed for the Cd-doped samples. Here, the value of β varies rather systematically as a function of temperature range, for both the ordinary and modified power laws with a much stronger variation for the ordinary power law. The theoretical expectation for mean field behaviour is represented by the dashed-dot line. The two curves seem to be converging as the lowest temperature employed in the fits approaches the transition temperature and the asymptotic behaviour indicates a value of β of about 0.5 consistent with mean field results. This value of β is clearly far removed from 3D XY behaviour observed in pure $CuGeO_3$.

Figure 5 shows the same results for the two Si-doped samples. In both cases, the modified power law, Eq. (4), produces rather robust results while the value of β obtained from the ordinary power law increases systematically as the lowest

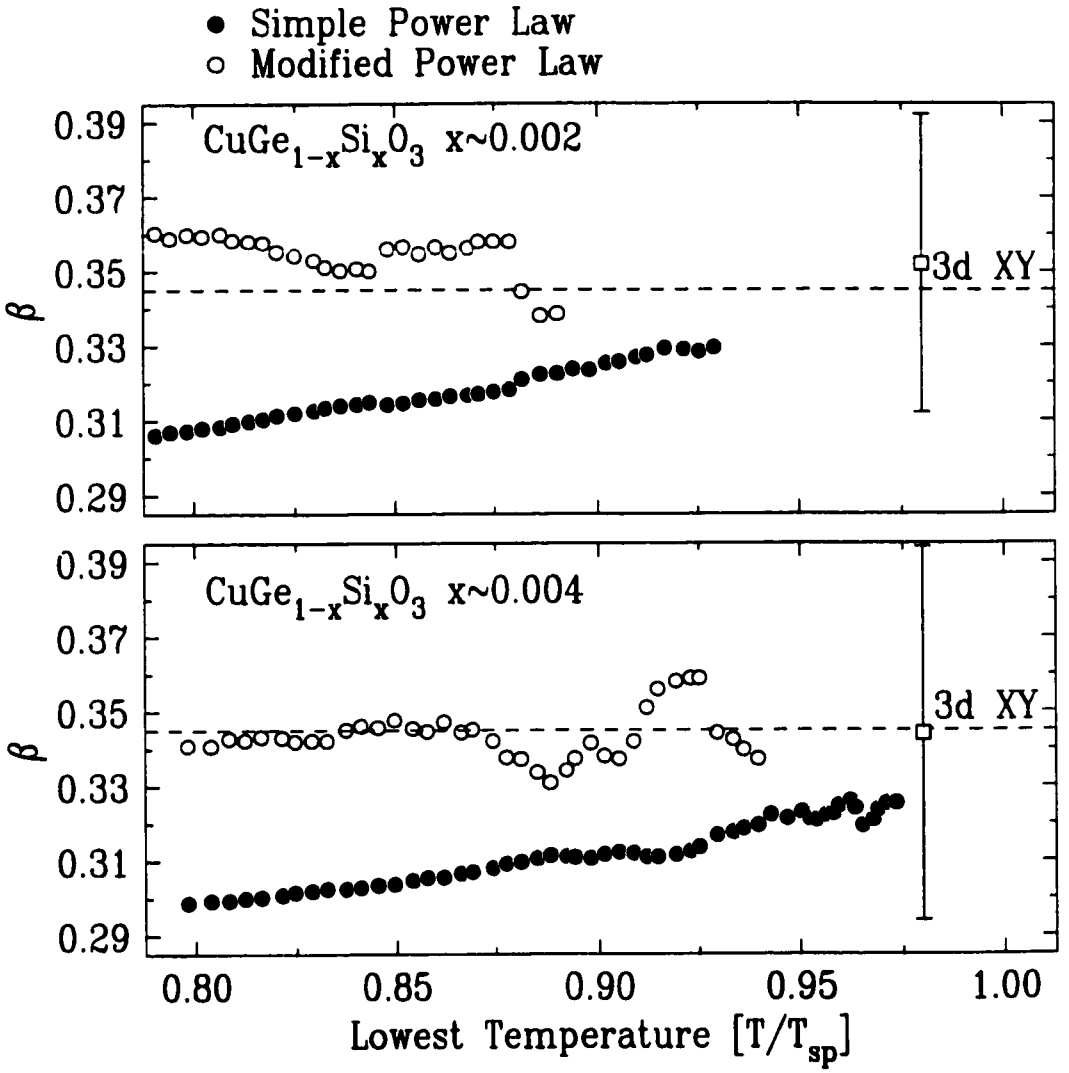

Figure 5: Values of the exponent β as a function of the lowest temperature included in the fits (plotted as T/T_{sp}) for the 0.2% Si-doped and 0.4% Si-doped samples as determined by fits to both an ordinary power law [Eq. (3)] and a power law with the first correction-to-scaling term included [Eq. (4)]. As suggested by the data presented in Fig. 2, the results for both samples are consistent with those obtained for pure $CuGeO_3$ and also consistent with 3D XY universality. Again, the uncertainty represented by the error bars is largely a result of the uncertainty in T_{sp}. The larger error bar on the higher doped Si sample is a consequence of the increased difficulty in determining the transition temperature with the rounding (due to concentration gradients) present near T_{sp}.

temperature employed in the fits is increased. The curves for the 0.2% Si-doped sample, shown in the upper panel of Fig. 5, were not able to be extended as close to the transition temperature as that for the other samples due to poorer quality of data as can be seen in the examination of the raw data in Fig. 1. Nevertheless, the value of β for both Si-doped samples are very consistent with the results obtained for the pure compound confirming the qualitative conclusions made previously.

In all panels of Figs. 4 and 5, the resulting values of β and the corresponding error bars are represented by the single square data point. It is clear in all cases that the error in the value of the exponent is considerably larger than the spread in the fitted values represented on these figures. In fact, the error in the value of β, as is the case with almost all critical exponent determinations, is dominated by the error in the chosen value of the transition temperature. The curves presented in Figs. 4 and 5 are all obtained from fits with a fixed transition temperature and thus don't reflect the true error in the critical exponent which was obtained by detailed analysis of the dependence of these curves on the chosen transition temperature.

C. Discussion

The final results for the extracted value of the critical exponent β as well as the value of the transition temperature are summarized in Table 1. This table shows the dopant ion, concentration of this dopant, the replaced ion, the change in ionic radius (ionic radius of dopant - ionic radius of replaced ion), and the extracted transition temperature and exponent β. The larger error in β for the 0.4% Si-doped sample is a consequence of the larger error in the value of the transition temperature due to inhomogeneities in dopant concentration as was discussed earlier. The last row of

Dopant	Conc.(%)	Replaced Ion	Δi.r.	T_{sp}	β
-	-	-	-	14.05±0.02	0.345±0.03
Zn^{2+}	0.1	Cu^{2+}	0.02	13.68±0.02	0.345±0.03
Si^{4+}	0.2	Ge^{4+}	-0.11	13.03±0.03	0.355±0.04
Si^{4+}	0.4	Ge^{4+}	-0.11	12.15±0.05	0.345±0.06
Cd^{2+}	0.1	Cu^{2+}	0.25	13.93±0.03	0.50±0.04
†Ga^{3+}	1.0	Ge^{4+}	0.09	13.3	0.5

Table 1: Summary of the order parameter analysis for the pure and lightly doped $CuGeO_3$ samples. The values for the ionic radii[20] are taken to be Cu^{2+} 0.72 Å, Ge^{4+} 0.52 Å, Zn^{2+} 0.74 Å, Si^{4+} 0.42 Å, Cd^{2+} 0.97 Å, and Ga^{3+} 0.62 Å. †The values for the Ga^{3+} doped samples were taken from the Raman scattering measurements of a folded phonon.[23]

this table shows approximate results for a Ga-doped sample obtained from Raman scattering measurements of a folded phonon by Weiden et. al.[23] This point will be discussed in more detail later.

The results for the pure, Zn-doped, and Si-doped samples are all consistent with one another. In terms of the Harris criterion, this suggests results consistent with 3D XY behaviour and inconsistent with 3D Ising behaviour where a change in critical properties is expected. As mentioned before, the expected change in β is from 0.326 in the pure Ising model to 0.35 in the random Ising system. While this change in β is within the uncertainty for all extracted exponents, the change in the nominal value of β for all four measurements is much less than the uncertainty in any particular estimate, indicating that the results are very consistent with one another. This provides another piece of evidence supporting 3D XY universality, but it is not definitive as some crossover from pure to random critical behaviour is expected and it is not clear

that such a crossover is complete for the examined doped samples.

One result which is clear is that the extracted exponent β for the Cd-doped samples is inconsistent with that for the pure compound and consistent with mean field behaviour. Similar results are seen in a Ga-doped $CuGeO_3$ sample where Ga^{3+} replaces Ge^{4+}.[23] The measurements on this sample were Raman scattering measurements of the intensity of a folded phonon. This intensity is not obviously proportional to the square of the order parameter, but the same measurement on pure $CuGeO_3$ produces data consistent with diffraction measurements of the intensity of superlattice Bragg peaks. Consequently, we infer from this that this Raman scattering intensity of this folded phonon is indeed proportional to the square of the order parameter. The results for the Ga-doped samples indicated linear behaviour in this phonon intensity, similar to the linear behaviour observed in our measurements of Cd-doped $CuGeO_3$ and, consequently, we suggest a value of the exponent β of 0.5 and this is indicated by the last row in Table 1.

To interpret these results, let us consider the change in ionic radius (dopant - replaced) as shown in Table 1. We can see that if this quantity is very slightly positive (Zn-doped $CuGeO_3$) or negative (Si-doped $CuGeO_3$), no change in critical properties is observed. However, if the change in ionic radius is substantially positive (Cd and Ga-doped $CuGeO_3$), the critical phenomena change from 3D XY behaviour to mean field. This suggests critical phenomena which are dependent on the presence of relatively long-range local strain fields induced by the presence of a larger dopant ion.

To emphasize this point, Fig. 6 shows the exponent β plotted as a function of a quantity which we take as a measure of the internal strain present, namely, the the relative change in ionic radius. In this figure, we see that a change in ionic

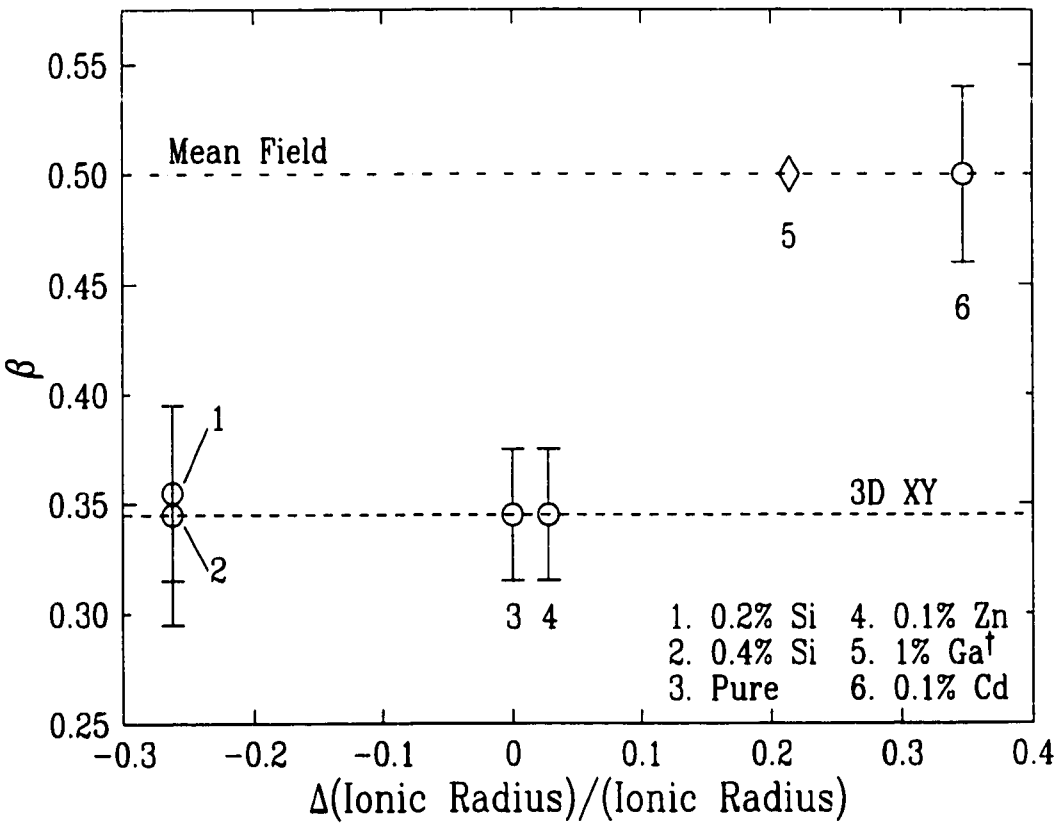

Figure 6: Values of the exponent β, determined by the fits to the modified power law, as a function of the relative change in ionic radius of the dopant compared to the substituted ion. One can see that for a change in ionic radius which is substantially positive, there appears to be a change in the critical phenomena from 3D XY behaviour to mean field behaviour and this jump appears to be independent of concentration. The diamond symbol † represents results taken from Raman scattering measurements of a folded phonon on a Ga^{3+} doped sample.[23]

radius which is slightly positive or negative yields an exponent consistent with 3D XY behaviour whereas a substantially positive change in ionic radius produces mean field results. This change in behaviour seems independent of the concentration of dopant as is evidenced by the very small amount of Cd present in the crystals studied in this paper (in addition, the Ga-doped measurements were performed on several samples with different levels of dopant and no change in behaviour was observed[23]). It seems reasonable that it is the long-range nature of these strain fields which drives the system to mean-field behaviour. This suggests that internal strains are a relevant perturbation to the order parameter, which is not surprising as the SP transition is magnetoelastic in nature and dependent on the elastic properties of the lattice. Related to this is the fact that a spontaneous strain is known to accompany the SP phase even in pure $CuGeO_3$.[24–26]

As a final point of note, we feel that the change in critical properties for the Cd-doped samples have no relevance with respect to the Harris criterion and the inferred universality of pure $CuGeO_3$. The Harris criterion assumes randomness induced by the simple removal of spins from a model system and in no way takes into account changes in the local lattice structure and the effects of these changes on the critical behaviour.

IV. LATTICE CONSTANTS

Previous high resolution measurements of lattice constants in pure $CuGeO_3$ indicated the presence of spontaneous strains below the transition temperature whose magnitude scaled with the square of the order parameter.[24–26] These strains were first observed using diffraction techniques for the b lattice constant[24,25] and later

confirmed using high resolution capacitance dilatometry to exist in all three crystal directions.[26] We have performed detailed measurements of the spontaneous strains on a 0.1% Zn-doped, 0.2% Si-doped and one 0.1% Cd-doped (sample 1) crystal. The Cd-doped sample shows significant deviations in the order parameter, as compared to pure $CuGeO_3$, so it is particularly interesting to examine the spontaneous strains in this sample to see if the same scaling with the square of the order parameter occurs and we will concentrate our discussion on these results.

Experimentally, the measurements were performed on the same samples as the order parameter measurements using the same instrument, the same sample environment and the same thermometry. This allows for detailed comparisons between the spontaneous strains and order parameter to be made with no adjustment of the transition temperature. The only technical difference between these measurements and those of the order parameter was that the vertically focusing PG (002) monochromator crystal was replaced by a flat, perfect single crystal Ge (111) monochromator to provide the resolution necessary to examine small lattice constant changes. The Ge (111) crystal allowed the measurements to be performed with Cu $K\alpha_1$ radiation, Cu $K\alpha_2$ being removed by distance collimation.

As was the case for previous lattice constant measurements on pure $CuGeO_3$,[19] we could not obtain the sensitivity required to allow for detailed comparisons to the order parameter using a conventional method. The conventional approach consists of aligning all angles and performing a detailed longitudinal scan following each change in temperature. The peak position and thus the lattice constant are then obtained from detailed lineshape analysis. To overcome this, we developed an alternative method to measure these relative lattice constant changes and this technique has been described previously.[19] The basic idea is to measure intensity changes for some

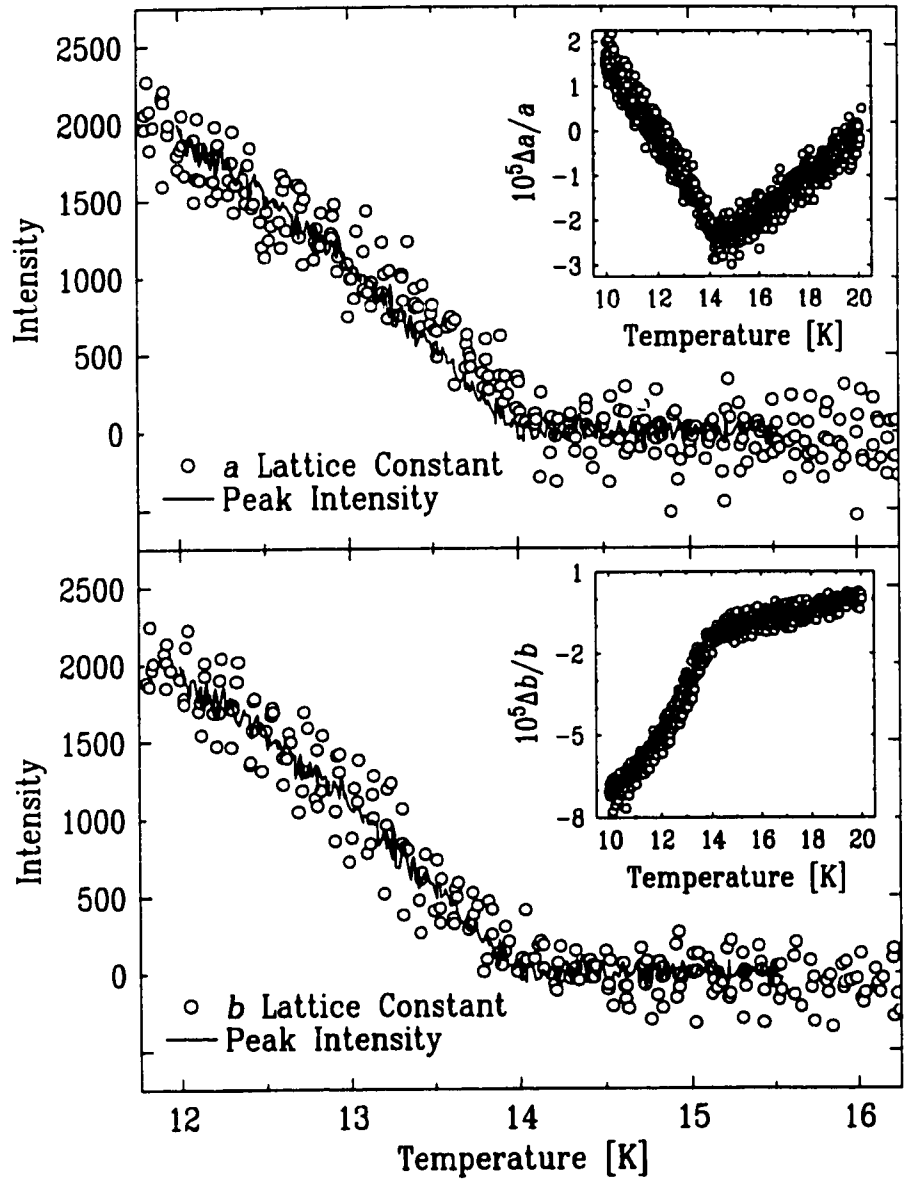

Figure 7: Relative changes in lattice constant as a function of temperature, background subtracted and normalized to agree with the order parameter at T=12.5 K for the 0.1% Cd-doped sample. The upper panel shows the results for the a lattice constant while the lower panel shows the corresponding results for the b lattice constant. The inset in both panels show the raw data plotted as $\Delta l/l$ and normalized to zero at T=20K. The data shows that the spontaneous strains scale with the order parameter squared even though the shape of the order parameter changes with Cd doping. This clearly indicates a coupling of the spontaneous strains to the order parameter, as observed previously in pure $CuGeO_3$.[24–26]

point on the sharply varying part of the lineshape and from this, together with a detailed knowledge of the lineshape, we can extract the peak position and thus the lattice constant as a function of temperature. This method assumes a fixed lineshape over the temperature range of interest and this is checked by periodically performing longitudinal scans. Reproducibility is checked by performing the measurements on both warming and cooling and the resulting relative lattice constant changes for Cd-doped $CuGeO_3$, shown in the insets of Fig. 7, are composed of 3 warming runs and 3 cooling runs.

The data obtained for the relative lattice constant changes for both the a and b lattice constants are shown in the insets of Fig. 7. The data are plotted in such a way that $\Delta l/l$ is set to zero at T=20 K. We can clearly see the presence of spontaneous strains below the transition temperature for both directions. To extract the spontaneous strains from these relative lattice constant changes, we fit the data from 16 to 20 K to an appropriate polynomial. The form of this polynomial was taken from previous measurements of a sample of $Cu_{1-x}Zn_xGeO_3$ with $x\sim0.05$ where the SP transition had been completely suppressed below the temperature range of interest in these measurements.[19] From these measurements, the background for the a lattice constant was well described by:

$$a = a_0[1 + A(T - T_0)^2] \tag{5}$$

and the b lattice constant was fit to a T^4 behaviour as expected for the thermal expansion of an insulator where the thermal expansion coefficient exhibits T^3 behaviour:[25]

$$b = b_0(1 + AT^4). \tag{6}$$

The best fit to these polynomials was then subtracted from the data and the resulting spontaneous strain data is scaled to agree with the peak intensity data as is shown in

Fig. 7. Here, for both the a and b lattice constants, we see very good agreement with the square of the order parameter, given by the peak intensity data. Similar results are obtained for the 0.1% Zn-doped sample and the 0.2% Si-doped sample both of which indicate spontaneous strains which scale with the order parameter squared. We have concentrated on the Cd-doped sample as it shows mean field behaviour in the order parameter which differs substantially from the behaviour observed in pure $CuGeO_3$. The fact that the spontaneous strains change their behaviour from that observed in pure $CuGeO_3$ to coincide with the square of the mean field-like order parameter show that the two are indeed intimately related.

V. SUMMARY

In summary, we observe critical behaviour very similar to that for pure $CuGeO_3$ in samples of lightly doped $CuGeO_3$ where Cu^{2+} is replaced by Zn^{2+} and Ge^{4+} is replaced by Si^{4+}. This result is consistent with 3D XY universality for pure $CuGeO_3$ by virtue of the Harris criterion. However, in samples where Cu^{2+} is replaced by Cd^{2+}, the critical properties change dramatically and the 3D XY behaviour observed in the pure compound is replaced by mean field behaviour. We interpret these changes as a consequence of long-range internal strain fields which couple to the order parameter due to the magnetoelastic nature of the SP transition. In addition, lattice constant measurements on several doped samples of $CuGeO_3$ indicate the presence of spontaneous strains below the transition temperature which scale with the square of the order parameter as was observed in pure $CuGeO_3$.

ACKNOWLEDGMENTS

This work was supported by NSERC of Canada and the OCMR of Ontario. It is a pleasure to acknowledge discussions with M.L. Plumer.

References

[1] M. Hase, I. Terasaki, and K. Uchinokura, Phys. Rev. Lett. **70**, 3651 (1993).

[2] J.P. Pouget, L.P. Regnault, M. Ain, B. Hennion, J.P. Renard, P. Veillet, G. Dhalenne, and A. Revocolevschi, Phys. Rev. Lett. **72**, 4037 (1994).

[3] O. Kamimura, M. Terauchi, M. Tanaka, O. Fujita, and J. Akimitsu, J. Phys. Soc. Jpn. **63**, 2467 (1994).

[4] M. Nishi, O. Fujita, and J. Akimitsu, Phys. Rev. B **50**, 6508 (1994).

[5] O. Fujita, J. Akimitsu, M. Nishi, and K. Kakurai, Phys. Rev. Lett. **74**, 1677 (1995).

[6] See J.W. Bray, L.V. Interrante, I.S. Jacobs, and J.C. Bonner, in *Extended Linear Chain Compounds*, edited by J.S. Miller (Plenum Press, New York, 1983), Vol. 3, p.353, and references therein.

[7] H. Völlenkle, A. Wittman, and H. Notwotny, Monatsh. Chem. **98**, 1352 (1967).

[8] M. Hase, I. Terasaki, Y. Sasago, K. Uchinokura, and H. Obara, Phys. Rev. Lett. **71**, 4059 (1993).

[9] S.B. Oseroff, S-W. Cheong, B. Aktas, M.F. Hundley, Z. Fisk, and L.W. Rupp, Jr., Phys. Rev. Lett. **74**, 1450 (1995).

[10] J-G. Lussier, S.M. Coad, D.F. McMorrow, and D. McK. Paul, J. Phys. Condens. Matter **7**, L325 (1995).

[11] Y. Sasago, N. Koide, K. Uchinokura, Michael C. Martin, M. Hase, K. Hirota, and G. Shirane, Phys. Rev. B **54**, R6835 (1996).

[12] J.P. Renard, K. Le Dang, P. Veillet, G. Dhalenne, A. Revcolevschi, and L.P. Reg-

nault, Europhys. Lett. **30**, 475 (1995).

[13] L.P. Regnault, J.P. Renard, G. Dhalenne, and A. Revcolevschi, Europhys. Lett. **32**, 579 (1995).

[14] M. Poirier, R. Beaudry, M. Castonguay, M.L. Plumer, G. Quirion, F.S. Razavi, A. Revcholevschi, and G. Dhalenne, Phys. Rev. B **52**, R6971 (1995).

[15] A.B. Harris, J. Phys. C **7**, 1671 (1974).

[16] A.B. Harris and T.C. Lubensky, Phys. Rev. Lett. **33**, 1540 (1974).

[17] M.F. Collins, *Magnetic Critical Scattering* (Oxford University Press, New York, 1989).

[18] K.G. Newman and E.K. Riedel, Phys. Rev. B **25**, 264 (1982).

[19] M.D. Lumsden, B.D. Gaulin, and H. Dabkowska, Phys. Rev. B **57**, 14097 (1998).

[20] *Handbook of Physics and Chemistry 62nd Edition*, edited by R.C. Weast (CRC Press, Boca Raton, FL, 1981).

[21] See, for example, M. Plischke and B. Bergersen, *Equilibrium Statistical Physics* (Prentice Hall, Englewood Cliffs, NJ, 1989).

[22] A. Aharony and G. Ahlers, Phys. Rev. Lett. **44**, 782 (1980).

[23] M. Weiden, W. Richter, C. Geibel, F. Steglich, P. Lemmens, B. Eisener, M. Brinkmann, and G. Güntherodt, Physica B **225**, 177 (1996).

[24] J.E. Lorenzo, K. Hirota, G. Shirane, J.M. Tranquada, M. Hase, K. Uchinokura, H. Kojima, I. Tanaka, and Y. Shibuya, Phys. Rev. B **50**,1278 (1994).

[25] Q.J. Harris, Q. Feng, R.J. Birgeneau, K. Hirota, K. Kakurai, J.E. Lorenzo, G.

Shirane, M. Hase, K. Uchinokura, H. Kojima, I. Tanaka, and Y. Shibuya, Phys. Rev. B **50**, 12606 (1994).

[26] H. Winkelmann, E. Gamper, B. Büchner, M. Braden, A. Revcolevschi, and G. Dhalenne, Phys. Rev. B **51**, 12884 (1995).

Chapter 6

Critical Properties in $MEM(TCNQ)_2$

Throughout the measurements on both pure and doped $CuGeO_3$, the critical properties associated with the SP transition could only be studied through examination of the order parameter as the critical scattering was not easily observed in these compounds. The organic SP systems have been shown to exhibit a large amount of critical scattering (Moncton et al. 1977, van Bodegom et al. 1981), but this scattering has not been examined quantitatively. Surprisingly, despite their discovery over 20 years ago, the critical phenomena associated with the SP transition in the organic SP systems have not been studied in any detail. Consequently, we report measurements of the critical phenomena at the SP transition for the organic compound $MEM(TCNQ)_2$. These results are presented in the following article entitled, "Critical phenomena at the spin-Peierls transition in $MEM(TCNQ)_2$" which was submitted for publication in Physical Review B, September 21, 1998.

Critical Phenomena at the Spin Peierls Transition in $MEM(TCNQ)_2$

M.D. Lumsden and B.D. Gaulin

Department of Physics and Astronomy, McMaster University,

Hamilton, Ontario, L8S 4M1, Canada

Abstract

We have performed a detailed x-ray scattering study of the critical phenomena associated with the spin-Peierls phase transition in the organic compound $MEM(TCNQ)_2$. Analysis of the superlattice reflection intensity indicates an order parameter with an associated critical exponent β=0.35±0.06 consistent with 3D behaviour, as seen in the inorganic compound $CuGeO_3$, and clearly inconsistent with mean field behaviour, as indicated in previous studies. Measurements of lattice constants indicate the presence of spontaneous strains below the transition temperature, the first such observation in an organic spin-Peierls system. The measured critical scattering is not well described by an Ornstein-Zernike, Lorentzian, lineshape. An adequate description is obtained with a Lorentzian^x with x varying or with a Lorentzian+Lorentzian^2 lineshape. The latter descriptor is reminiscent of previous high-resolution x-ray scattering studies where a two-component lineshape has been observed. Analysis using such a lineshape indicate critical exponents γ and ν, obtained from the Lorentzian component, consistent with the results obtained for the order parameter.

Submitted to Physical Review B September 21,1998

I. INTRODUCTION

The spin-Peierls (SP) transition[1] occurs in antiferromagnetic Heisenberg spin-1/2 chains in the presence of strong magnetoelastic coupling with the 3D lattice vibrations. Below the SP transition temperature (T_{sp}), a lattice dimerization occurs which increases progressively as the temperature is lowered, together with the concomitant appearance of an energy gap in the spectrum of magnetic excitations. This gap separates a nonmagnetic singlet ground state from a triplet of excited states. Such a transition is characterized by a rapid, isotropic drop in the magnetic susceptibility below T_{sp}, due to the nonmagnetic nature of the ground state, the appearance of a gap in the excitation spectrum, and the appearance of new, superlattice Bragg peaks resulting from new periodicities introduced by the lattice dimerization.

The organic compound MEM(TCNQ)$_2$ is composed of planar TCNQ molecules which stack along the crystallographic (0,0,l) direction producing quasi-one-dimensional chains.[2] Above 335 K, the chains are uniform and the system is metallic, but at this temperature, MEM(TCNQ)$_2$ undergoes a metal-insulator transition, characterized as an electronic Peierls transition,[3] and the uniform chains become dimerized. Between 335 K and 17.1 K, there is a single spin-1/2 magnetic moment present on each dimer and the crystal structure is triclinic with lattice parameters a=7.824(5) Å, b=15.426(16) Å, c=6.896(5) Å, α=113.59(8)°, β=73.27(7)°, and γ=112.71(8)° at 113 K.[4] At 17.1 K, MEM(TCNQ)$_2$ undergoes an additional phase transition producing a second dimerization of the chains.[4] This second transition has been shown to exhibit all of the characteristics of a SP phase transition. The uniform drop in the magnetic susceptibility[2,5] and the appearance of superlattice Bragg peaks with indices $(h, k, l/2)$[4,6] have been observed (These Miller indices and those quoted in the

remainder of this paper refer to the room temperature crystal structure not the structure above the 335 K transition). The gap in the excitation spectrum has not been directly observed with inelastic neutron scattering due to the low density of magnetic moment,[7] but its presence has been inferred from recent μSR studies.[8] Finally, the characteristic behaviour in a magnetic field has been observed,[9] where T_{sp} decreases with increasing field until a critical field is reached above which the system enters into a different, incommensurate phase.[1]

The critical phenomena associated with the SP transition have not been extremely well characterized. The most comprehensive work has involved measurements of the exponent β associated with the order parameter in the inorganic SP compound $CuGeO_3$ where an exponent β=0.345±0.03 was found consistent with a 3D universality class.[10] Measurements of the exponents γ and ν associated with the build up of fluctuations upon nearing the transition temperature have been very difficult to obtain in $CuGeO_3$. The majority of scattering studies have had great difficulty in observing any critical scattering[10–13] with the only success occurring using synchrotron x-ray radiation.[14] However, in these synchrotron studies, the observed critical scattering could not be described using a standard Ornstein-Zernike form, which yields Lorentzian lineshape in wavevector, but instead a much sharper lineshape, well described by a Lorentzian squared, was observed. As is typically the case with this so-called "second length scale" critical scattering,[15] the extracted critical exponents are larger in magnitude than expected and are inconsistent with any conventional universality class.

Examination of critical properties in organic SP systems has been less comprehensive with the only existing results indicating behaviour consistent with mean field theory.[3,16] This motivated us to carefully measure both the order parameter and

the critical fluctuations associated with the SP transition in the organic compound MEM(TCNQ)$_2$. Previous studies indicated the presence of substantial critical scattering but no quantitative lineshape analysis had been performed.[4] We expected that the presence of second length scattering which complicated the critical fluctuation measurements in $CuGeO_3$[14] would not occur in MEM(TCNQ)$_2$. These sharp fluctuations are generally attributed to defects in the near surface region[15] and are much more prevalent in x-ray scattering measurements where low penetration depths result in substantial surface sensitivity. However, the organic nature of MEM(TCNQ)$_2$ yields large x-ray penetration depths and consequently reduced surface sensitivity. Thus, we anticipated a single Lorentzian lineshape would be adequate to describe the critical scattering, as is typically seen in bulk neutron scattering measurements, allowing critical exponents consistent with traditional universality classes to be extracted.

In addition, we performed measurements of the thermal expansion of MEM(TCNQ)$_2$ in the vicinity of the SP transition temperature. Similar measurements on $CuGeO_3$[13,17,18] indicated the presence of spontaneous strains below the transition temperature which scaled with the square of the order parameter. We report such spontaneous strains for the first time in an organic SP system.

II. EXPERIMENTAL DETAILS

A single crystal of MEM(TCNQ)$_2$ with approximate dimensions $4\times1\times0.5$ mm^3 was mounted in a Be can in the presence of a He exchange gas. This sample was part of the larger crystal used in Ref. 4. This can was mounted on the cold finger of a closed-cycle He refrigerator and the temperature was kept stable to ±0.01 K for all reported measurements. The measurements were performed in a Huber four-circle

diffractometer, allowing access to a large portion of reciprocal space, and the incident radiation was CuKα radiation from a Rigaku 18 kW rotating anode x-ray generator. This radiation was further monochromatized by a flat PG (0,0,2) monochromator crystal.

The order parameter was measured at several wavevectors to ensure reproducible results. The critical scattering was measured at both the (1,6,-1/2) and (0,11,3/2) superlattice peaks as a check for consistency, these peaks being chosen due to their relative intensity when compared with approximately 120 other superlattice peaks. For the measurements of the thermal expansion, the (0,12,0) and (0,0,4) Bragg peaks were examined and the resolution was improved significantly by tightening the collimation which is controlled by a series of four slits, two before and two after the sample position.

III. ORDER PARAMETER

A. Experiment

The temperature dependence of the peak intensity of the (1,6,-1/2), (0,11,3/2),(1,5,3/2), and (0,0,5/2) superlattice reflections were measured for temperatures ranging from 10 K to 20 K and the resulting peak intensity as a function of temperature for the (0,11,3/2) reflection is shown in the upper panel of Fig. 1. In addition, the temperature dependence of the intensity integrated over a transverse scan was measured from 15 K to 18 K for the (1,6,-1/2) reflection. The results for all four peaks are consistent with one another leading to the conclusion that extinction effects are small as the peak intensities of the various reflections differed greatly (for instance, the (0,0,5/2) reflection produced a rather low peak intensity of about 150

counts/sec while the (0,11,3/2) reflection was much more intense yielding a count rate of about 4200 counts/sec).

B. Analysis

Determination of the transition temperature was achieved by careful examination of the peak intensity as a function of temperature and its first and second derivatives as shown in the lower panel of Fig. 1. In the absence of any critical scattering, one expects the first derivative to jump abruptly to zero at the transition temperature. However, critical scattering from fluctuations provides an additional contribution to the peak intensity which reaches its maximum value in **Q** at the ordering wavevector and in temperature at the transition temperature. Consequently, this critical scattering generates substantial curvature in the peak intensity near T_{sp} causing the first derivative to change in a much more gradual fashion. The range of temperatures over which this critical scattering is substantial relative to the Bragg component must be eliminated from the analysis to obtain accurate estimates of the critical exponent β. The observed first derivative can be seen to decrease steadily until about 16.3 K where it appears to level out. We take this to indicate the presence of substantial critical scattering and, consequently, the analysis was performed up to a maximum temperature of about 16.1 K, chosen as a conservative estimate, in order to consider data containing solely the Bragg component. This upper temperature is represented by the dotted, vertical line in the lower panel of Fig. 1.

The second derivative of the peak intensity as a function of temperature is also shown in the lower panel of Fig. 1. It can be seen to be strongly peaked at a temperature of about 17.1 K and this point, representing the point of maximum curvature,

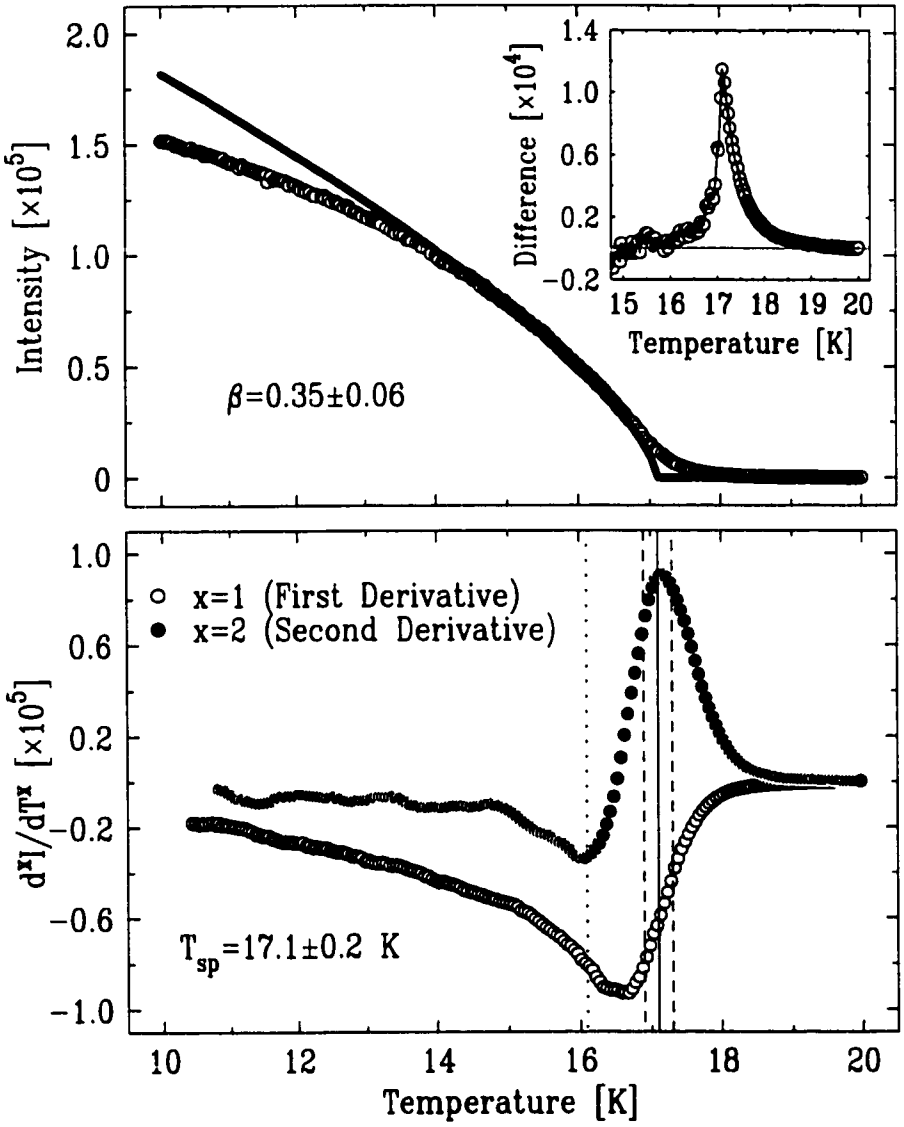

Figure 1: The upper panel shows the peak intensity as a function of temperature for the (0,11,3/2) superlattice reflection. The sold line represents the best fit to a simple power law, Eq. 1, with a value of the exponent β of about 0.35 and the inset shows the difference between this line and the measured intensity. Such a difference indicates the contribution due to fluctuations. The lower panel shows the first and second derivatives of the peak intensity as a function of temperature. The dotted line indicates the temperature above which fluctuations become substantial. The solid line and nearby dashed lines represent the best fit and extreme estimates of the transition temperature, respectively.

is taken to be indicative of the transition temperature. This maximum point could only be determined accurately to approximately ±0.2 K and thus we determine the transition temperature to be 17.1±0.2 K. This best estimate and the maximum and minimum values are represented by the solid line and two dashed lines, respectively, in the lower panel of Fig. 1.

To avoid difficulties resulting from changes in peak position, measurements of the intensity integrated over a transverse scan were performed on the (1,6,-1/2) superlattice reflection from 15 K up to about 18 K and this data will be used in the quantitative analysis which follows. In order to extract the proper critical behaviour of the order parameter, this data was fit to a power law in the reduced temperature, $t = 1 - T/T_{sp}$,

$$Intensity = I_o t^{2\beta} + Background. \quad (1)$$

This power law behaviour is expected to be valid in the asymptotic critical region, near T_{sp}, where the length scale associated with the fluctuations in the order parameter dominate over any other relevant length scales in the system. As the temperature is lowered below this region, this power law behaviour must be modified by successive correction-to-scaling terms,[19] the first of which is included in Eq. 2.,

$$Intensity = I_o t^{2\beta}(1 + At^{\Delta}) + Background \quad (2)$$

where the exponent Δ has an approximate value of 0.5 for 3D behaviour.

To investigate the extent of the asymptotic region, the dependence of the extracted value of β on the lowest temperature included in the fits was examined carefully and is shown in Fig. 2 for fits to the ordinary power law, Eq. 1, from 15 K up to the predetermined maximum temperature of 16.1 K. The plot presents results with the transition temperature fixed at the nominal value of 17.1 K and the maximum and

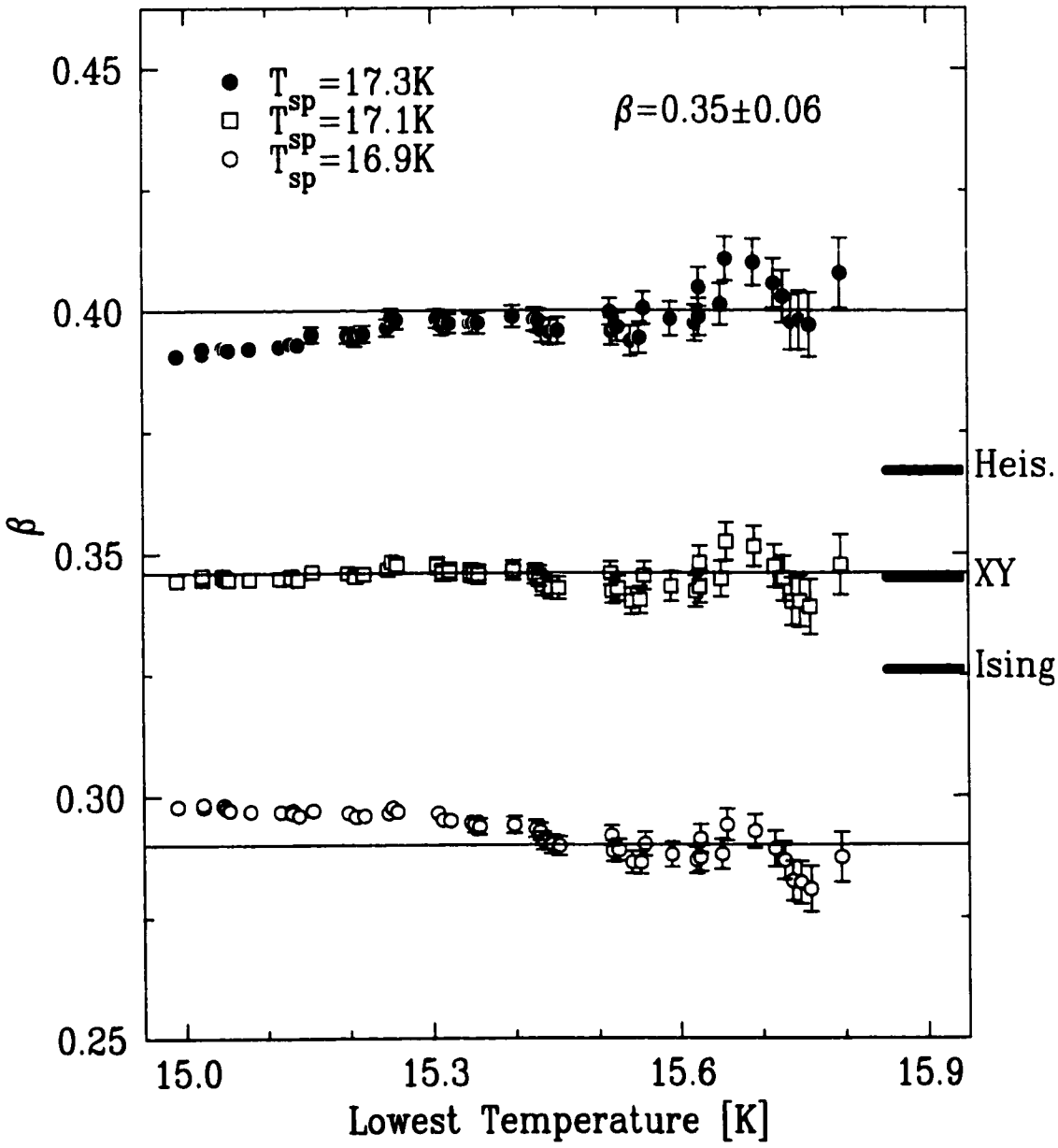

Figure 2: The extracted value of the exponent β obtained from the ordinary power law, Eq. 1, as a function of the lowest temperature included in the fits with T_{sp} fixed at values of 17.1 K, 17.3 K, and 16.9 K representing the best estimate, maximum, and minimum values respectively. The robust nature of the fits with respect to the lowest temperature is indicative of an asymptotic region which extends at least until 15 K. For reference, the theoretical predictions for 3D Ising, XY, and Heisenberg universality are indicated on the plot.

minimum temperatures of 17.3 K and 16.9 K respectively. Fits were also performed using the ordinary power law with a varying transition temperature. In all cases, the best fit value of T_{sp} fell within the previously determined range of values, namely, between 16.9 K and 17.3 K, validating the previously selected transition temperature. The results obtained with a T_{sp} of 17.1 K indicate no systematic behaviour with respect to the lowest temperature included in the fits producing a value of β of about 0.35. The upper and lower bounds to T_{sp} generate values of the exponent β approximately ± 0.06 around this nominal value. This error, determined by the error in the transition temperature, is by far the largest source of uncertainty in determination of the critical exponent and thus we arrive at an exponent $\beta = 0.35 \pm 0.06$. This value of β is consistent with conventional 3D behaviour, as was observed in $CuGeO_3$,[10] and is clearly inconsistent with mean field behaviour, as reported in previous studies.[3] For reference, the values of the exponent β for 3D Ising, XY, and Heisenberg universality[20] are indicated on Fig. 2.

The robust behaviour of the fits using the ordinary power law with respect to the range of data included suggests that the asymptotic region extends to at least 15 K. To check that this is indeed the case, the same examination of β as a function of lowest temperature was performed using the power law with first correction to scaling included, Eq. 2. The resulting extracted values of β sat directly on top of the results from the ordinary power law, Eq. 1, confirming that correction terms are unnecessary for temperatures as low as 15 K.

The solid line shown in the upper panel of Fig. 1 represents the best fit to Eq. 1 with a corresponding exponent, β, of 0.35. The difference between the data and this solid line is shown, for temperatures near the transition temperature, in the inset to the upper panel of Fig. 1. This difference, representing the contribution to the

peak intensity resulting from the critical fluctuations, can be seen to peak sharply at the transition temperature. One expects the same critical exponent above and below the transition temperature, but the amplitude of the power law describing the fluctuations should be smaller below T_{sp} due to the universal nature of the amplitude ratio. Consequently, the critical scattering should fall away faster below the transition temperature, a point which is qualitatively clear from the difference data presented in the inset.

C. Comparison to $CuGeO_3$

As mentioned previously, the asymptotic region in MEM(TCNQ)$_2$ extends to at least 15 K corresponding to a value of T/T_{sp} of about 0.88. This is in contrast to the results obtained on $CuGeO_3$ where the first correction to scaling term was needed for temperatures within 0.4 K of the transition temperature indicating an asymptotic region which extends no further than T/T_{sp}=0.96.

To allow for a more systematic comparison between MEM(TCNQ)$_2$ and $CuGeO_3$, Fig. 3 shows the peak intensity for both plotted as a function of T/T_{sp} normalized to unity at T/T_{sp}=0.9 (this value is chosen as it includes the range in both compounds where the order parameter has been quantitatively examined in detail). We can see agreement between the two from 0.9 to about 0.96 suggesting similar critical behaviour as quantitatively shown by the similar values for the exponent β. Above T/T_{sp} of about 0.96, the critical scattering present in MEM(TCNQ)$_2$ and much less evident in $CuGeO_3$ causes the peak intensities to deviate. Below T/T_{sp} of about 0.9, the peak intensity of $CuGeO_3$ seems to saturate much more rapidly with decreasing temperature than does the MEM(TCNQ)$_2$ intensity indicating very different non-

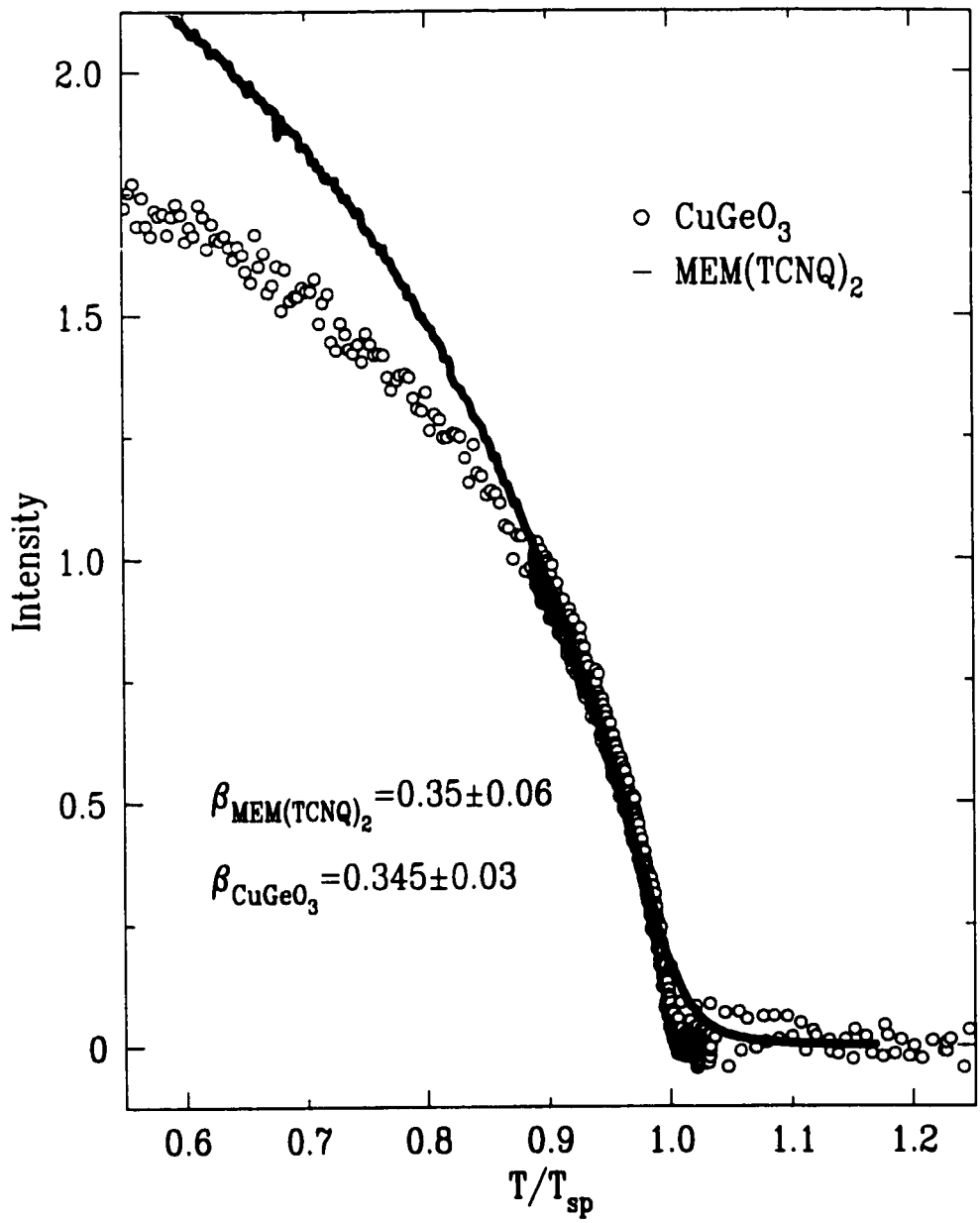

Figure 3: The peak intensity as a function of temperature normalized to the transition temperature for the inorganic SP compound $CuGeO_3$ and the organic system $MEM(TCNQ)_2$. The intensity is normalized to unity at a T/T_{sp} of about 0.9. There is good agreement between the two close to the transition as indicated by the similar values of the exponent β. The low temperature non-critical behaviour is rather different suggesting greater ease of deformation for $MEM(TCNQ)_2$.

critical behaviour between the two compounds. This implies that the MEM(TCNQ)$_2$ lattice is able to deform with greater ease than that of $CuGeO_3$, a fact that may be related to a soft phonon mode present in MEM(TCNQ)$_2$[21] which appears to be absent in $CuGeO_3$. Such deviations may also be related to differences in the nature of the dimerization wavevector which produces a single dimerization along the c^* axis for MEM(TCNQ)$_2$ and a doubly dimerized state, with dimerizations along a^* and c^*, for $CuGeO_3$.

IV. LATTICE CONSTANTS

Measurements of the temperature dependence of the lattice constants in the inorganic SP compound $CuGeO_3$ indicated the presence of spontaneous strains below the transition temperature whose magnitude scaled with the square of the order parameter.[10,13,17,18] We performed similar measurements on the (0,0,4) and (0,12,0) reflections of MEM(TCNQ)$_2$ in search of analogous effects in an organic SP system.

The (0,12,0) reflection was measured using a conventional approach wherein, following a change in temperature, all the angles were rocked and centered and a detailed longitudinal scan performed. The peak position was then extracted from lineshape analysis on this longitudinal scan. Such a conventional approach could not produce sufficient sensitivity for the (0,0,4) reflection largely due to inferior resolution at this reflection (the scattering angle for (0,12,0) was 2θ=86.98° while that for (0,0,4) was 2θ=59.70°). To obtain reasonable results for this peak, an alternative approach, described in detail in Ref. 10, was employed. The new approach involves measuring changes in intensity for some point on the sharply varying portion of the lineshape and from this, coupled with a detailed knowledge of the lineshape itself, the peak

position, and thus lattice constant as a function of temperature can be extracted. This method assumes a robust lineshape over the temperature range of interest, an assumption which is reasonable over a small range of temperatures. The enhancement in sensitivity is accomplished through an improvement in statistics as the time in measuring a single temperature now only includes measuring the intensity at a single point. This results in a measurement which is less intensity limited compared to the conventional approach and allows for improvement in the collimation, and thus resolution correspondingly.

The resultant lattice constants as a function of temperature are shown in Fig. 4. The data are plotted as Δd/d normalized to zero at a temperature of 25 K. The lower panel shows the results for the (0,12,0) reflection which indicates a clear change in thermal expansion at T_{sp}, indicated by the dashed line, demonstrating the presence of a spontaneous strain, as was observed in $CuGeO_3$. The upper panel shows the results for the (0,0,4) reflection and, while not as evident, appears to similarly show the existence of such a spontaneous strain.

To further emphasize this point, the derivative of the data is shown in the inset for both reflections. Here, one can clearly see an abrupt change in slope at the transition temperature in both reflections implying the presence of spontaneous strains in both directions. The presence of such strains in MEM(TCNQ)$_2$, coupled with previous observations of similar results in $CuGeO_3$ and in the recently proposed SP system α'-NaV_2O_5,[22] suggest that these spontaneous strains are indeed an inherent characteristic of a SP system.

We attempted to extract the spontaneous strains from the measurements of Δd/d to examine whether scaling with the square of the order parameter occurs, as was the case with $CuGeO_3$. However, without some independent measure of the background

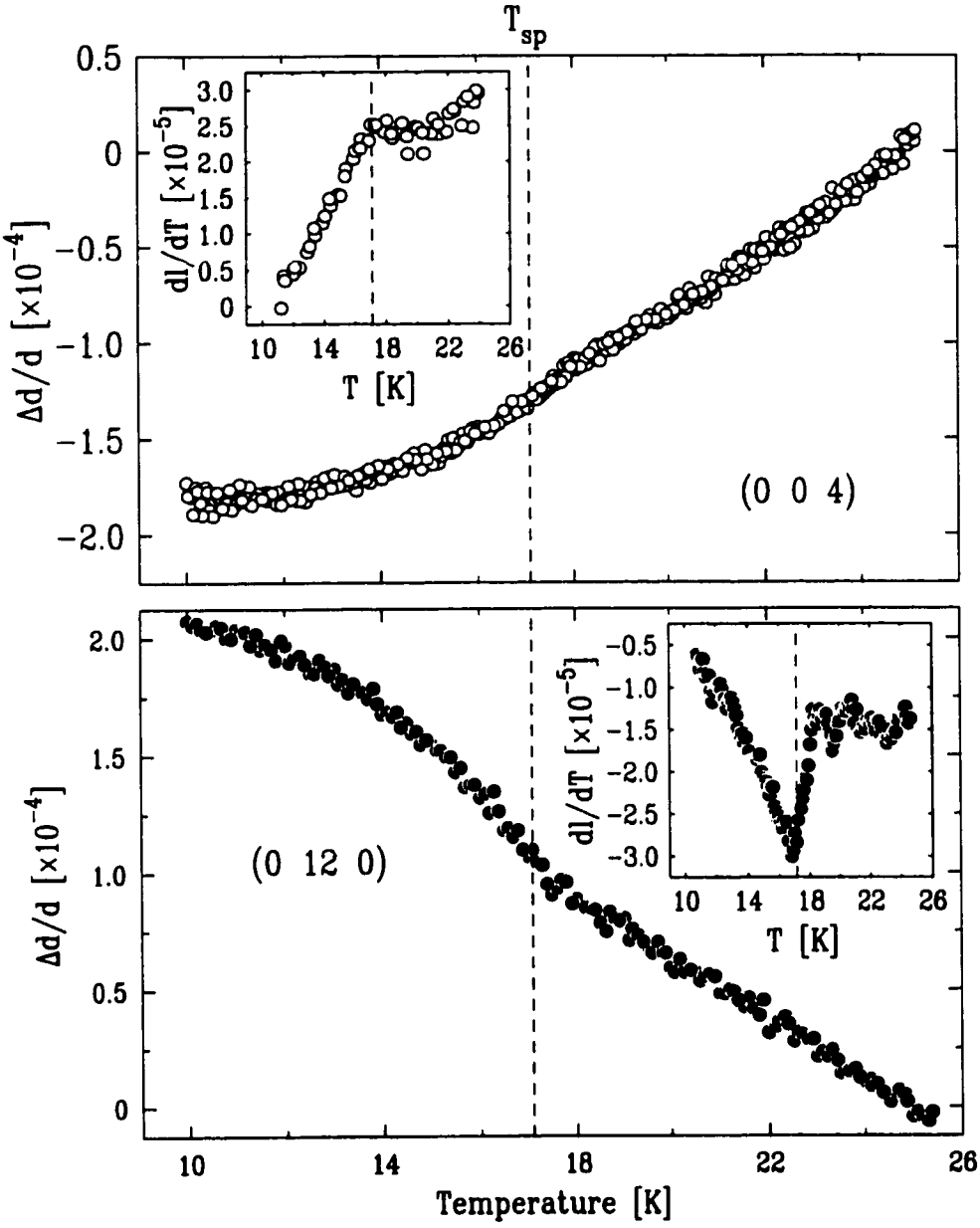

Figure 4: The relative change in d-spacing for the (0,0,4) and (0,12,0) Bragg peaks as a function of temperature. There are clear deviations in the data at the transition temperature suggesting the presence of spontaneous strains below T_{sp}. To further emphasize this point, the inset in both the upper and lower panels shows the temperature derivative of $\delta d/d$. This shows a clear change in slope at the transition temperature emphasizing the presence of spontaneous strains. The value of the transition temperature, T_{sp}=17.1 K, is indicated by the dashed line.

to be subtracted, representing the thermal expansion in the absence of the SP transition, it is very difficult to properly extract this information. Such an independent background determination was performed in $CuGeO_3$[10] by repeating the measurements on a dilute sample with sufficient dopant concentrations to suppress the SP transition below the temperature range of interest. Low solubility limits for dopants in MEM(TCNQ)$_2$ makes a similar study impossible, but perhaps, in the future, these measurements could be repeated in a magnetic field where the transition temperature can be sufficiently suppressed to allow for an independent background determination.

V. CRITICAL SCATTERING

The critical fluctuations accompanying the SP transition were carefully measured at two superlattice wavevectors, (1,6,-1/2) and (0,11,3/2), by performing detailed scans along the principal reciprocal lattice directions at a number of temperatures between 16 K and 20 K. In order to perform quantitative lineshape analysis, the anticipated cross section, $d\sigma/d\Omega(\mathbf{Q}\text{-}\mathbf{Q}')$ must be convoluted with the instrumental resolution function, $R(\mathbf{Q}')$,

$$I(\mathbf{Q}) = \int R(\mathbf{Q}')\frac{d\sigma}{d\Omega}(\mathbf{Q} - \mathbf{Q}')d\mathbf{Q}'. \quad (3)$$

Determination of the instrumental resolution function was performed by careful measurements at low temperatures (~9 K) where the scattering is assumed to be free of any critical scattering, and only a resolution limited Bragg peak remains. It became evident that finding an analytical description to adequately describe this resolution function would be a formidable task due to the existence of two large crystallites of roughly equal size constituting the mosaic single crystal. Figure 5 shows a mesh scan

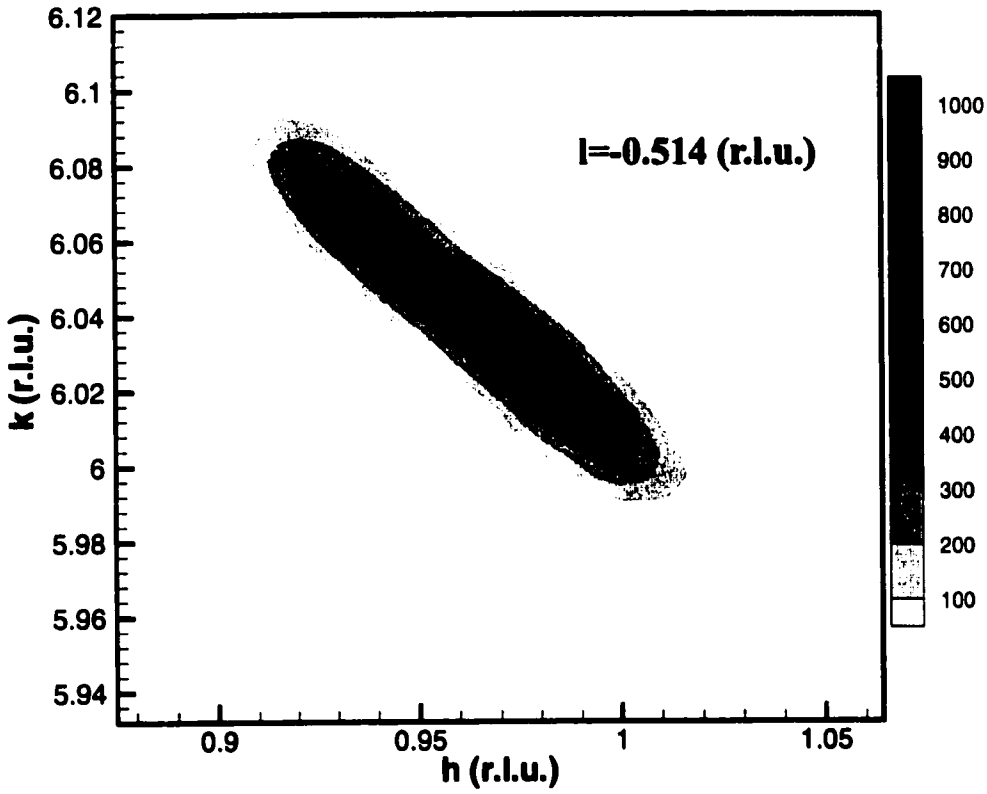

Figure 5: Low temperature ($\sim$ 9 K) mesh scan through the (1,6,-1/2) superlattice reflection in the h-k reciprocal lattice plane at a value of l slightly off the optimized peak position. This clearly shows the presence of two crystallites in the mosaic single crystal. This also shows that the resolution function is not aligned with the h and k axes in this scattering plane.

in the h-k reciprocal space plane at a value of l just off the optimized peak position. This contour plot clearly shows the presence of two distinct crystallites.

Approximately 30 mesh scans, similar to the one shown in Fig. 5, were measured to fully characterize the resolution function at all points in h, k, l space in the vicinity of the superlattice reflection. The two measured reflections were chosen due to their relative strength when compared to other reflections and to allow repetition of the measurements in two quite different scattering geometries. The relatively large intensity of these superlattice peaks allowed such a detailed mapping of the low temperature behaviour to be carried out in a reasonable amount of time.

This measured resolution function was then convoluted with the assumed cross-section numerically to generate the intensity at the relevant h, k, and l coordinates for the critical scattering measurements. To yield consistent results, the data were simultaneously fit to the set of three scan along the three principal reciprocal space directions at each temperature.

A. Possible Lineshapes

The fluctuation-dissipation theorem relates the spin-pair correlation function, and thus the scattering cross-section, to the static susceptibility.[23] The Ornstein-Zernike form for the **Q**-dependent susceptibility is a Lorentzian in **Q**,

$$\begin{aligned} \frac{d\sigma}{d\Omega} &\sim T\chi(\mathbf{Q},T) \\ &\sim \frac{T\chi(T)}{1+\frac{\mathbf{Q}^2}{\kappa^2}}. \end{aligned} \tag{4}$$

$\mathbf{Q}^2$ represents the square of the distance in reciprocal space relative to the superlattice peak position and the width, κ, was allowed to vary independently along h, k, and l.

The full form for $\mathbf{Q}^2/\kappa^2$ for a triclinic single crystal, as was employed in the analysis, is shown in the appendix.

Fits were performed using the convoluted Lorentzian lineshape and the resulting best fit at a temperature of 17.7 K, well above the transition temperature of 17.1 K, is represented by the solid line shown in the left panel of Fig. 6. This figure shows the data taken along the l reciprocal space direction as this direction exhibited the sharpest resolution and, hence, allows for easier comparison of fit quality (similar scans were obtained along the h and k directions). The fit to the single Lorentzian is clearly not a satisfactory description of the data as the solid line sits inside the data near the peak and overestimates the data away from the peak position. The obtained value of the goodness-of-fit parameter, χ^2, at 17.7 K was 9.13 for the combined fit over the three sets of data incorporating scans along h, k, and l.

As the single Lorentzian cross-section did not adequately describe the observed data, an alternative form was required. Many recent measurements of critical fluctuations using x-ray scattering have been shown to exhibit two length scales.[15] The first, describing the fluctuations in the bulk of the crystal, are well described by an Ornstein-Zernike, Lorentzian cross-section with extracted critical exponents consistent with conventional universality classes. The second, larger length scale, typically well described by a Lorentzian squared lineshape, has been attributed to defects in the near surface region and most commonly generates critical exponents larger than those obtained from the bulk fluctuations. Such observations were first made for the cubic to tetragonal structural phase transition in some of the perovskites[24–31] and later observations were made in magnetic x-ray scattering experiments on Ho,[32,33] Tb,[34,35] and some U based compounds.[36–38]

The data obtained for MEM(TCNQ)$_2$ did not clearly exhibit two distinct line-

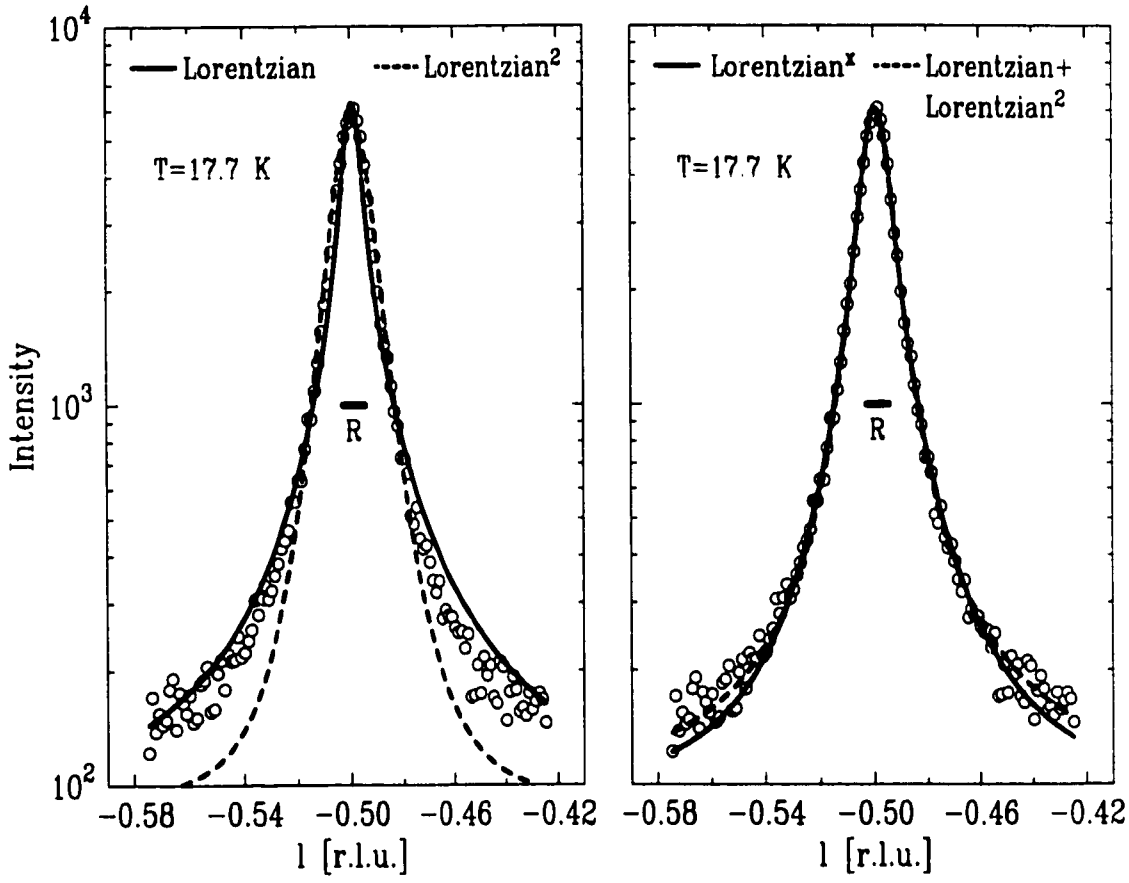

Figure 6: The data obtained from scans along l for a temperature of about 17.7 K chosen to be clearly above the transition temperature. The solid line in the left panel indicates the best fit to a convoluted Lorentzian cross-section while the dashed line represents the best fit using a Lorentzian^2 cross-section. Neither are good descriptors of the data. The lines in the right panel are taken from best fits to a convoluted Lorentzian^x where x is a varying parameter (solid line) and a Lorentzian + Lorentzian^2 (dashed line). Both forms provide good descriptions of the data. For reference, the measured resolution is indicated by the horizontal bar.

shapes and, consequently, fits were first attempted to a convoluted Lorentzian squared lineshape alone,

$$\frac{d\sigma}{d\Omega} \sim \frac{T\chi(T)}{(1+\frac{\mathbf{Q}^2}{\kappa^2})^2}. \tag{5}$$

Such a lineshape has been observed in several high resolution synchrotron measurements including the inorganic SP system $CuGeO_3$.[14]

The best fit using the above cross-section at a temperature of 17.7 K is indicated by the dashed line in the left panel of Fig. 6. One can see that this curve also does not yield an adequate description of the data, severely underestimating the data away from the peak position. The goodness-of-fit parameter for the fits at 17.7 K was 8.93 indicating a fit of equally poor quality as that provided by the single Lorentzian cross-section.

As the lineshape generated using Lorentzian and Lorentzian squared cross-sections produced poor descriptions of the data and there are not two distinct lineshapes present in the raw data, fits were also performed using a cross-section given by a Lorentzian with a varying power,

$$\frac{d\sigma}{d\Omega} \sim \frac{T\chi(T)}{(1+\frac{\mathbf{Q}^2}{\kappa^2})^x} \tag{6}$$

where x is a varying parameter of the fits. The Lorentzian cross-section overestimated the scattering away from the peak position and the Lorentzian squared underestimated this same scattering, thus one would expect to obtain a best estimate of the power x lying somewhere between 1 and 2.

The best fit to such a form at a temperature of 17.7 K is represented, for the scan along the l direction, by the solid line in the right panel of Fig. 6. At this particular temperature, the best fit value of the power, x, was found to be 1.31 confirming the expectation of a value lying between 1 and 2. This solid line can be seen to be a

much improved description of the data yielding a goodness-of-fit parameter of 1.67 at 17.7 K, a substantial improvement over the previous values for the Lorentzian or Lorentzian squared cross-sections.

To examine the progression of the obtained power, x, as the temperature is raised above the transition temperature, the extracted value of x, as a function of temperature is shown in Fig. 7 for both the (1,6,-1/2) and (0,11,3/2) reflections. For both reflections, the value of x can be seen to decrease steadily from about 1.35 near the transition to a value of about 1, consistent with a single Lorentzian, at higher temperatures near 19 K. This indicates behaviour closer to a Lorentzian squared near the transition with the data adequately described by a single Lorentzian well above T_{sp}. This observation is consistent with that observed in other systems which exhibit two length scale scattering. In such systems, the amplitude of the Lorentzian squared component diminishes more rapidly with increasing temperature when compared to the corresponding Lorentzian amplitude and, eventually, the sharper fluctuations become negligible in comparison to the bulk fluctuations.

Consequently, fits were performed using a Lorentzian + Lorentzian^2 cross-section,

$$\frac{d\sigma}{d\Omega} \sim \frac{T\chi_1(T)}{1+\frac{\mathbf{Q}^2}{\kappa_1^2}} + \frac{T\chi_2(T)}{(1+\frac{\mathbf{Q}^2}{\kappa_2^2})^2} \tag{7}$$

where the subscript 1 refers to the Lorentzian component and the subscript 2 refers to the Lorentzian squared. The best description of the data using the above form is indicated by the dashed line in the right panel of Fig. 6. As was the case for the Lorentzian with a varying power, this form also describes the data very well with a resultant goodness-of-fit parameter of 1.86 at a temperature of 17.7 K. The cross-sections represented by Eq. 6 and Eq. 7 both generate excellent descriptions of the data and it is very difficult to distinguish between the two.

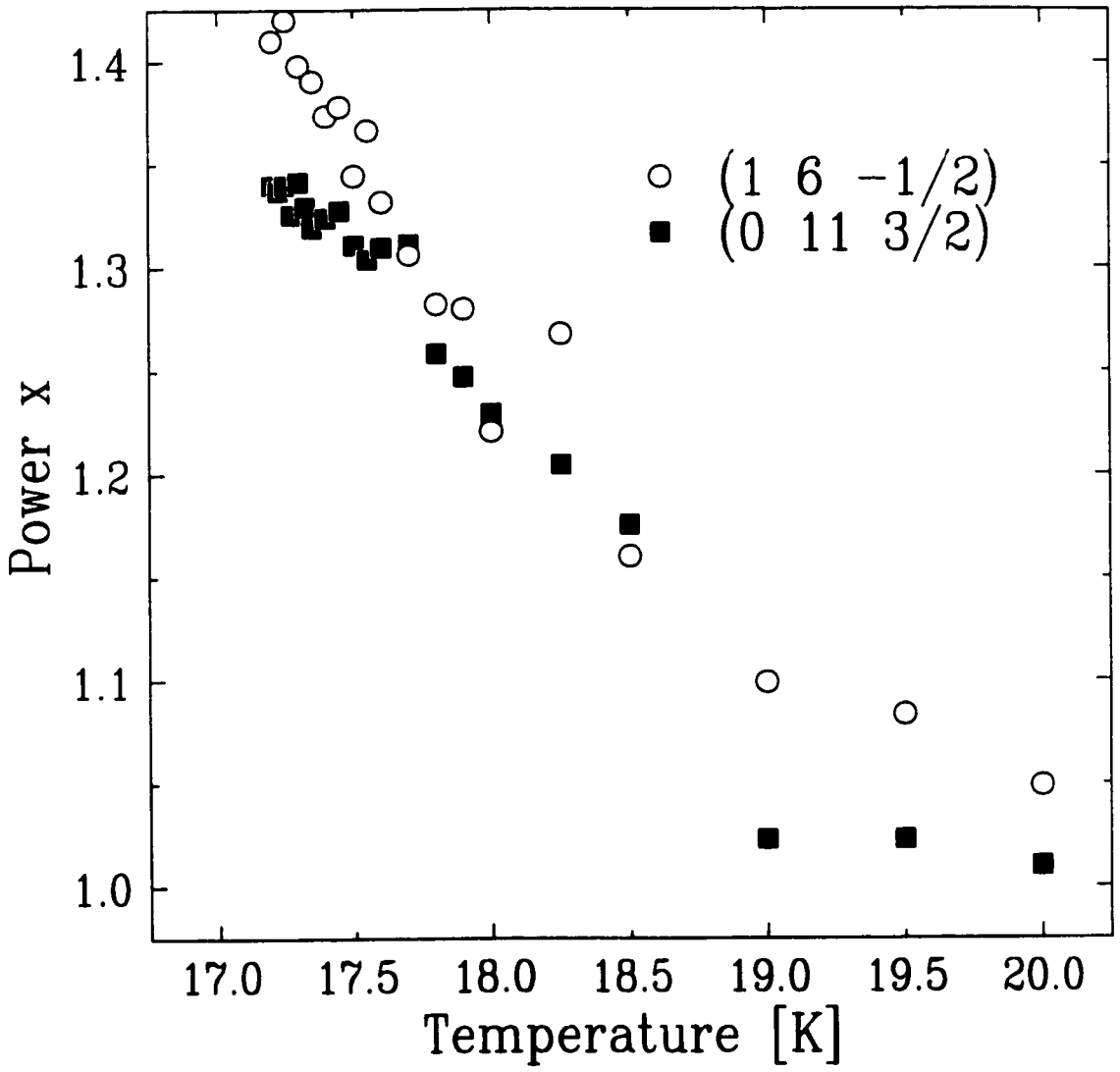

Figure 7: The extracted power, x, from fits to a Lorentzian^x convoluted with the instrumental resolution as a function of temperature for both the (1,6,-1/2) and (0,11,3/2) superlattice reflections. The power of x has a best fit value of about 1.35 near T_{sp} (17.1 K) and falls off steadily with increasing temperature to a value of about unity, consistent with a single Lorentzian cross-section.

T(K)	χ^2 Lor.	χ^2 Lor.^{2}	χ^2 Lor.^{x}	χ^2 Lor.+Lor.^{2}	χ^2 Lor.$^{1.35}$
17.4	29.44	15.86	2.45	3.12	2.58
17.5	23.84	14.87	2.14	2.18	2.14
17.7	9.13	8.93	1.67	1.86	1.69
18	3.87	5.99	1.87	1.77	2.12
19	1.55	3.37	1.45	2.08	1.77
20	1.50	2.53	1.50	1.66	1.71

Table 1: The goodness-of-fit parameter $\chi^2=\chi_h^2+\chi_k^2+\chi_l^2$ where χ_x^2 is taken from the scan along the x direction (where x=h,k,or l) and $\chi_x^2 = \sum_i[(I_{obs}(i) - I_{calc}(i))/\Delta(I_{obs}(i))]^2$ at several temperatures above the transition temperature. Results are shown for fits using a Lorentzian, Lorentzian^2, Lorentzian^x, Lorentzian+Lorentzian^2, and Lorentzian$^{1.35}$ cross-section convoluted with the instrumental resolution function. The values shown are for the (1,6,-1/2) superlattice reflection.

The discussion to this point centered on the data at a single temperature of 17.7 K chosen to be clearly above the transition temperature. To examine the behaviour at differing temperatures, Table 1 shows the goodness-of-fit parameter χ^2 for the four cross-sections discussed previously at several temperatures between 17.4 K and 20 K. The inferior nature of the fits using the Lorentzian or Lorentzian squared cross-sections in the vicinity of T_{sp} are clearly indicated by the large magnitude of χ^2. In fact, the Lorentzian^2 lineshape does not appear to adequately describe the data at any temperature while the Lorentzian can be seen to produce good fit quality only for data sufficiently above the transition temperature. The Lorentzian with a varying power and the Lorentzian + Lorentzian^2 both generate good descriptions of the data at all temperatures and, in addition, although not previously mentioned, one can also obtain reasonable quality by fixing the varying power x to a value of about

1.35. This value corresponds to that obtained for temperatures close to the transition temperature and the resulting goodness-of-fit parameters using such a cross-section are shown in the last column of Table 1. Thus, we have shown that the Lorentzian cross-section expected for Ornstein-Zernike fluctuations does not adequately describe the data near T_{sp} and have provided three alternative forms which produce good descriptions of the data.

B. Critical Exponents

Of the possible cross-sections which produce reasonable descriptions of the data, the only one expected to yield meaningful exponents is the Lorentzian + Lorentzian^2, Eq. 7. This expectation is derived from previous x-ray and neutron measurements of critical scattering where two length scales were observed.[15] The resulting susceptibility, χ_1, and the correlation length, $\xi_1 \sim 1/\kappa_1$, versus reduced temperature, with T_{sp}=17.1 K, is shown in Fig. 8 on a logarithmic plot. Initially, the width κ_1 was allowed to vary independently along h,k, and l, but the widths were found to be related to each other by a simple multiplicative constant and hence, the values along k and l were fixed to be some ratio of the width along h to lower the number of varying fit parameters. The widths for the Lorentzian and Lorentzian^2 components were allowed to vary independently. Scaling theory of continuous phase transitions indicates that both χ_1 and ξ_1 should obey power law behaviour in the immediate vicinity of T_{sp},

$$\chi_1 \sim t^{-\gamma_1} \qquad \xi_1 \sim t^{-\nu_1} \tag{8}$$

where the critical exponents γ_1 and ν_1 are universal quantities which help to define the universality class for a given phase transition.

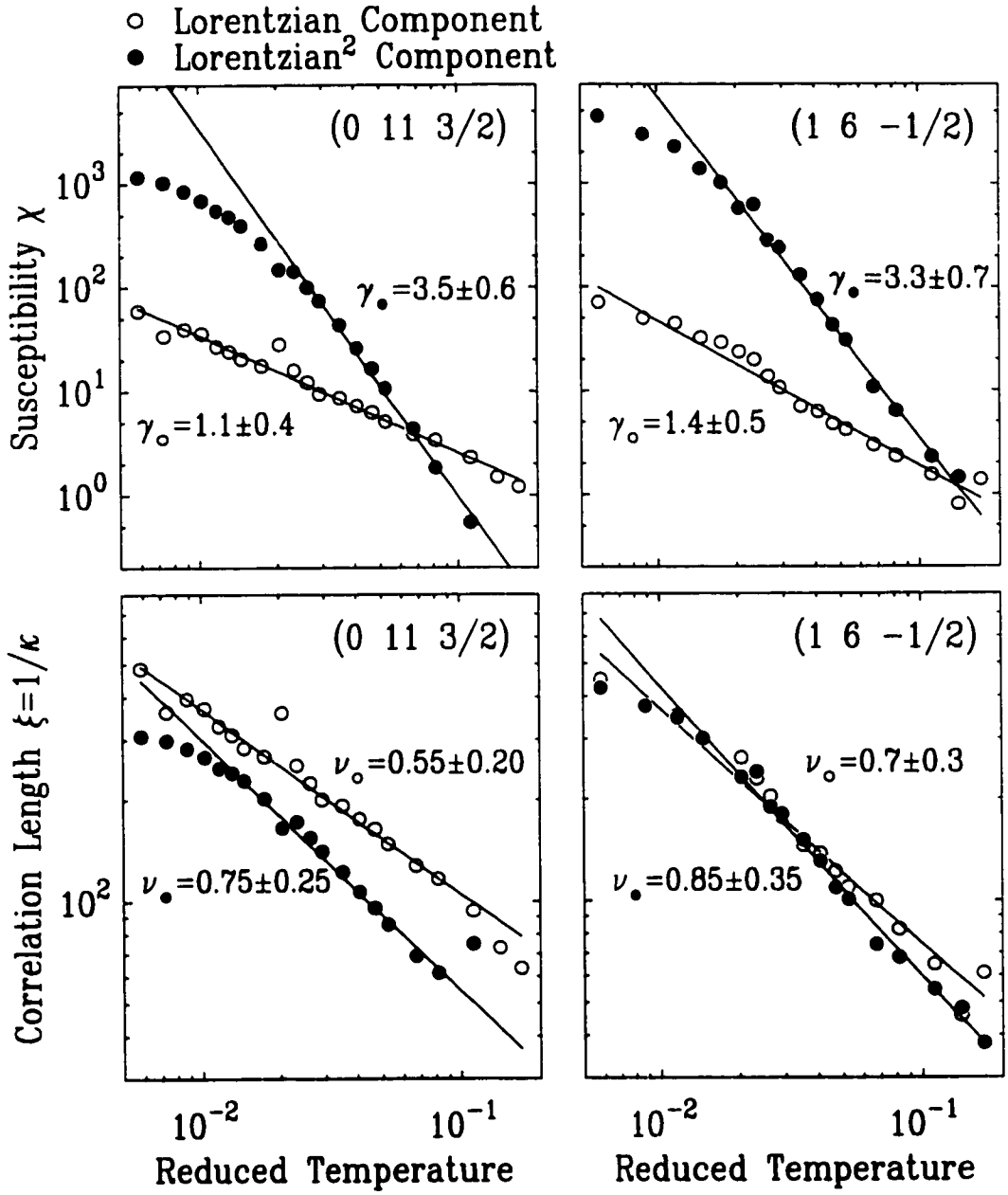

Figure 8: The resulting susceptibility, χ, and the correlation length $\xi = 1/\kappa$ from the fits to the Lorentzian + Lorentzian^2 cross-sections convoluted with the instrumental resolution as a function of reduced temperature on a logarithmic plot for both measured superlattice reflections. The solid lines represent best fits to a power law and the resulting critical exponents are indicated on the plot where the subscript • refers to the Lorentzian^2 component while the subscript o refers to the Lorentzian.

The solid lines shown in Fig. 8 represent the best power law description of the data and yields exponents for the Lorentzian component of the lineshape of γ_1=1.1±0.4 and γ_1=1.4±0.5 for the (0,11,3/2) and (1,6,-1/2) reflections with corresponding values of ν_1 of 0.55±0.20 and 0.7±0.3. Such values are indeed consistent with conventional 3D behaviour as suggested from the detailed order parameter analysis presented previously (the theoretical values of γ for 3D Ising, XY, and Heisenberg behaviour are 1.24, 1.32, and 1.39 respectively with corresponding values of ν of 0.63, 0.67, and 0.71[20]). The relatively large error bars on these critical exponent determinations does not allow distinction between 3D behaviour and mean field behaviour (where γ=1 and ν=0.5[39]) as was possible with the exponent β extracted from the order parameter. However, all previous measurements of two length scale scattering have occurred in systems exhibiting non-mean field critical behaviour.[15] This may suggest that the potential observation of such scattering in MEM(TCNQ)$_2$ is, in itself, indicative of critical behaviour inconsistent with mean field theory, as confirmed by the β exponent determination.

Although the extracted exponents are largely meaningless in terms of the assignment of a universality class, fits to the power law represented by Eq. 8 were also performed for the Lorentzian^2 component. The exponents obtained can be seen to be consistent between the two superlattice reflections yielding values of γ_2 of 3.5±0.6 and 3.3±0.7 and values of ν_2 of 0.75±0.25 and 0.85±0.35 for the (0,11,3/2) and (1,6,-1/2) reflections respectively. As had been suggested from previous second length scale observations,[15] these exponents are larger than those obtained for the bulk exponents, particularly for the exponent, γ, describing the susceptibility. One can also see from the data presented in Fig. 8 that the Lorentzian^2 component only seems to exhibit power law behaviour for reduced temperatures in excess of about 0.02 deviating sub-

stantially from the solid line below this value. The nature of such a deviation is unclear and may be indicative of either problems with the Lorentzian + Lorentzian^2 description of the data for temperatures very close to T_{sp} or a crossover to a regime where the two components exhibit similar exponents.

C. Discussion

The observed scattering appears to produce results consistent with the observation of two length scales in previous x-ray scattering measurements but there are a number of striking differences which should be mentioned. The most significant difference is the relative magnitude of the correlation lengths for the Lorentzian and Lorentzian^2 components. The best fit width κ for the Lorentzian component of the lineshape is the same size or smaller than the corresponding width for the Lorentzian^2 component as can be seen from the extracted widths in the lower panel of Fig. 8 and also from Fig. 9 where the Lorentzian+Lorentzian^2 components of the best fit at 17.7 K are shown. This indicates a length scale for the Lorentzian component which is of roughly the same size or perhaps even larger than the associated length scale for the Lorentzian^2 portion. This is in contrast to the majority of two length scale observations obtained previously where the Lorentzian^2 is noticeably sharper in **Q** indicating a larger associated length scale.[15]

The second difference between these observations and typical two length scale measurements is in the fall off of the Lorentzian^2 component. Most measurements show the presence of a sharp Lorentzian^2 lineshape which usually disappears with increasing temperature by a reduced temperature of about 0.04.[15] From Fig. 8, one can clearly see that the Lorentzian^2 remains until a reduced temperature of about 0.1

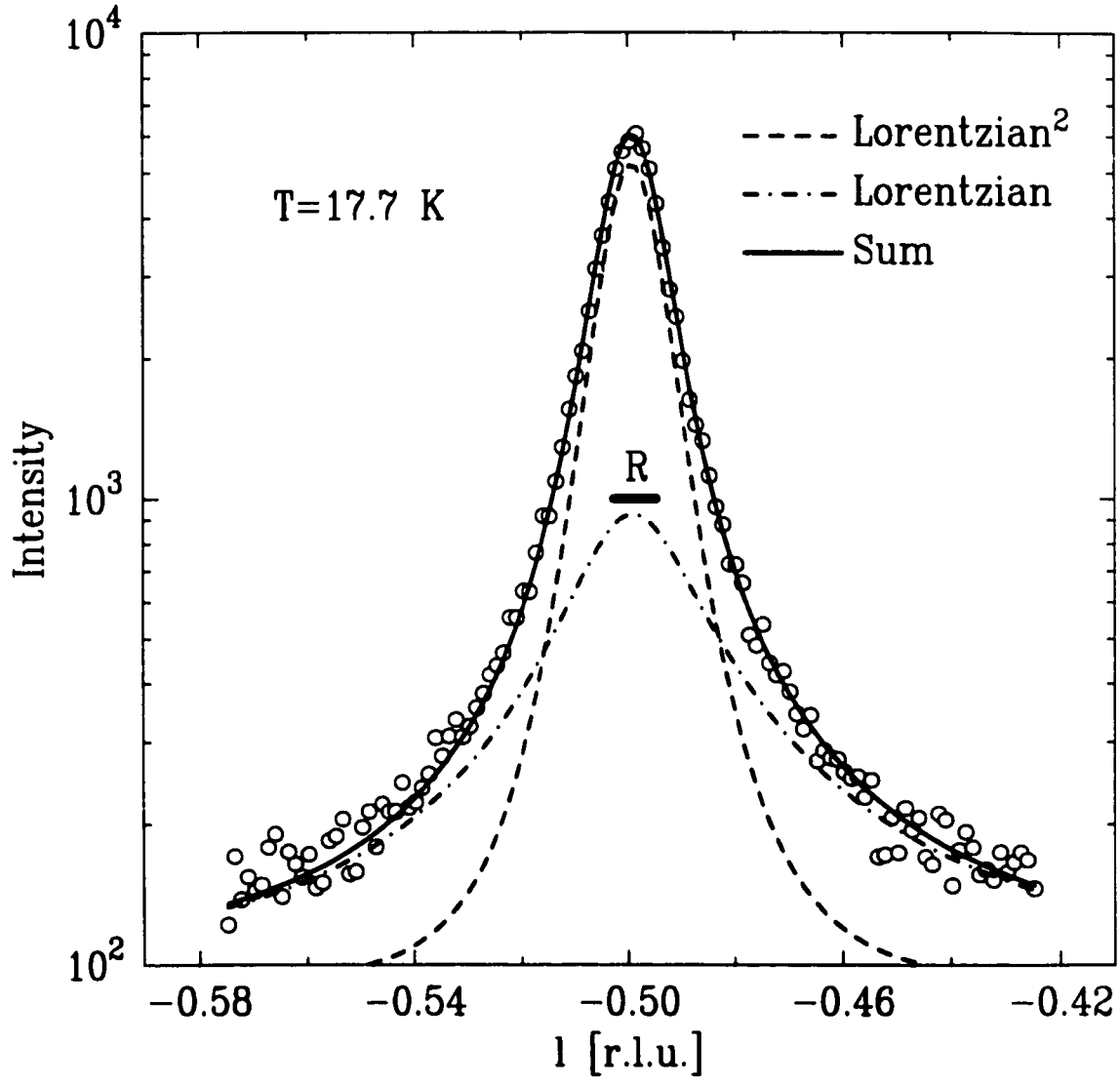

Figure 9: The data obtained for a scan along l at a temperature of 17.7 K. The solid line shows the best fit to a Lorentzian+Lorentzian^2 cross-section convoluted with the instrumental resolution. The dashed line shows the Lorentzian^2 component of this best fit and the dash-dot line shows the Lorentzian component. For reference, the resolution in indicated by the horizontal bar.

above which the observed scattering is well described by a single Lorentzian.

The appearance of two length scale scattering is typically observed in the presence of substantial surface sensitivity, as is the case for most x-ray scattering measurements resulting from relatively small penetration depths. This fact is partially responsible for the characterization of the second length scale as a near surface effect. However, the organic nature of MEM(TCNQ)$_2$ should produce large penetration depths for the 8 keV x-rays employed in this study and, consequently, surface sensitivity is weak. As a result, this measurement more closely resembles typical neutron scattering experiments where large penetration depths cause the bulk of the crystal to be sampled and, in such measurements, only one length scale is typically observed. The potential observation of such scattering in MEM(TCNQ)$_2$ is unexpected. It is possible that it may have resulted from a sampled scattering volume which overlapped with a large section of the near surface region yielding substantial surface sensitivity despite the large penetration depths. Such a possibility is more likely with x-rays than with neutron as distance collimation employed in x-ray measurements results in a very narrow beam and a resulting small scattering volume whereas with neutrons, collimation is typically provided by Soller slits producing a beam with a size on the order of a few centimeters. The observation of such scattering at two distinct wavevectors seems inconsistent with such a possibility as the scattering geometries differ greatly between the two. However, the ratio of amplitudes for the Lorentzian to Lorentzian^2 components differ between the two reflections by a factor of three. This indicates a much weaker Lorentzian^2 component at the (0,11,3/2) reflection, a difference which could be attributed to differences in scattering geometry.

A similar scenario has been observed previously with high energy synchrotron x-ray experiments performed on the perovskite $SrTiO_3$.[27] In these experiments, high-

energy ($\sim$ 100 keV) x-rays were used in an attempt to increase the penetration depths. As a result, only a single component lineshape, well described by a Lorentzian, was observed with a temperature dependence consistent with neutron measurements. However, when the experiment was configured to sample a near surface volume element, the second length scale was observed.

Another possible explanation of the existence of a two component lineshape is that such a cross-section is intrinsic to the system and not a consequence of defects in the near surface region. The observation of such scattering in MEM(TCNQ)$_2$ with no obvious surface sensitivity would seem to be consistent with such a possibility. This possibility was discussed by Cowley[15], and if such an explanation is correct, it indicates short-comings in scaling theory of continuous phase transitions when applied to such a system using such a probe.

Although we cannot distinguish between the three possible lineshapes, the observed scattering bears a striking resemblance to previous neutron measurements on a dilute 2d random Ising antiferromagnet in a magnetic field.[40] In these measurements, scattering was observed which was not well described by a single Lorentzian lineshape and the suggested lineshapes were identical to those reported in this paper, namely a Lorentzian with a varying power and a Lorentzian + Lorentzian^2. Indeed it was such similarities which lead to the possible description of the two length scale scattering in term of random defects distributed in the quasi-two-dimensional near surface region.

VI. SUMMARY

Measurements of the temperature dependence of the intensity of the superlattice Bragg peaks indicate a transition temperature of 17.1±0.2 K and an order parameter characterized by a critical exponent β of 0.35±0.06. This exponent is consistent with conventional 3D universality as observed previously in the inorganic SP compound $CuGeO_3$ and is clearly inconsistent with previous measurements where behaviour consistent with mean field theory was reported. Analysis of the critical behaviour of the order parameter indicated that the correction-to-scaling term is not needed for temperatures as low as two degrees below the transition temperature. This indicates a much gentler variation of the order parameter as compared with $CuGeO_3$ where the correction term was needed for temperatures within about 0.5 K of the transition temperature.

Lattice constant measurements on the (0,0,4) and (0,12,0) Bragg reflections indicate the presence of spontaneous strains below the transition temperature as observed in previous work on $CuGeO_3$. This represents the first observation of such spontaneous strains in an organic SP system and suggests that their presence is an intrinsic characteristic of the SP phase transition.

Measurements of fluctuations indicate the presence of substantial critical scattering, as had been observed previously. This scattering, however, cannot be adequately described by a single Lorentzian lineshape as expected from scaling theory of continuous phase transitions. The data can be adequately described by a Lorentzian with a varying power or a Lorentzian + Lorentzian^2. Similar lineshapes have previously been observed in x-ray scattering measurements of critical fluctuations where two length scales are observed, one corresponding to the bulk fluctuations well described

by a Lorentzian while the second, larger length scale is typically well described by a Lorentzian^2. Analysis using this form for the cross-section allows bulk exponents γ and ν to be extracted from the Lorentzian component and such an effort yields exponents consistent with 3D behaviour, as seen with the order parameter, but not inconsistent with mean field theory. Exponents extracted from the Lorentzian^2 portion of the lineshape are larger than those for the Lorentzian component, particularly for γ, in a manner similar to previous two length scale studies.

ACKNOWLEDGMENTS

This work was supported by NSERC of Canada and OCMR of Ontario. We thank H.A. Mook for making the single crystal available to us.

APPENDIX: FULL FORM OF Q^2 FOR A TRICLINIC CRYSTAL

The square of the distance in reciprocal space, Q^2, for a triclinic single crystal with lattice parameters a,b,c,α,β,γ in terms of the Miller indices h,k,l, can be shown to be

$$\begin{aligned} Q^2 &= 4\pi^2(1 + 2\,cos\alpha cos\beta cos\gamma - cos^2\alpha - cos^2\beta - cos^2\gamma)^{-1} \\ &\times \left[sin^2\alpha \frac{h^2}{a^2} + sin^2\beta \frac{k^2}{b^2} + sin^2\gamma \frac{l^2}{c^2} \right. \\ &\quad +2(cos\alpha\, cos\beta - cos\gamma)\frac{hk}{ab} + 2(cos\beta\, cos\gamma - cos\alpha)\frac{kl}{bc} \\ &\quad \left. +2(cos\gamma\, cos\alpha - cos\beta)\frac{hl}{ac} \right]. \end{aligned} \tag{A1}$$

The distance in reciprocal space away from some position, h',k', l', divided by a width κ with allowance for differing widths along h,k,l will then be given by

$$\begin{aligned}\frac{Q^2}{\kappa^2} &= 4\pi^2(1+2cos\alpha cos\beta cos\gamma - cos^2\alpha - cos^2\beta - cos^2\gamma)^{-1} \\ &\times \left[\frac{sin^2\alpha}{a^2}\frac{(h-h')^2}{\kappa_h^2} + \frac{sin^2\beta}{b^2}\frac{(k-k')^2}{\kappa_k^2} + \frac{sin^2\gamma}{c^2}\frac{(l-l')^2}{\kappa_l^2}\right. \\ &+2\frac{(cos\alpha\ cos\beta - cos\gamma)}{ab}\frac{(h-h')(k-k')}{\kappa_h\kappa_k} \\ &+2\frac{(cos\beta\ cos\gamma - cos\alpha)}{bc}\frac{(k-k')(l-l')}{\kappa_k\kappa_l} \\ &\left.+2\frac{(cos\gamma\ cos\alpha - cos\beta)}{ac}\frac{(h-h')(l-l')}{\kappa_h\kappa_l}\right]. \end{aligned} \tag{A2}$$

The above equation is the full expression which is substituted for Q^2/κ^2 in Eqs. 4.5.6 and 7.

References

[1] See J.W. Bray, L.V. Interrante, I.S. Jacobs, and J.C. Bonner, in *Extended Linear Chain Compounds*, edited by J.S. Miller (Plenum Press, New York, 1983), Vol. 3, p.353, and references therein.

[2] B. van Bodegom, Acta Cryst. B **37**, 863 (1981).

[3] S. Huizinga, J. Kommandeur, G.A. Sawatzky, B.T. Thole, K. Kopinga, W.J.M. de Jonge, and J. Roos, Phys. Rev. B **19**, 4723 (1979).

[4] B. van Bodegom, B.C. Larson, and H.A. Mook, Phys. Rev. B **24**, 1520 (1981).

[5] P.I. Kuindersma, G.A. Sawatzky, and J. Kommandeur, J. Phys. C **8**, 3005 (1975).

[6] R.J.J. Visser, S. Oostra, C. Vettier, J. Voiron, Phys. Rev. B **28**, 2074 (1983).

[7] G. Aeppli, J.L. deBoer, J.P. Pouget, and G. Shirane, Phys. Rev. B **29**, 5165 (1984).

[8] S.J. Blundell, F.L. Pratt, P.A. Pattenden, M. Kurmoo, K.H. Chow, S. Tagagi, Th Jestädt, and W. Hayes, J. Phys. Condens. Matter **9**, L119 (1997).

[9] D. Bloch, J. Voiron, J.W. Bray, I.S. Jacobs, J.C. Bonner, and J. Kommandeur, Physics Letters, **82A**, 21 (1981).

[10] M.D. Lumsden, B.D. Gaulin, and H. Dabkowska, Phys. Rev. B **57** 14097 (1998).

[11] J.P. Pouget, L.P. Regnault, M. Ain, B. Hennion, J.P. Renard, P. Veillet, G. Dhalenne, and A. Revocolevschi, Phys. Rev. Lett. **72**, 4037 (1994).

[12] K. Hirota, D.E. Cox, J.E. Lorenzo, G. Shirane, J.M. Tranquada, M. Hase, K. Uchinokura, H. Kojima, Y. Shibuya, and I. Tanaka, Phys. Rev. Lett. **73**, 736 (1994).

[13] Q.J. Harris, Q. Feng, R.J. Birgeneau, K. Hirota, K. Kakurai, J.E. Lorenzo, G. Shirane, M. Hase, K. Uchinokura, H. Kojima, I. Tanaka, and Y. Shibuya, Phys. Rev. B **50**, 12606 (1994).

[14] Q.J. Harris, Q. Feng, R.J. Birgeneau, K. Hirota, G. Shirane, M. Hase, and K. Uchinokura, Phys. Rev. B **52**, 15420 (1995).

[15] A good review of two length scale phenomena is provided in, R.A. Cowley, Physica Scripta **T66**, 24 (1996).

[16] D.E. Moncton, R.J. Birgeneau, L.V. Interrante, and F. Wudl, Phys. Rev. Lett. **39**, 507 (1977).

[17] J.E. Lorenzo, K. Hirota, G. Shirane, J.M. Tranquada, M. Hase, K. Uchinokura, H. Kojima, I. Tanaka, and Y. Shibuya, Phys. Rev. B **50**,1278 (1994).

[18] H. Winkelmann, E. Gamper, B. Büchner, M. Braden, A. Revcolevschi, and G. Dhalenne, Phys. Rev. B **51**, 12884 (1995).

[19] A. Aharony and G. Ahlers, Phys. Rev. Lett. **44**, 782 (1980).

[20] M.F. Collins, *Magnetic Critical Scattering* (Oxford University Press, New York, 1989).

[21] Y. Tanaka, N. Satoh, and K. Nagasaka, J. Phys. Soc. Japan **59**, 319 (1990).

[22] M. Köppen, D. Pankert, R. Hauptmann, M. Lang, M. Weiden, C. Geibel, and F. Steglich, Phys. Rev. B **57**, 8466 (1998).

[23] H. Eugene Stanley, *Introduction to Phase Transitions and Critical Phenomena* (Clarendon Press, Oxford, 1971).

[24] S.R. Andrews, J. Phys. C **19**, 3721 (1986).

[25] R.J. Nelmes, P.E. Hatton, and H. Vass, Phys. Rev. Lett. **60** 2172, (1988).

[26] D.F. McMorrow, N. Hamaya, S. Shimomura, Y. Fujii, S. Kishimoto, and H. Iwasaki, Solid State Commun. **76**, 443 (1990).

[27] H.-B. Neumann, U. Rütt, J.R. Schneider, and G. Shirane, Phys. Rev. B **52** 3981 (1995).

[28] K. Hirota, J.P. Hill, S.M. Shapiro, G. Shirane, and Y. Fujii, Phys. Rev. B **52** 13195 (1995).

[29] U.J. Nicholls and R.A. Cowley, J. Phys. C **20** 3417 (1987).

[30] T.W. Ryan, R.J. Nelmes, R.A. Cowley, and A. Gibaud, Phys. Rev. Lett. **56**, 2704 (1986).

[31] A. Gibaud, R.A. Cowley, and P.W. Mitchell, J. Phys. C **20** 3849 (1987).

[32] T.R. Thurston, G. Helgesen, Doon Gibbs, J.P. Hill, B.D. Gaulin, and G. Shirane, Phys. Rev. Lett. **70**, 3151 (1993).

[33] T.R. Thurston, G. Helgesen, J.P. Hill, Doon Gibbs, B.D. Gaulin, and P.J. Simpson, Phys. Rev. B **49**, 15730 (1994).

[34] K. Hirota, G. Shirane, P.M. Gehring, and C.F. Majkrzak, Phys. Rev. B **49**, 11967 (1994).

[35] P.M. Gehring, K. Hirota, C.F. Majkrzak, and G. Shirane, Phys. Rev. B **51**, 3234 (1995).

[36] G.M. Watson, B.D. Gaulin, Doon Gibbs, T.R. Thurston, P.J. Simpson, S.M.

Shapiro, G.H. Lander, Hj. Matzke, S. Wang, and M. Dudley, Phys. Rev. B **53**. 686 (1996).

[37] S.G. Perry, W.J. Nuttall, W.G. Stirling, G.H. Lander, and O. Vogt, Phys. Rev. B **54**, 15234 (1996).

[38] A. Stunault, S. Langridge, C. Vettier, Doon Gibbs, N. Bernhoeft, Phys. Rev. B **55**. 423 (1997).

[39] See, for example, M. Plischke and B. Bergersen, *Equilibrium Statistical Physics* (Prentice Hall, New Jersey, 1989).

[40] R.J. Birgeneau, H. Yoshizawa, R.A. Cowley, G. Shirane, and H. Ikeda, Phys. Rev. B **28**, 1438 (1983).

Chapter 7

Summary

The behaviour of a system in the immediate vicinity of a critical phase transition has been a field of considerable theoretical and experimental interest for the past 30 years. As we approach such a point, a number of physically measurable quantities are found to diverge exhibiting a power law dependence on the reduced temperature in the immediate vicinity of the transition temperature. The critical exponents which define these power law divergences help to define a universality class for a given phase transition. Scattering techniques, both neutron and x-ray, are the single most powerful probe for the study of these critical properties as they allow for measurement of the exponents β, γ, and ν which describe the order parameter, susceptibility, and correlation length respectively.

X-ray scattering techniques have been used in the study of the spin-Peierls phase transition. Such a transition occurs in quasi-one-dimensional S=1/2 Heisenberg spin chains with antiferromagnetic coupling between spins. In the presence of strong magnetoelastic coupling, the spin chains undergo a dimerization, which proceeds continuously below some transition temperature. This dimerization is accompanied by the appearance of a gap in the magnetic excitation spectrum. We have studied the

critical behaviour in pure and dilute samples of the inorganic spin-Peierls system, $CuGeO_3$, and also in the organic compound $MEM(TCNQ)_2$.

Measurements of the order parameter associated with the SP transition in pure $CuGeO_3$ show the presence of a continuous phase transition below a transition temperature of T_{sp}=14.05±0.01 K. The critical exponent, β, describing the order parameter was found to be 0.345±0.03 consistent with conventional 3D behaviour and most closely consistent with 3D XY universality as had been suggested by previous theoretical studies (Plumer 1996). The results indicate a rather narrow asymptotic critical region which is likely responsible for the wide range of values of β reported in previous measurements.

Careful measurements of relative lattice constant changes as a function of temperature have also been performed for pure $CuGeO_3$ using a novel approach. These measurements indicate the clear presence of spontaneous strains below the transition temperature. Through the use of an independent background determination, the spontaneous strains were extracted and found to scale with the square of the order parameter as had been suggested in previous studies (Winkelmann, Gamper, Büchner, Braden, Revcolevschi & Dhalenne 1995).

Measurements of the critical properties under the influence of impurities have also been performed on a series of doped samples of $CuGeO_3$ with Cu^{2+} replaced with both Zn^{2+} and Cd^{2+} and Ge^{4+} replaced with Si^{4+}. Order parameter results under the influence of either Zn or Si doping indicate results consistent with the pure material. Such results are suggestive of 3D XY universality for the pure compound by virtue of the Harris criterion which suggests changes in critical properties in the presence of impurities for 3D Ising systems but not 3D XY or Heisenberg systems. (this is based on the value of the exponent α). However, substantially different mean-field results are observed for the Cd doped sample where the order parameter is found

to differ greatly from that displayed in the pure material. This change in behaviour from 3D to mean field universality is described as arising from relatively long-range local strain fields induced by the presence of a substantially larger dopant ion.

The temperature dependence of relative lattice constant changes were measured for these doped samples and, as was the case in the pure material, indicate the presence of spontaneous strains which scale with the square of the order parameter. This scaling was even observed for the Cd doped sample, where the order parameter exhibits mean field behaviour, suggesting an intimate connection between the order parameter and the spontaneous strains.

Finally, the critical properties associated with the SP transition in the organic compound MEM(TCNQ)$_2$ were examined. Unlike $CuGeO_3$, substantial critical scattering was observed in MEM(TCNQ)$_2$ allowing for a determination of not only the critical exponent β but also the exponents γ and ν. Measurements of the order parameter indicate a critical exponent β of 0.35±0.06 consistent with 3D behaviour, as was observed for $CuGeO_3$, and inconsistent with mean field behaviour which had been suggested previously. Critical scattering measurements showed scattering which could not be well described by an Ornstein-Zernike form with a lineshape which is Lorentzian in wavevector. The scattering can be described by either a Lorentzian^x with x varying or a Lorentzian+Lorentzian^2. The later descriptor is reminiscent of recent x-ray scattering measurements of structural phase transitions in some perovskites and magnetic x-ray scattering measurements on Ho, Tb, and some U-based compounds. In these studies, the critical scattering exhibits two components, a bulk component well described by a Lorentzian and a sharper component, attributed to defects in the near surface region, well described by a Lorentzian^2. Such scattering was unexpected in MEM(TCNQ)$_2$ as the organic nature of the compound should result in large penetration depths and, thus, weak surface sensitivity. Extraction of

critical exponents γ and ν from the Lorentzian component of the lineshape indicate values which are consistent with the universality class suggested from the exponent β, but not distinguishable from the mean field values.

Appendix A

Resolution Convolution

As mentioned in Chapter 3, when an x-ray scattering measurement is performed, the measured intensity is a convolution of the actual scattering cross-section, $d\sigma/d\Omega(\mathbf{Q}\text{-}\mathbf{Q}')$, with the instrumental resolution function, $R(\mathbf{Q}')$. Consequently, the scattered intensity at some wavevector $\mathbf{Q}$ will be given by,

$$I(\mathbf{Q}) = \int R(\mathbf{Q}')\frac{d\sigma}{d\Omega}(\mathbf{Q} - \mathbf{Q}')d\mathbf{Q}'. \tag{A.1}$$

Many scattering experiments can be performed without the necessity to perform such a convolution as one is often not interested in the details of the lineshape. However, for critical scattering measurements, it is the components of the lineshape which provide a measure of the response function and the correlation length and, thus, such a convolution is essential.

If one considers the measurement of a Bragg peak, for which,

$$\frac{d\sigma}{d\Omega}(\mathbf{Q} - \mathbf{Q}') \sim \delta(\mathbf{Q} - \mathbf{Q}'), \tag{A.2}$$

then insertion of this delta function into equation A.1 gives an intensity

$$I(\mathbf{Q}) \sim R(\mathbf{Q}). \tag{A.3}$$

Consequently, measurement of a Bragg reflection will provide a direct measurement of the resolution function of the instrument. For our measurements of the critical scattering in $MEM(TCNQ)_2$, these measurements were performed at our base temperature, ~9 K, which should be sufficiently below the transition temperature, T_{sp} ~17 K, to ensure that diffuse critical scattering will be negligible with only the resolution limited Bragg feature remaining. As the superlattice peak intensity was rather strong and there were no urgent time constraints on the experiment, this resolution function was mapped out fully through a series of approximately 30 mesh scans in the h-k recipricol lattice plane at a number of different values of l. This provides a complete experimental characterization of the resolution function, a process which is often impossible to perform due to time constraints which exist at large scale facilities, be they neutron or synchrotron laboratories. Several of the resultant mesh scans for the (1,6,-1/2) superlattice reflection are shown in Fig. A.1 where one can clearly see the presence of two distinct crystallites.

This discrete array of points representing the resolution function is then used to numerically perform the integral, Eq. A.1. The method used in this process is referred to as the *Centres of Scattering* (Rogge 1994) technique. Within this approach, one treats every individual point in the resolution array as a scattering centre with the assumed cross-section, $d\sigma/d\Omega$, centred about this point. We then calculate the contribution of this cross-section to the scattering at the observation point, with wavevector **Q**, and modulate the contribution by the amplitude of the resolution function at this particular scattering centre. The total scattering at **Q** is then obtained by summing the contribution from all scattering centres contained in the discrete array which constitutes the resolution function. Mathematically, the scattering at some

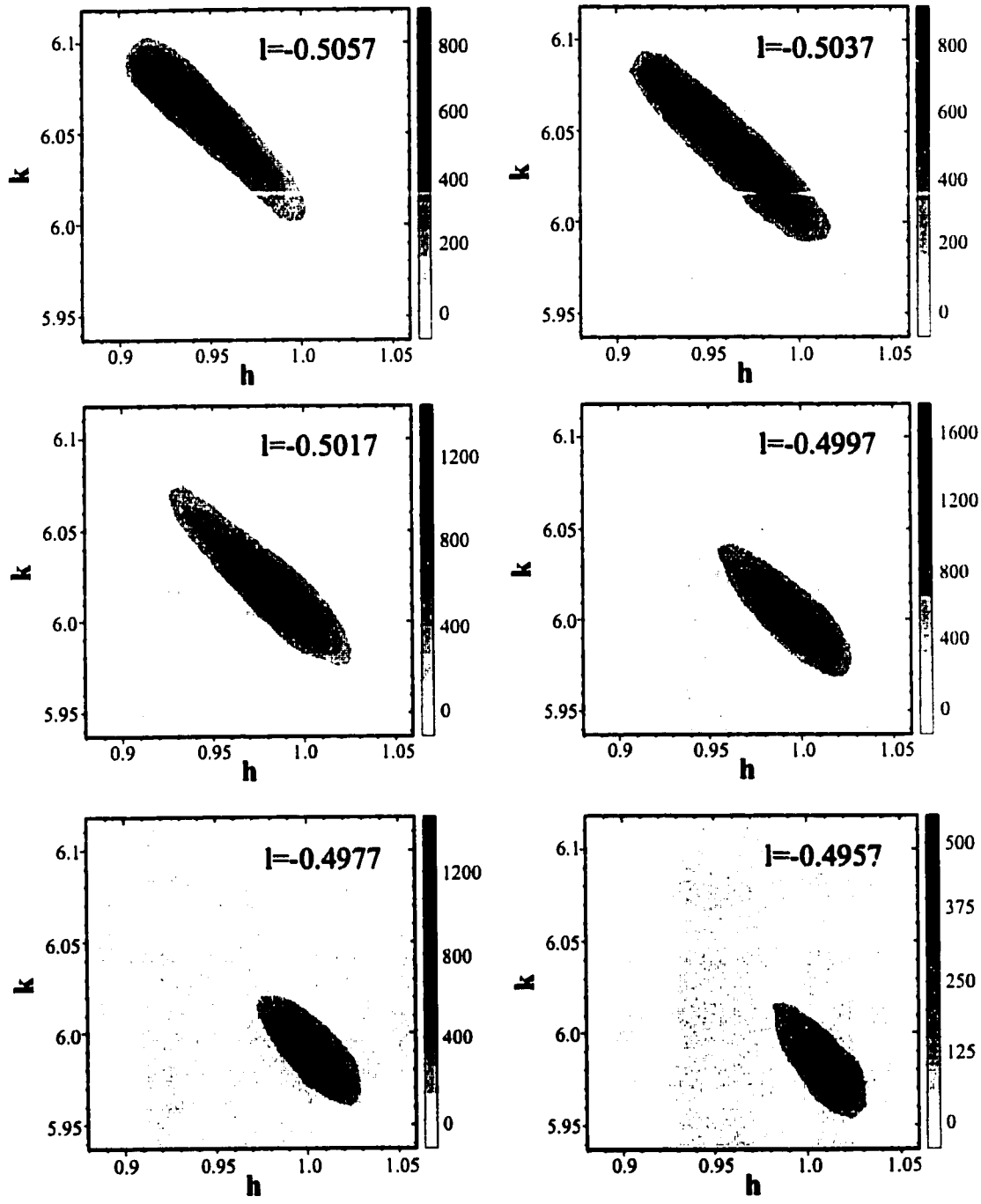

Figure A.1: Representative scans of the measurement of the resolution function for the (1,6,-1/2) superlattice reflection. The entire resolution function was directly measured with a series of ~30 h-k mesh scans at differing l values.

point **Q**, described by the recipricol lattice coordinates (h,k,l), is given by,

$$I(h,k,l) = \sum_{h_i}\sum_{k_i}\sum_{l_i} R(h_i,k_i,l_i)\frac{d\sigma}{d\Omega}(h-h_i, k-k_i, l-l_i) \qquad (A.4)$$

where the sums are over the points in the resolution array. To improve the speed of computation, this triple sum was replaced by a single sum,

$$I(h,k,l) = \sum_{n=1}^{ngrid} R(h_n,k_n,l_n)\frac{d\sigma}{d\Omega}(h-h_n, k-k_n, l-l_n) \qquad (A.5)$$

where the sum is now over the *ngrid* points which make up the resolution array. In fact, these two summations, Eq. A.4 and A.5, are identical. The enhancement in speed of computation for Eq. A.5 occurs because the large majority of the points in the resolution array have negligible intensity. The triple sum requires a uniform array of points and such a restriction is lifted by using the single summation. Consequently, one can remove all negligible points before the computation begins and this reduces the number of points which need to be considered by typically a factor of 20 correspondingly enhancing the speed of calculation.

Equation A.5 generates the intensity at a single point and this process must be repeated for each of the 363 points which compose a set of three scans along h,k,and l respectively at each temperature (3 scans of 121 points). This generates a representation of the scattering and a best fit is obtained by minimizing an overall goodness-of-fit parameter, χ^2, with respect to the parameters which describe the assumed cross-section. This overall χ^2 is a sum of the individual goodness-of-fit parameters for the three scans along h,k, and l. i.e.,

$$\chi^2 = \frac{\chi_h^2 + \chi_k^2 + \chi_l^2}{n_h + n_k + n_l - n_{params}} \quad where$$
$$\chi_i^2 = \sum_{n=1}^{n_i}\left[\frac{I_{meas}(n) - I_{calc}(n)}{\Delta I_{meas}(n)}\right]^2 \qquad (A.6)$$

where i=h,k, or l and n_h,n_k, and n_l are the number of points contained in the h, k, and l scans respectively and n_{params} are the number of variable parameters.

The minimization was accomplished through the use of a nonlinear least-squares fitting routine contained in the MINUIT library which is part of the CERNLIB suite of data analysis libraries.

The measured resolution array contained 31×31×31 points. However, it was necessary, particularly close to the transition temperature where the scattering is sharp in wavevector, to increase the density of points contained in this array allowing for a more accurate numerical approximation to the integral. To accomplish this, new grids were generated by performing a 3D linear interpolation of the measured data. The FORTRAN routine used in this process was taken from Press, Flannery, Teukolsky & Vetterling (1990) where the provided routines for 1D and 2D linear interpolations were extended to the 3D case. This routine basically performs an average of the 8 nearest neighbours, weighted by the relative distance to each neighbour, to attain the value at the point in question. Such a process was also used to check whether the finite size of the array caused any difficulties with the numerical approximation to the integral. Fits to a single Lorentzian lineshape were performed using three different arrays, the first of which started with 121×121×121 points (of which many were eliminated due to negligible intensity) the second and third containing twice and three times this number of points along each direction. Fits to data at the (1,6,-1/2) wavevector, at a temperature of 17.7 K using the three grids generated best fit representations which were indistinguishable from each other with corresponding values of χ^2 of 9.13, 9.01, and 9.03 respectively. These numbers are effectively identical suggesting that there are no finite size difficulties in the numerical approximation to the integral.

Bibliography

Aeppli, G., de Boer, J. L., Pouget, J. P. & Shirane, G. (1984), *Phys. Rev. B* **29**, 5165.

Ashcroft, N. W. & Mermin, N. D. (1976), *Solid State Physics*, Sauders College Publishing, Toronto.

Bloch, D., Voiron, J., Bray, J. W., Jacobs, I. S., Bonner, J. C. & Kommandeur, J. (1981), *Physics Letters* **82A**, 21.

Blundell, S. J., Pratt, F. L., Pattenden, P. A., Kurmoo, M., Chow, K. H., Takagi, S., Jestädt, T. & Hayes, W. (1997), *J. Phys. Condens. Matter* **9**, L119.

Bonner, J. C. & Fisher, M. E. (1964), *Phys. Rev.* **135**, A640.

Bragg, W. H. & Bragg, W. L. (1913), *Proceedings of the Royal Society London* **A88**, 428.

Bragg, W. L. (1913), *Proceedings of the Cambridge Philosophical Society* **17**, 43.

Bragg, W. L. (1914), *Proceedings of the Royal Society London* **A89**, 248.

Bray, J. W., Hart, H. R., Interrante, L. V., Jacobs, I. S., Kasper, J. S., Watkins, G. D., Wee, S. H. & Bonner, J. C. (1975), *Phys. Rev. Lett.* **35**, 744.

Bray, J. W., Interrante, L. V., Jacobs, I. S. & Bonner, J. C. (1983), *Extended Linear Chain Compounds*, Vol. 3, Plenum Press, chapter The Spin-Peierls Transition, pp. 353–415.

Bulaevskii, L. N., Buzdin, A. I. & Khomskii, D. I. (1978), *Solid State Commun.* **27**, 5.

Collins, M. F. (1989), *Magnetic Critical Scattering*, Oxford University Press, New York.

Cullity, B. D. (1967), *Elements of X-ray Diffraction*, Addison-Wesley, Don Mills, Ontario.

Fisher, M. E. (1964), *J. Math. Phys.* **5**, 944.

Fisher, M. E. & Burford, R. J. (1967), *Phys. Rev.* **156**, 583.

Friedrich, W., Knipping, P. & Laue, M. (1912), *Proceedings of the Royal Bavarian Academy of Science* p. 303.

Fujita, M., Ubukata, K., Arai, M., Tonegawa, T., Mino, M., Motokawa, M., Knight, K., Forsyth, B., Bennington, S. M., Akimitsu, J. & Fujita, O. (1996), *Physica B* **219 and 220**, 95.

Fujita, O., Akimitsu, J., Nishi, M. & Kakurai, K. (1995), *Phys. Rev. Lett.* **74**, 1677.

Fukuyama, H., Tanimoto, T. & Saito, M. (1996), *J. Phys. Soc. Japan* **65**, 1182.

Grenier, B., Renard, J.-P., Veillet, P., Paulsen, C., Calemczuk, R., Dhalenne, G. & Revcolevschi, A. (1998), *Phys. Rev. B* **57**, 3444.

Guggenheim, E. A. (1945), *J. Chem. Phys.* **13**, 253.

Hamamoto, T., Adachi, N., Kido, G., Hase, M., Sasago, Y. & Uchinokura, K. (1994), *J. Phys. Soc. Japan* **63**, 1218.

Harris, A. (1974), *J. Phys. C* **7**, 1671.

Harris, A. & Lubensky, T. (1974), *Phys. Rev. Lett.* **33**, 1540.

Hase, M., Terasaki, I., Sasago, Y., Uchinokura, K. & Obara, H. (1993), *Phys. Rev. Lett.* **71**, 4059.

Hase, M., Terasaki, I. & Uchinokura, K. (1993), *Phys. Rev. Lett.* **70**, 3651.

Hase, M., Terasaki, I., Uchinokura, K., Tokunaga, M., Miura, N. & Obara, H. (1993), *Phys. Rev. B* **48**, 9616.

Hirota, K., Cox, D. E., Lorenzo, J. E., Shirane, G., Tranquada, J. M., Hase, M., Uchinokura, K., Kojima, H., Shibuya, Y. & Tanaka, I. (1994), *Phys. Rev. Lett.* **73**, 736.

Huizinga, S., Kommandeur, J., Sawatzky, G. A., Thole, B. T., Kopinga, K., de Jonge, W. J. M. & Roos, J. (1979), *Phys. Rev. B* **19**, 4723.

Jackson, J. D. (1975), *Classical Electrodynamics*, second edn, John-Wiley and Sons, Toronto.

Kadanoff, L. P. (1966), *Physics* **2**, 263.

Kadanoff, L. P. (1976), *Phase Transitions and Critical Phenomena*, Academic Press, chapter Scaling, Unversality and Operator Algebras, pp. 1–34.

Kiryukhin, V. & Keimer, B. (1995), *Phys. Rev. B* **52**, R704.

Köppen, M., Pankert, D., Hauptmann, R., Lang, M., Weiden, M., Geibel, C. & Steglich, F. (1998), *Phys. Rev. B* **57**, 8466.

Kosterlitz, J. M. (1974), *J. Phys. C.* **7**, 1046.

Kosterlitz, J. M. & Thouless, D. J. (1973), *J. Phys. C.* **6**, 1181.

Landau, L. D. & Lifshitz, E. M. (1969), *Statistical Physics*, Addison-Wesley, Reading, Mass.

Laue, M. (1912), *Proceedings of the Royal Bavarian Academy of Science* p. 363.

Lumsden, M. D. & Gaulin, B. D. (1998), X-ray diffraction study of the spin-peierls transition in NaV_2O_5.

Manabe, K., Ishimoto, H., Koide, N., Sasago, Y. & Uchinokura, K. (1998), *Phys. Rev. B* **58**, R575.

McConnell, H. M. & Lynden-Bell, R. (1962), *J. Chem. Phys.* **36**, 2393.

Mermin, N. D. & Wagner, H. (1966), *Phys. Rev. Lett.* **17**, 1133.

Moncton, D. E., Birgeneau, R. J., Interrante, L. V. & Wudl, F. (1977), *Phys. Rev. Lett.* **39**, 507.

Nishi, M., Fujita, O. & Akimitsu, J. (1994), *Phys. Rev. B* **50**, 6508.

Ornstein, L. S. & Zernicke, F. (1914), *Proc. Sect. Sci. K. Med. Akad, Wet.* **17**, 793.

Oseroff, S., Cheong, S.-W., Aktas, B., Hundley, M., Fisk, Z. & L.W. Rupp, J. (1995), *Phys. Rev. Lett.* **74**, 1450.

Peierls, R. E. (1955), *Quantum Theory of Solids*, Oxford University Press, London.

Plischke, M. & Bergersen, B. (1989), *Equilibrium Statistical Physics*, Prentice Hall, Englewood Cliffs, New Jersey.

Plumer, M. (1996), *Phys. Rev. B* **53**, 594.

Poirier, M., Beaudry, R., Castonguay, M., Plumer, M., Quirion, G., Razavi, F., Revcholevschi, A. & Dhalenne, G. (1995), *Phys. Rev. B* **52**, R6971.

Pouget, J. P., Regnault, L. P., Ain, M., Hennion, B., Renard, J. P., Veillet, P., Dhalenne, G. & Revcolevschi, A. (1994), *Phys. Rev. Lett.* **72**, 4037.

Press, W. H., Flannery, B. P., Teukolsky, S. A. & Vetterling, W. T. (1990), *Numerical recipes in FORTRAN*, Cambridge University Press, New York.

Regnault, L., Renard, J., Dhalenne, G. & Revcolevschi, A. (1995), *Europhys. Lett.* **32**, 579.

Renard, J., Dang, K. L., Veillet, P., Dhalenne, G., Revcolevschi, A. & Regnault, L. P. (1995), *Europhys. Lett.* **30**, 475.

Roentgen, W. C. (1895), Presented to the president of the Wurzburg Physical-Medical Society, Dec. 28, 1895.

Rogge, R. B. (1994), Neutron scattering techniques in the study of phase transitions, PhD thesis, McMaster University.

Sasago, Y., Koide, N., Uchinokura, K., Martin, M. C., Hase, M. & Hirota, K. (1996), *Phys. Rev. B* **54**, R6835.

Stanley, H. E. (1971), *Introduction to Phase Transitions and Critical Phenomena*, Clarendon Press, Oxford.

Tanaka, Y., Satoh, N. & Nagasaka, K. (1990), *J. Phys. Soc. Japan* **59**, 319.

van Bodegom, B. (1981), *Acta Cryst.* **B37**, 857.

van Bodegom, B. & Bosch, A. (1981), *Acta Cryst.* **B37**, 863.

van Bodegom, B., Larson, B. C. & Mook, H. A. (1981), *Phys. Rev. B* **24**, 1520.

van der Waals, J. D. (1873), PhD thesis, University of Leiden.

Visser, R. J. J., Oostra, S., Vettier, C. & Voiron, J. (1983), *Phys. Rev. B* **28**, 2074.

Völlenkle, H., Wittman, A. & Nowotny, H. (1967), *Monatsh. Chem.* **98**, 1352.

Warren, B. E. (1990), *X-Ray Diffrction*, Dover Publications, Inc., New York.

Winkelmann, H., Gamper, E., Büchner, B., Braden, M., Revcolevschi, A. & Dhalenne, G. (1995), *Phys. Rev. B* **51**, 12884.